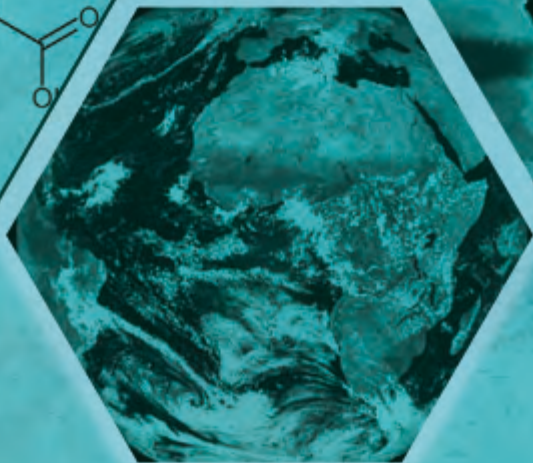
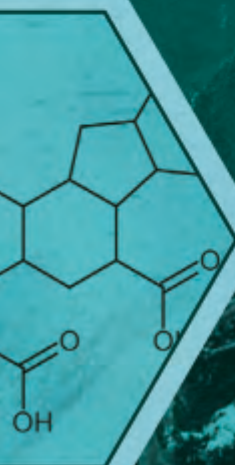


DYNAMICS OF MARINE DISSOLVED ORGANIC MATTER: OCEAN METABOLISM AND CLIMATE TRANSITIONS

PATRICIA DE LA FUENTE GAMERO



 **CSIC**
Consejo Superior de Investigaciones Científicas

ICM Institut de Ciències del Mar

 **UNIVERSITAT POLITÈCNICA DE CATALUNYA BARCELONATECH**

BARCELONA
2019



UNIVERSITAT POLITÈCNICA
DE CATALUNYA
BARCELONATECH

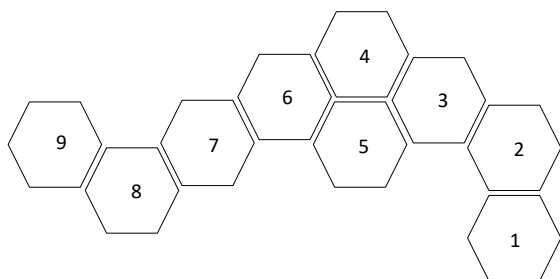
Dynamics of marine dissolved organic matter: ocean metabolism and climate transitions.

Patricia De La Fuente Gamero

ADVERTIMENT La consulta d'aquesta tesi queda condicionada a l'acceptació de les següents condicions d'ús: La difusió d'aquesta tesi per mitjà del repositori institucional UPCommons (<http://upcommons.upc.edu/tesis>) i el repositori cooperatiu TDX (<http://www.tdx.cat/>) ha estat autoritzada pels titulars dels drets de propietat intel·lectual **únicament per a usos privats** emmarcats en activitats d'investigació i docència. No s'autoritza la seva reproducció amb finalitats de lucre ni la seva difusió i posada a disposició des d'un lloc aliè al servei UPCommons o TDX. No s'autoritza la presentació del seu contingut en una finestra o marc aliè a UPCommons (*framing*). Aquesta reserva de drets afecta tant al resum de presentació de la tesi com als seus continguts. En la utilització o cita de parts de la tesi és obligat indicar el nom de la persona autora.

ADVERTENCIA La consulta de esta tesis queda condicionada a la aceptación de las siguientes condiciones de uso: La difusión de esta tesis por medio del repositorio institucional UPCommons (<http://upcommons.upc.edu/tesis>) y el repositorio cooperativo TDR (<http://www.tdx.cat/?locale-attribute=es>) ha sido autorizada por los titulares de los derechos de propiedad intelectual **únicamente para usos privados enmarcados** en actividades de investigación y docencia. No se autoriza su reproducción con finalidades de lucro ni su difusión y puesta a disposición desde un sitio ajeno al servicio UPCommons No se autoriza la presentación de su contenido en una ventana o marco ajeno a UPCommons (*framing*). Esta reserva de derechos afecta tanto al resumen de presentación de la tesis como a sus contenidos. En la utilización o cita de partes de la tesis es obligado indicar el nombre de la persona autora.

WARNING On having consulted this thesis you're accepting the following use conditions: Spreading this thesis by the institutional repository UPCommons (<http://upcommons.upc.edu/tesis>) and the cooperative repository TDX (<http://www.tdx.cat/?locale-attribute=en>) has been authorized by the titular of the intellectual property rights **only for private uses** placed in investigation and teaching activities. Reproduction with lucrative aims is not authorized neither its spreading nor availability from a site foreign to the UPCommons service. Introducing its content in a window or frame foreign to the UPCommons service is not authorized (*framing*). These rights affect to the presentation summary of the thesis as well as to its contents. In the using or citation of parts of the thesis it's obliged to indicate the name of the author.



Front and back cover images

[1] R/V Hespérides. Photo from Carmen Herrero Photography.

[2] Spectrofluorometer for fluorescent dissolved organic matter (FDOM) analysis. Photo from Patricia De La Fuente Gamero. Thanks to Raquel, Lab technician at ICM-CSIC.

[3] Modis-aqua satellite image, level-3: Monthly climatology (2003 - 2018) of Chlorophyll concentration (mg m⁻³). 4km resolution. From <https://oceancolor.gsfc.nasa.gov>.

[4] SeaBird 911 Plus CTD system mounted in a 24 Niskin bottle rosette in the MOC2-equatorial Cruise on board the R/V Hespérides. Photo from Marc Gasser i Rubinat.

[5] View one quarter of Earth's disc from European weather satellite Meteosat Second Generation (MSG). European Space Agency (<https://www.esa.int/ESA>).

[6] Recalcitrant biomolecule: α -carboxylic – rich alicyclic compounds. Taken from *Dittmar (2015)*ⁱ.

[7] Quartz cubette for FDOM analysis. Photo from Patricia De La Fuente Gamero. Thanks to Raquel, Lab technician at ICM-CSIC.

[8] Carbon dioxide records and temperature anomaly over the past 800 kyr. Taken from *Lüthi (2008)*ⁱⁱ.

[9] R/V Hespérides. Photo from Marc Gasser i Rubinat.

ⁱ Dittmar, T., Kattner, G., (2003). The biogeochemistry of the river and shelf ecosystem of the Arctic Ocean: a review. *Mar. Chem.* 83, 103–120.

ⁱⁱ Lüthi, D., et al. (2008). High-resolution carbon dioxide concentration record 650,000–800,000 years before present, *Nature*, 378, 379–382.

Dynamics of Marine Dissolved Organic Matter: Ocean Metabolism and Climate Transitions.

Patricia De La Fuente Gamero

Dissertation submitted to obtain the doctoral degree

Universitat Politècnica de Catalunya. PhD program in Marine Science.

Advisors:

Pr. Dr. Josep Lluís Pelegrí

Physical and Technological Oceanography

Institut de Ciències del Mar (CSIC)

&

Dr. Celia Marrasé

Marine Biology and Oceanography

Institut de Ciències del Mar (CSIC)

PhD Dissertation by compendium of publications

Barcelona, 2019

“The Ocean is the major component determining the Earth’s health”ⁱ

“Every component of the Earth community has three rights:
the right to be, the right to habitat, and the right to fulfil its role,
in the ever-renewing processes of the Earth community”ⁱⁱ

ⁱ Pelegrí, J., Alonso, I., Arístegui, J. (2001). The ocean, our climate and the earth's health. *Sci. Mar.*, 65(S1), 3-5.

ⁱⁱ Compson, J. (2008). Evening Thoughts: Reflecting on Earth as Sacred Community – Edited by Thomas Berry and Mary Evelyn Tucker . The Dream of the Earth – By Thomas Berry. *Reviews in Religion & Theology*, 15: 597-599.

Dedication

To my beloved parents, **Tomás & Nieves**,

thanks for everything.

Without you, nothing would have been possible

To **Alvaro Nawel**, my strong son,

thanks for illuminating and revealing me the true way.

To **Antonio**, my love,

thanks for walking by my side.

To my dear Auntie **Maite Vela**,

thanks for your support and your wise words.

Preface and Acknowledgments

This PhD thesis has been carried out in the Institute of Marine Sciences (ICM, Spanish Research Council, CSIC), at both the Physical and Technological Oceanography and the Marine Biology and Oceanography Departments.

The research was funded by the Secretary of Universities and Research of the Ministry of Business and Knowledge of the Generalitat of Catalonia, with the support of the European Social Fund through a FI-AGAUR fellowship. And it was carried out in the frame of the following projects: MOC2 (CTM2008-06438-C02), TIC-MOC (CTM2011-28867) and DOREMI (CTM2012-34294) funded by the R+D Spanish research program, FISIOCEAN (PIF08-006-1) funded by CSIC's frontier program and ECLIPSE project financed by Total Foundation.

We kindly thank Elsevier, American Meteorological Society and Wiley their permission to make available the author's scientific publications for this PhD Thesis and its public defense.

I clearly remember the first time I heard to Josep Lluís Pelegrí Llopart talking about the climate oceanic memory and about the possibility of studying the homeostatic equilibrium of the Earth's climate using a physiological analogy with temporal rhythms in living beings. I was studying the master's degree in Global Change in Mallorca and my heart speeded up as I was listening to his explanations. Because, by then, far from fully understanding with the intellect, I had a strong intuition that it was a path that could offer multiple new possibilities. Not only for a novel understanding of the climate of the Earth complex system but also as an opportunity to send a message that the humanity forms an integral part of our planet, a vital Unity consciousness so necessary in the face of the current planetary crisis that we are living. I was imagining the planet Earth as in a feverish state, just like a living being that suffers a kind of "internal fever" due to a thermal imbalance of the body by metabolic disorders, which alters its metabolism and increases entropy, hence difficulting the maintenance of structures and life. The human being is depriving the natural systems that allow regulating the temperature of the Earth, its chemistry and its metabolism, propitiating an approximation towards the threshold (perhaps in temperature or carbon dioxide) from which the processes are irreversible, at least on a human scale.

Thus, the day that Josep Lluís Pelegrí Llopart offered me the opportunity to participate in the FISIOCEAN project: a physiological approach to the study of natural and anthropogenic climate change in the Earth System, it was one of the happiest days of my life.

So, I started this PhD adventure with the oceanographic cruise MOC2-equatorial, the first of the Spanish physical oceanography in the equatorial Atlantic, one of the most important regions for the balance of the climate. The MOC2 project (oceanic memory of the climate x meridional overturning circulation = MOC squared) had the main objective of improving our

Preface and Acknowledgments

knowledge of the role of the oceans as regulators of the planet's climate. During 45 days on board the Oceanographic Research Vessel (R/V) Hespérides, I was working together with an incredible staff, technicians and scientists (Spanish and other nationalities), collecting data for many variables. Specifically, the 7.5°N section was being repeated for the fourth time in the history of oceanography, measuring physical, biological and biogeochemical parameters that were not sampled in the previous editions. The biogeochemical and physical measurements used in the thesis work came from this MOC2-equatorial cruise, so I would like to thank the R/V Hesperides crew and technical UTM personnel for their invaluable support and professional assistance during that oceanographic cruise.

I give special thanks to Josep Lluís Pelegrí Llopart and Celia Marrasé Peña, tireless researchers, whose curiosity has no limit. Thank you for the opportunity you have given me, for your availability, for your advice. Thank you for your enthusiasm, professionalism and human quality. Thank you for sharing with me the passion for making science, always with respect to others and nature.

Thanks to my family and friends, for your trust in me and for your invaluable support. Thanks to my dear colleagues of the ICM, for teaching me a lot, personally and professionally. Thank you very much for sharing who you are with me.

Thanks, thanks, thanks.

With love,

Patricia De La Fuente Gamero

Abstract

The Global Ocean is the largest Earth compartment holding carbon and nutrients that reaches the upper-ocean at temporal scales ranging from months to 10 kyr. The availability of these nutrients is fundamental to sustain primary production and the concentration of dissolved inorganic carbon (DIC) in surface waters controls the glacial-interglacial changes in atmospheric CO_2 . One process that influences both nutrients and carbon availability is the Microbial Carbon Pump (MCP), which refers to the production of refractory dissolved organic carbon (RDOC) compounds via heterotrophic microbial activity. Variations in the RDOC pool affect long-term carbon storage in the ocean, hence influencing the carbon cycle and climate.

The general objective of this thesis is to expand our understanding of the connections between RDOC production by MCP and the ocean metabolism (understood as the upper-ocean net autotrophic community production), paying special attention to the role of the marine microbial processes in the glacial-interglacial transitions of the Earth system.

The RDOC production by MCP is inferred through the lineal dependence of fluorescent dissolved organic matter (FDOM) with apparent oxygen utilization (AOU) and nutrients. This relationship, however, depends on the preformed content in the water masses. In this thesis, a valuable dataset, obtained from a high-resolution spatial sampling along $7.5^\circ N$ in the equatorial Atlantic Ocean, is used to distinguish the variability of FDOM distribution associated with in situ production from that related to the water properties at origin. A simple objective nonlinear-global methodology for resolving the non-conservative fraction of biogeochemical variables distribution is presented. The approach focuses on fitting high-order polynomial models over the entire temperature-salinity space. The differences between the modelled values and the observations are identified as biogeochemical anomalies. The goodness of the method is compared, for each water stratum, with the traditional approach, which is based on the local linear mixing of a maximum of three source water masses. The new methodology has good skill at distinguishing between the conservative and non-conservative contributions to biogeochemical variables, lending information about biogeochemical processes, stoichiometric ratios and patterns of connectivity within a certain region. For the first time, a general relationship between humic-like FDOM and AOU in the dark equatorial Atlantic Ocean is formulated, irrespective of the water masses. The results endorse the idea that FDOM is mostly produced in situ in the dark ocean.

In the second part of the thesis, the role of RDOC pool in quaternary climate transitions is explored. The glacial-interglacial transitions are considered as functional states of the complex Earth system, with different energetic conditions in terms of solar energy conversion through marine photosynthesis. However, the oceanic system capacity to capture and transform the incident solar radiation depends on the availability of DIC and nutrients to the productive

Abstract

upper ocean. The supply of DIC and nutrients by the Meridional Overturning Circulation (MOC) and the DOM pool are evaluated through a simple two-box and two-state relaxation-type model for the DIC and nutrients in the upper ocean. The model, inspired on physiological concepts, considers the upper ocean to switch between basal (glacial) and enhanced (interglacial) metabolic states. The model reproduces well the atmospheric CO_2 time series for the last 420 kyr, providing a solution for the size and temporal dependence of the MOC and setting global constraints on primary production and remineralization in the upper ocean. The RDOC accumulates during the glacial period and its availability at the end of this cycle sets the metabolic intensity of the subsequent interglacial, in what constitutes a central component of the Earth's pulsating homeostatic organization.

Resumen

El Océano Global es el mayor reservorio de carbono y nutrientes que llegan al océano superior en escalas temporales de meses hasta 10.000 años. La disponibilidad de nutrientes es fundamental para la producción primaria y la concentración de carbono inorgánico disuelto (DIC en inglés) en las aguas superficiales controla los cambios glacial-interglacial del CO₂ atmosférico. La bomba de carbono microbiana (MCP en inglés) se refiere a la producción de compuestos refractarios de carbono orgánico disuelto (RDOC en inglés) a través de la actividad microbiana heterotrófica siendo un proceso que influye tanto en los nutrientes como en la disponibilidad de carbono. Las variaciones en el reservorio de RDOC afectan al almacenamiento de carbono a largo plazo en el océano, influyendo en el ciclo del carbono y el clima.

El objetivo general de esta tesis es ampliar la comprensión de las conexiones entre la producción de RDOC por la MCP y el metabolismo oceánico (entendido como la producción comunitaria autótrofa neta del océano superior), prestando especial atención al papel de los procesos microbianos en las transiciones glacial - interglacial del sistema terrestre.

La producción de RDOC por la MCP se infiere a través de la dependencia lineal de la materia orgánica disuelta fluorescente (FDOM, en inglés) con la utilización aparente de oxígeno (AOU, en inglés) y los nutrientes. Dicha relación depende del contenido preformado en las masas de agua. A partir de datos obtenidos a lo largo de 7.5⁰N en el Océano Atlántico ecuatorial, se evalúa que variabilidad de la distribución de FDOM corresponde con producción in situ y cual a las propiedades del agua en origen. Se presenta una metodología objetiva y simple, no lineal y global para resolver la fracción no conservativa de la distribución de variables biogeoquímicas mediante el ajuste de modelos polinomiales en todo el espacio de temperatura y salinidad. Se evalúa la bondad del método para cada estrato de agua comparándolo con el enfoque tradicional, basado en la mezcla lineal y local de un máximo de tres masas de agua fuente. La nueva metodología distingue entre las contribuciones conservativas y no conservativas de las variables biogeoquímicas, proporciona información de procesos biogeoquímicos, relaciones estequiométricas y patrones de conectividad dentro de una región. Por primera vez, se formula una relación general entre FDOM tipo húmico y AOU en el Océano Atlántico ecuatorial, independiente de las masas de agua. Los resultados respaldan la idea de que el FDOM se produce principalmente in situ en el océano profundo.

En la segunda parte de la tesis, se explora el papel del RDOC en las transiciones climáticas del cuaternario. Las transiciones glacial-interglacial se consideran estados funcionales del sistema terrestre, con diferentes condiciones energéticas en términos de conversión de la energía solar a través de la fotosíntesis. La capacidad del sistema oceánico para capturar y transformar la radiación solar incidente depende de la disponibilidad de DIC/nutrientes en el

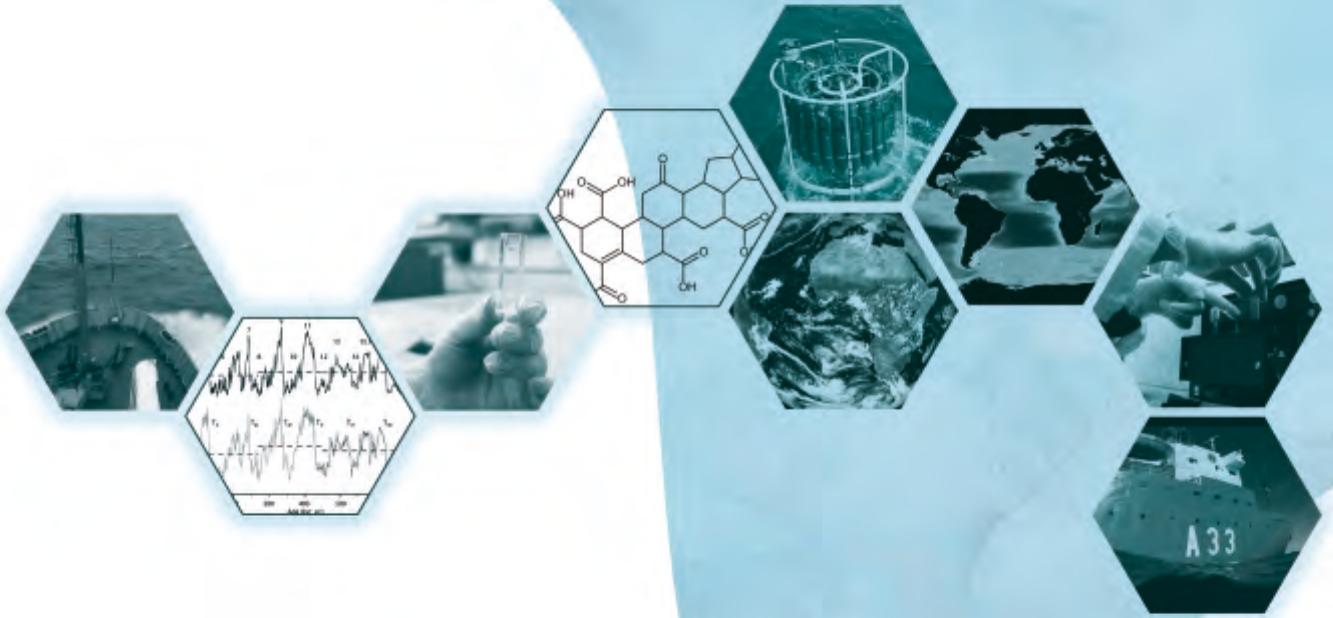
Resumen

océano superior. El aporte de DIC/nutrientes por el Bucle Latitudinal (MOC, en inglés) y el reservorio de materia orgánica disuelta se evalúan a través de un modelo simple de dos cajas y de relajación de dos estados para el DIC/nutrientes en el océano superior. El modelo, inspirado en conceptos fisiológicos, considera que el océano superior cambia entre dos estados metabólicos diferentes, basal (glacial) y excitado (interglacial). El modelo reproduce la serie temporal de CO_2 atmosférico de los últimos 420 kyr, proporcionando la magnitud y dependencia temporal de la MOC y estableciendo restricciones en la producción primaria y la remineralización en el océano superior. El RDOC acumulado en el período glacial y su disponibilidad al final de este ciclo establece la intensidad metabólica del interglacial subsiguiente, constituyendo por tanto un componente central de la organización homeostática pulsante de la Tierra.

Index

| | |
|---|-----|
| General introduction and aims of the thesis | 19 |
| Influence of mixing of water masses and microbial activity on the spatial variability of refractory dissolved organic matter (RDOC) in the deep ocean: | |
| I. <i>A simple nonlinear and end-member-free approach for obtaining ocean remineralization patterns</i> | 45 |
| II. <i>Does a general relationship exist between fluorescent dissolved organic matter and microbial respiration? - The case of the dark equatorial Atlantic Ocean</i> | 67 |
| A “two-box” ocean model to characterize and understand the role of the RDOC over the glacial-interglacial transitions, via the microbial carbon pump: | |
| III. <i>Global constraints on net primary production and inorganic carbon supply during glacial and interglacial cycles</i> | 81 |
| General discussion and conclusions..... | 111 |

GENERAL INTRODUCTION AND AIMS OF THE THESIS



1. Ocean carbon cycle and atmospheric CO_2 variability

The incoming solar radiation to the planet Earth is of short wavelength. More than half of the Sun's radiation either is reflected back into space (primarily by clouds) or enters the atmosphere and is emitted back to space. The remaining fraction reaches the Earth's surface and is radiated out at much longer wavelengths (i.e. in the infrared band, typically between 5 and 20 μm); most of this outgoing radiation is trapped by the atmosphere (the greenhouse effect) which then radiates back to the Earth and towards space. For the Earth's temperature to be stable over long periods of time, the incoming and outgoing energy, due to the short-and long-wave radiation respectively, have to be equal (this state of balance is called radiative equilibrium). In the case with no atmosphere, the equilibrium temperature for the Earth would be -18°C . The presence of an atmosphere with trace gases that absorb at infrared wavelengths, i.e. greenhouse gases, turns Earth into a much more habitable planet. The thermal energy absorbed by these greenhouse gases in the atmosphere is emitted to a substantial degree in a downward direction, heating up the lower atmosphere and causing the Earth's surface temperature to rise (giving the observed Earth's average surface temperature value of about 15°C) (Sarmiento & Gruber, 2006).

The atmospheric gas that exerts the principal control over the strength of the terrestrial greenhouse effect is the long-lived carbon dioxide (CO_2), hence playing a critical role in the Earth's average surface temperature (Arrhenius, 1869; Falkowsky, 2000; Doney & Schimel, 2007; Lacis et al., 2010; Ciais et al., 2013; Myhre et al., 2013). Over a range of geological and historical timescales, global averaged Earth's temperature fluctuations are associated with variations in the levels of CO_2 in the atmosphere (Petit et al., 1999; Royer, 2006; Royer et al., 2007; Doney & Schimel, 2007). For instance, the analysis from ice-cores over the late Pleistocene glacial-interglacial cycles showed the parallel rise and fall of temperature and atmospheric CO_2 (Fig.1) (Petit et al., 1999; Royer et al., 2007; Lüthi et al., 2008; Bereiter et al., 2015). It suggests that changes in atmospheric CO_2 play a significant role in the energetics of glacial-interglacial cycles and illustrates the close coupling of the global carbon cycle and the Earth's climate system response to orbital forcing at these geological timescales (Hays, 1976; Berger & Loutre, 1991; Imbrie et al., 1992; Imbrie et al., 1993; Petit et al., 1999; Falkowsky, 2000; EPICA community members, 2004).

The world ocean is one of the main constituents of the climate system and it can influence the climate system being part of the planetary energy cycle (due to its heat storage capacity, heat transport and sea-ice cover) and by participating in the biogeochemical cycles and exchanging gases with the atmosphere (Sarmiento & Gruber, 2006; Rahmstorf, 2002).

In the global carbon cycle, the World Ocean with 38000 petagrams of carbon ($\text{Pg C} = 10^{15} \text{ g C}$) is the largest non-geological reservoir of carbon (65 times that atmosphere and 17 times that the terrestrial biosphere). Together with the fact that the sequestration of carbon into the ocean interior avoids re-equilibration with the atmosphere on centennial and millennial timescales, the cause for the glacial-interglacial variations of atmospheric CO_2 must rely on the biological, physical and chemical processes controlling the carbon cycle in the ocean at these geological timescales (Kanwisher, 1960; Broecker, 1982; Sigman & Boyle, 2000; Falkowsky, 2000; Prentice et al., 2001; Marinov & Sarmiento, 2004; Sarmiento & Gruber, 2006; Doney & Schimel, 2007; Heinze et al., 2015).

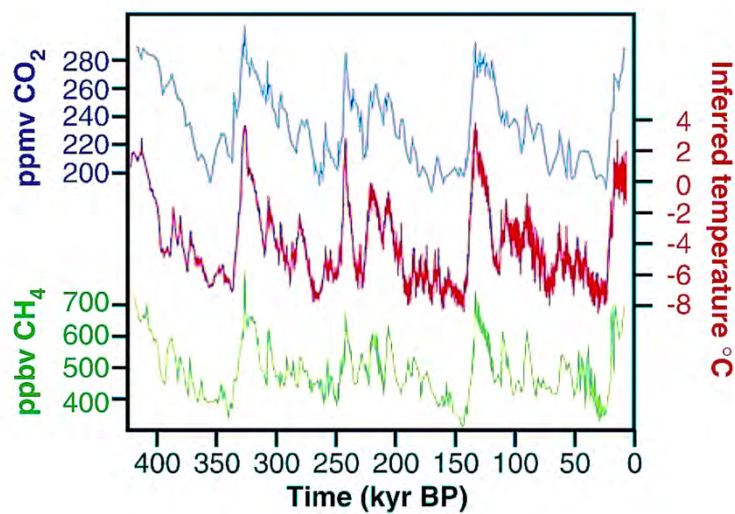


Fig.1. The 420000-year Vostok (Antarctica) ice core record of the green-house gasses: atmospheric CO_2 (ppmv, parts per million by volume) and methane CH_4 (ppbv, parts per billion by volume), and inferred temperature ($^{\circ}\text{C}$) through the four glacial-interglacial cycles (figure extracted from Steffen et al., 2004)

1.1. How does the ocean exert the control on atmospheric CO_2 ?

The absorption of atmospheric CO_2 by the ocean is partly due to dissociation into ions and their interactions with sea water constituents (Wanninkhof, 1992; Le Quéré & Metzl, 2004; Marinov & Sarmiento, 2004; Sarmiento & Gruber, 2006; Wanninkhof, 2014; Prentice et al., 2015). When atmospheric CO_2 dissolves in the ocean surface by molecular diffusion, it reacts with seawater forming dissolved CO_2 (CO_2^{aq}), bicarbonate ion (HCO_3^-) and carbonate ion (CO_3^{2-}) (Kanwisher, 1960; Sarmiento & Gruber, 2006). The sum of these components is named total dissolved inorganic carbon (DIC).

Most of the DIC is in the form of bicarbonate (91%) and carbonate ions (8%) and less than 1% of the total DIC is CO_2^{aq} , which is the only form that is exchangeable with the atmosphere

(Le Quéré & Metzl, 2004; Marinov & Sarmiento, 2004; Sarmiento & Gruber, 2006; Prentice et al., 2015). A measure of the extent to which CO_2 has reacted with water to form CO_3^{2-} and HCO_3^- is the concentration of total alkalinity (Alk), which is roughly the seawater's acid-buffering capacity, representing approximately the contribution of CO_3^{2-} and HCO_3^- to the charge balance of seawater (Gruber & Sarmiento, 2002; Sigman et al., 2010).

The amount of CO_2^{aq} is proportional to the partial pressure of dissolved CO_2 in surface ocean (pCO_2^{oc}) (Le Quéré & Metzl, 2004; Marinov & Sarmiento, 2004) and the air-sea difference in CO_2 partial pressures represents the main potential thermodynamic conduction for the air-sea gas transfer of CO_2 between the atmosphere and the surface ocean (Siegenthaler & Sarmiento, 1993; Wanninkhof, 1992; Le Quéré & Metzl, 2004; Marinov & Sarmiento, 2004; Sarmiento & Gruber, 2006).

Because the variability of pCO_2^{oc} is far greater than in the atmosphere, the observed variations in the air – sea difference in CO_2 partial pressures reflect mainly those variations in the oceanic pCO_2^{oc} values (Sarmiento & Gruber, 2006). The pCO_2^{oc} variation in mixed layer water is determined by temperature and salinity, DIC speciation (CO_2^{aq} , HCO_3^- , CO_3^{2-}) and DIC and alkalinity gradient between the surface ocean and the ocean interior (the surface concentration of DIC and alkalinity is respectively about 15% and 5% lower than deep ocean concentrations) (Zeebe and Wolf-Gladrow, 2001; Sarmiento & Gruber, 2006).

The vertical DIC and alkalinity gradients have the major consequences for atmospheric CO_2 . If the Global Ocean was allowed to mix uniformly by the ocean circulation, atmospheric CO_2 would almost reach 50% over its preindustrial concentration (from about 280 parts per million, ppm, to more than 420 ppm) (Gruber & Sarmiento 2002; Sarmiento & Gruber, 2006); remarkably, the value reached in April 2019 (413 ppm) is not far from this figure (<https://www.co2.earth>). The mechanisms that maintain these gradients against the continuous action of ocean transport and mixing are traditionally syncretized into two conceptual carbon pumps: the “solubility” pump, and the “biological” pump, both them driving (or vertical pumping) carbon away from the sea surface into deep ocean, allowing the storage of carbon (Siegenthaler & Wenk, 1984; Volk and Hoffert, 1985; Sigman & Boyle, 2000; Falkowsky et al., 2000; Zeebe and Wolf-Gladrow, 2001; Le Quéré & Metzl, 2004; Marinov & Sarmiento, 2004; Sarmiento & Gruber, 2006; Kohfeld & Ridgwell, 2009; Ridgwell & Arndt, 2015). Recently, a third carbon pump, the “microbial” carbon pump (MCP), was considered as an additional path for repartitioning carbon within the marine ocean carbon cycle (Jiao et al., 2010; Jiao & Azam, 2011; Jiao et al., 2014). The MCP results in long-term carbon sequestration in the dissolved organic carbon phase throughout the water column (the reservoir formed is

depth-independent), from the ocean surface to the ocean interior (*Jiao et al., 2010; Jiao & Azam, 2011; Carlson & Hansell, 2015*).

The ocean carbon pumps together with the effects of large scale flow patterns, mixing and ventilation rates of the Global Ocean, contribute to the net uptake of atmospheric CO_2 by the ocean, maintaining the huge oceanic carbon reservoir and setting the time scale for the equilibration of dissolved CO_2 with the atmosphere. How do they work?. It is explained in the following sections.

1.2. Ocean circulation

Global ocean circulation can be divided into two major components: the fast, wind-driven, upper-ocean circulation which is named thermocline circuit and the slow, deep-ocean circulation driven by fluxes of heat and freshwater across the sea surface and the associated pressure gradients, which is named thermohaline circulation (*Rahmstorf, 2006*). These two components act simultaneously in a non-linear way to drive the Meridional Overturning Circulation (MOC, *Broecker, 1991*), the movement of seawater across basins and depths (*Rahmstorf, 2006; Talley et al., 2011*).

The wind-driven circulation is associated with the prevailing winds, primarily the easterlies in the tropics and the westerlies in the mid-latitude. General patterns of the wind-driven circulation are conformed by a series of zonal currents, eastern boundary currents, and western boundary currents that form the subtropical and subpolar gyres. These waters recirculate isopycnally (along surfaces of constant density) in the permanent thermocline of the subtropical gyre and in the adjacent tropical and subpolar gyres, in relatively short periods of time (~ 10 years).

Deep ocean circulation begins at high latitudes, in the subpolar oceans. During each respective winter, dense waters form abruptly by events of intense surface cooling. As a consequence, waters sink to the sea floor and begin their trip through all the deep oceans of the Earth. During the deep-water formation process, heat, salt, and organic and inorganic carbon and nutrients are incorporated to the deep oceans. In the northern hemisphere winter, the North Atlantic Deep Water (NADW) is formed at Labrador Sea and Greenland Sea from where it flows to the Southern Hemisphere (*Ganachaud & Wunsch, 2000*). The MOC also has its origin, with a time lag of six months, in the Southern Hemisphere winter. It originates at the continental shelf around the Antarctic continent as Antarctic Bottom Water (AABW) and the Lower Circumpolar Deep Water (LCDW) (*Orsi et al., 1999, Ganachaud & Wunsch, 2000; Talley et al., 2011*). The deep waters formed in both hemispheres are dense enough to produce the

crossing to the Indian and Pacific oceans via the Antarctic Circumpolar Current. This long circuit takes of the order of 1000 years to return to the starting point through the formation of mode and intermediate waters and their slow transformations into surface waters, via upwelling along the pathway of the Antarctic Circumpolar Current (Orsi, *et al.*, 1999) and after following a much longer latitudinal pathway into the subpolar regions of the North Atlantic (Talley *et al.*, 2011) (Fig.2).

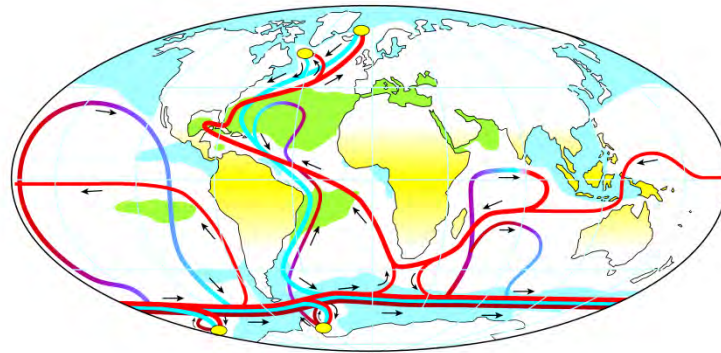


Fig.2. Schematic view of the MOC, with the near-surface waters shown as red lines, the deep currents in blue and the bottom currents in purple. The three main deep-water formation regions are showed as yellow ovals, with the shading indicating surface salinity above 36‰ (green) and below 34‰ (blue)(Figure and text modified from *Rahmstorf (2000)*).

The moderately shallow Sub-Antarctic Mode Waters (SAMW) are formed south of the subantarctic fronts (Sarmiento *et al.*, 2004). A fraction forms in the South Atlantic and another fraction is formed in the Indian Ocean, from where it reaches the Atlantic region via the Agulhas Current (Williams *et al.*, 2006). The Antarctic Intermediate Waters (AAIW) formed in the southeast Pacific penetrate at deeper layers, under the SAMW to reach the eastern tropical and equatorial Atlantic regions where vertical mixing and equatorial upwelling take place (Gouriou and Reverdin, 1992). Eventually, these nutrient- and carbon-rich new surface waters will continue north either as eastern and mainly western boundary currents to eventually cross the entire subtropical gyre and reach the North Atlantic subpolar gyre (Machín and Pelegrí, 2006; Rahmstorf, 2006; Williams *et al.*, 2006). The tropical and equatorial Atlantic Ocean is extraordinary complex, a neural centre connecting austral, subtropical and tropical waters, with currents that travel predominantly zonally between America and Africa. The intense meridional flow along the north coast of South America, the North Brazil Current (NBC), collects most of these westward currents and becomes a source of carbon and nutrients for the Gulf Stream, which ultimately reach the northernmost part of the North Atlantic (Pelegrí & Csanady, 1991; Gouriou and Reverdin, 1992; Williams *et al.*, 2006; Machín and Pelegrí, 2006; Rahmstorf, 2006).

The ultimate transport to the North Atlantic subpolar gyre of these nutrient- and DIC-rich waters replaces the losses of nutrients and carbon that take place during the winter deep convection. Therefore, the recirculation of the intermediate waters and their reincorporation to the equatorial surface waters through epipychnal advection and diapycnal mixing processes are of great importance to close the balance of heat, mass, nutrients and carbon of the MOC (Pelegri *et al.*, 2006). Moreover, the returning MOC waters bring temperature, salinity, carbon and nutrients characteristic of the deep ocean, both retaining a trace of the properties they acquired during their formation (a memory of past climates of the Earth) and of the transformations they have undergone through biological, chemical and physical processes during their journey.

1.3. Ocean carbon pumps

The solubility pump, (Fig.3) or physical pump is the term used to describe the physical and chemical process by which CO_2 is transported from the atmosphere to the deep-ocean. It operates as a result of the strong temperature dependence of the solubility of gaseous CO_2 in water, being more soluble in cold than in warm waters (net cooling of surface waters tends to drive CO_2 uptake) (Le Quéré & Metzl, 2004; Sarmiento & Gruber, 2006). The sequestration of atmospheric CO_2 via the solubility pump is controlled by the MOC. As a consequence, the ocean dissolved carbon is effectively prevented from re-equilibrating with the atmosphere until waters from the ocean interior are brought back to the surface hundreds of years later (Volk and Hoffert, 1985; Falkowsky *et al.*, 2000; Prentice *et al.*, 2001; Feely *et al.*, 2001; Steffen *et al.*, 2004; Kohfeld & Ridgwell, 2009; Legendré *et al.*, 2015; Ridgwell & Arndt, 2015).

The carbonate pump (Fig.4), a component of the biological carbon pump, involves the biological precipitation at sea surface of calcium carbonate ($CaCO_3$) either as aragonite or as calcite by shell- and skeleton-building marine organisms (e.g. coccolithophores and foraminifera), and the export of these calcium carbonate particles below the surface ocean (Volk and Hoffert, 1985; Kohfeld & Ridgwell, 2009; Heinze *et al.*, 2015). During the precipitation process at surface, alkalinity decreases by consuming HCO_3^- and CO_2^{aq} is released to the surrounding waters and from there to the atmosphere (Fig. 4). As a result, DIC and the ability of surface water to absorb atmospheric CO_2 diminish (Falkowsky *et al.*, 2000; Legendré *et al.*, 2015). The dissolution of some fraction of these calcium carbonate particles formed at the surface, releases HCO_3^- while they sink in the water column (Fig. 4). This dissolution process increases both alkalinity and DIC with depth and the ability of deep waters to absorb atmospheric CO_2 when these waters are brought back to the surface at the timescale of the

deep ocean circulation, on time scales of the order of 1000 years (Falkowsky *et al.*, 2000; Legendré *et al.*, 2015).

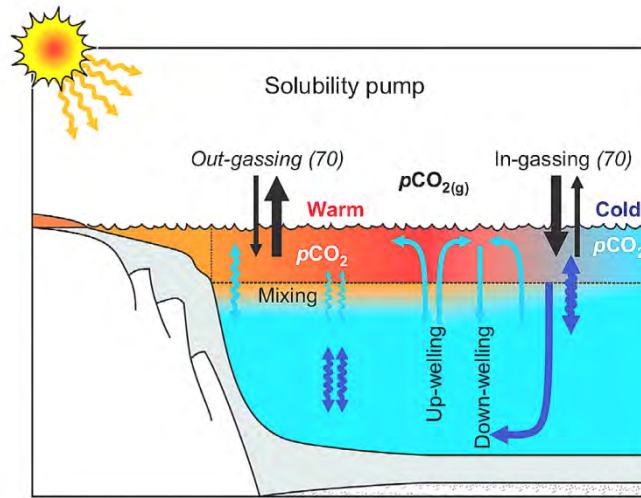


Fig.3. Outline of the solubility pump, (figure and text modified from Ridgwell & Arndt 2015).

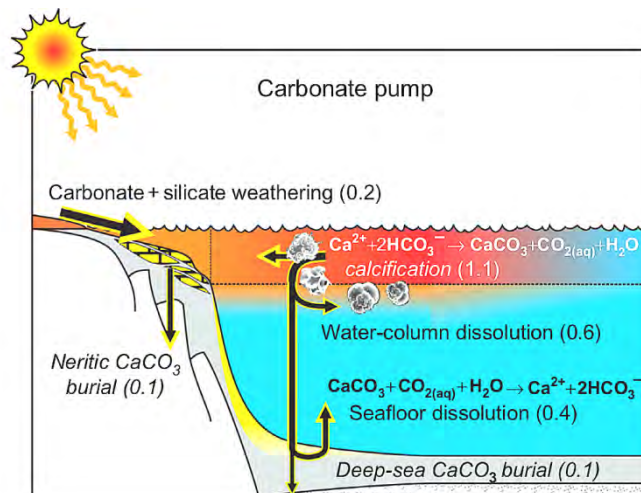


Fig.4. Outline of the carbonate pump. Carbon fluxes (Pg C) into the ocean are shown in normal font and sinks in italics (figure and text modified from Ridgwell & Arndt 2015).

The soft-tissue pump, also a component of the biological carbon pump (Fig. 5), is the process by which photosynthetically-produced organic matter in the ocean in the form of particulate organic carbon (POC) and dissolved organic carbon (DOC) descends from the euphotic or seasonal surface mixed layer to depth by a combination of sinking particles, physical mixing and downwelling of water parcels and active transport by zooplankton migration (Siegel *et al.*, 2016). During the downward flux, the biogenic material is remineralized through heterotrophic respiration mainly by bacteria and archaea (Azam, 1983), thus maintaining the strong vertical gradient of DIC (Volk and Hoffert, 1985; Ducklow *et al.*, 2001; Sarmiento & Gruber, 2006; Aristegui *et al.*, 2009; Hansell *et al.*, 2009; Turner *et al.*, 2015;

Zhang et al., 2018). Most of the downward flux of organic carbon is re-mineralised in the mesopelagic zone and the CO_2 produced returns to the atmosphere for the period corresponding to the residence time of mesopelagic waters (months to years) (Fig.5) (*Aristegui et al., 2002; Aristegui et al., 2005; Hansell et al., 2009; Legendré et al., 2015; Zhang et al., 2018*). Some of the organic carbon escapes microbial degradation in the mesopelagic and reaches the bathypelagic zone, where it may be respired and sequestered as CO_2 for centuries until it is ventilated to the surface again by the overturning circulation, allowing exchange with the atmosphere (*Ducklow et al., 2001; Aristegui et al., 2009; Jiao et al., 2010; Hansell, 2013a; Ridgwell & Arndt, 2015; Zhang et al., 2018*). About 0.3% of organic carbon escapes mineralization and is buried in marine sediments for hundreds of millions of years (*Dunne et al., 2007; Zhang et al., 2018*).

Hence, the farther the POC and the DOC sink before the associated carbon is released back to the DIC pool, the more effective the partition of DIC between the surface and the deep ocean will be (*Ridgwell & Arndt, 2015*). Thus, any reduction or increase in the efficiency of the organic carbon pump influence the ocean's ability to store biologically fixed carbon and hence affects atmospheric CO_2 . For instance, *Kwon et al. (2009)* calculated that, when the depth at which 63% of sinking carbon is respired increases by 24 m globally, atmospheric carbon dioxide concentrations fall by 10 – 27 ppm. This illustrates that a reduction in atmospheric carbon dioxide concentration can result from the redistribution of re-mineralized carbon from intermediate waters to bottom waters.

The ocean holds a huge dissolved organic carbon reservoir (670 Pg C, *Hansell et al., 2009*) equivalent in amount with the current total inventory of CO_2 in the atmosphere (750 Pg C, *Siegenthaler & Wenk, 1993*). The majority (> 90%) of the DOC that conform this reservoir is refractory (RDOC), being resistant to biological degradation and assimilation, thus allowing to accumulate (*Jiao & Azam, 2011; Hansell, 2013b*). The modelled lifetime of RDOC is ~16.000 years (*Hansell et al., 2012*), hence RDOC can survive several cycles of ocean ventilation playing an important role in carbon sequestration and climate regulation (*Hansell et al., 2012; Owaga & Tanoue, 2003; Rothman et al., 2003; Hopkinson & Vallino, 2005; Peltier et al., 2007; Jiao et al., 2010; Benner & Herldn, 2011; Jiao & Azam, 2011; Lechtenfeld et al., 2015; Carlson & Hansell, 2015*).

The microbial carbon pump (MCP) refers to the production of RDOC compounds via heterotrophic microbial processes (for a review see *Carlson & Hansell, 2015*) (Fig. 5). It is a conceptual framework that encompasses the processes of RDOC production as a consequence of the activity of marine pelagic microbes and its relevant role in the storage of carbon in the ocean (*Jiao et al., 2010*). Through the successive microbial processing of more bioavailable

carbon, the MCP pumps low concentrations of reactive carbon to high concentrations of RDOC, contributing to the huge oceanic RDOC pool (Jiao *et al.*, 2010). In addition, MCP transfers into RDOC more carbon than organic nitrogen and phosphorous, thus providing essential nutrients (Jiao *et al.*, 2010; Hopkinson & Vallino, 2005).

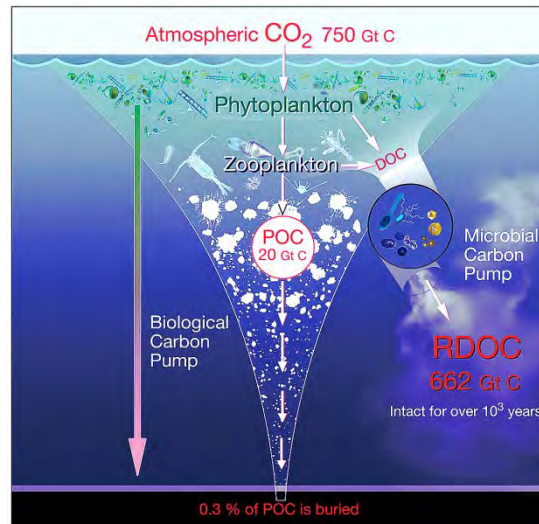


Fig.5. Schematic view for the cycling of carbon through biological and microbial carbon pumps (figure and text modified from Zhang *et al.*, 2018).

Three pathways of the MCP are identified: RDOC generated directly from microbial cell materials (i.e. direct exudation from growing bacterial cells, viral lysis of microbial cells, and protozoan grazing), RDOC derived from bacterial and archaeal degradation of particulate organic matter, and residual RDOC after microbial utilization of the bulk DOC (Jiao *et al.*, 2010; Jiao & Azam, 2011). At least 25% of the oceanic RDOC is of bacterial origin (Benner & Herndl, 2011; Kaiser & Benner, 2008) indicating that RDOC generation by the MCP might be an important mechanism for long term storage of fixed atmospheric carbon by the ocean (Jiao *et al.*, 2010; Jiao & Azam, 2011; Jiao *et al.*, 2014; Jiao *et al.*, 2018).

2. Modelling RDOC production

The previous section highlights that variations in RDOC production and utilization will affect long-term carbon storage in RDOC and hence the ocean carbon cycle and climate (Jiao *et al.*, 2010, 2011; Jiao & Azam, 2011; Jiao *et al.*, 2014). Therefore, for modelling the role of RDOC in the past and future Earth's climate, it is crucial to advance the current understanding of the sources, mechanisms and rates of RDOC generation.

As will be explained in more detail throughout this section, the biochemical characteristics of RDOC can be linked to its optical properties and these optical properties can be used as an

indicator to infer quantitative and qualitative changes in marine RDOC. Moreover, the optical properties of RDOC provide important insights into the origin of each water mass and the biogeochemical transformations of those waters during transport and mixing (*Bricaud et al., 1981; Mopper & Schultz, 1993; Green & Blough, 1994; Hansell & Carlson, 1998; Coble, 2007; Helms et al., 2008; Yamashita et al., 2008; Nelson & Coble, 2010; Nelson et al. 2007; Nelson et al., 2010; Hansell, 2013; Stedmon & Nelson, 2015*).

2.1. Fluorescent dissolved organic matter

The chromophoric dissolved organic matter (CDOM) is the fraction of the dissolved organic matter pool (DOM) that absorbs light at those bands found at the Earth's surface: UVB, UVA, and visible light (280–700 nm) (*Nelson & Coble, 2010; Coble et al., 2014*). After absorption of light (energy), a fraction of the CDOM will also emit light as blue fluorescence and such fraction is referred as fluorescent DOM (FDOM) (*Kalle, 1966; Coble et al., 2014*). The chromophore (and fluorophore) pool include, among others, aromatic amino acids and humic substances that are operationally quantified and characterized by spectroscopic methods, in particular UV-visible absorption spectroscopy and fluorescence spectroscopy (*Coble 1996; Del Vecchio & Blough, 2004; Nelson & Coble, 2010*).

The fluorescent properties of FDOM are largely limited to excitation wavelengths between 240-500 nm and emission wavelengths between 300-600 nm (*Coble, 1996*). It is possible to distinguish two main groups of FDOM substances depending of their excitation and emission (Ex/Em) wavelengths. The protein-like substances, which fluoresce at wavelengths characteristic of the aromatic amino acids (Ex/Em at 280/350 nm for peak-T), and the humic-like substances, which fluoresce at wavelengths characteristic of humic acids such as tannins, lignin, polyphenols and melanins among others (Ex/Em at 250/435 nm for peak-A, Ex/Em at 320/410 nm for peak-M, and Ex/Em at 340/440 nm for peak-C) (*Coble, et al., 1993; Coble, 1996, 2007*).

Abundance and distribution of FDOM in the global ocean appears to be controlled by in situ production, photochemical bleaching, terrestrial input, and by ocean ventilation processes (*Hayase et al., 1989; Chen & Bada, 1992; Hayase & Shinozuka 1995; Determann et al., 1996; Benner & Bloddanda, 1998; Yamashita & Tanoue, 2008; Romera-Castillo et al., 2010; Romera-Castillo et al., 2011a; Jørgensen et al., 2011; Jørgensen et al., 2014; Álvarez-Salgado et al., 2013; Hansell, 2013; Romera-Castillo et al., 2013; Stedmon & Nelson, 2015; Catalá et al., 2016*).

The components of humic-like FDOM were found ubiquitous in the marine environment with turnover times occurring at centennial timescales, suggesting that these fractions belong

to the RDOC pool (Yamashita & Tanoue, 2008; Jørgensen et al., 2011; Nelson et al., 2007; Álvarez-Salgado et al., 2013; Catalá et al., 2015). From here, two important considerations show out. First, production of RDOC via microbial oxidation of organic matter can be inferred from the positive and significant relationship of humic-like FDOM measurements with both apparent oxygen utilization (AOU) and inorganic nutrients (both proxies of microbial remineralization in the ocean) (Hayase et al., 1989; Chen and Bada, 1992; Hayase and Shinozuka, 1995; Nieto-Cid et al., 2005; Nieto-Cid et al., 2006; Yamashita and Tanoue, 2008; Yamashita et al., 2010; Jørgensen et al., 2011; Catalá et al., 2016). Second, humic-like FDOM substances can be used as a semi-conservative tracer of ocean interior ventilation and biogeochemical processes (Romera-Castillo et al., 2011a; Álvarez-Salgado et al., 2013; Hansell & Carlson, 2013; Hansell, 2013; Catalá et al., 2015).

2.2. Impact of ocean mixing and mineralization process on RDOC production

Several studies through simple regression models have found that more than 80% of the humic-like FDOM variability is explained by AOU in the Pacific and Indian basins, showing a clear association of the production of RDOC with water mass aging (Hayase et al., 1989; Hayase and Shinozuka, 1995; Yamashita and Tanoue, 2008; Jørgensen et al., 2011). Instead, in the Atlantic Ocean the correlation is weak (Jørgensen et al., 2011), which suggests a significant role for ocean mixing and general circulation in the distribution of those biogeochemical properties (Nelson et al., 2007; Nelson et al., 2010; Swan et al., 2009; Nelson & Siegel, 2013).

The relationship between any pair of non-conservative biogeochemical variables, such as FDOM and AOU, depends on the conservative mixing of waters with different preformed values (properties values that are initially present in seawater at the time of down-welling) and non-conservative processes (i.e. remineralization of organic matter) that occur during mixing. Hence, in order to infer biological processes from biogeochemical relationships, the data have to be analysed such as to separate the contribution that is not attributable to any biological alteration (Carlson et al., 2010; Schneider et al., 2015).

Different statistical procedures had been used to separate the thermohaline variability from the distribution of a biogeochemical property: binary mixing models (Swan et al., 2009; Carlson et al., 2010), multiple linear regressions (Perez et al., 1993; Nieto-Cid et al., 2005; Castro et al., 2006;) and multi-parameter water analysis (Reinthal et al., 2013; Alvarez-Salgado et al., 2013; Catalá et al., 2015). From those statistical approximations a relationship for the Atlantic between humic-like FDOM and AOU finally arise but only when observations from the North Atlantic waters are not considered in the statistical analysis (Fig.6) (Jørgensen et al., 2011; Alvarez-Salgado et al., 2013; Catalá et al., 2015).

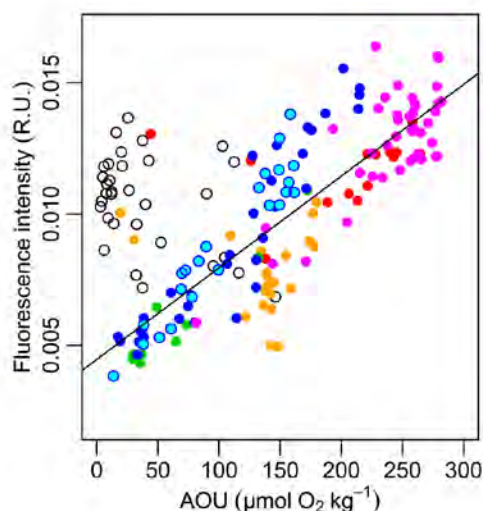


Fig.6. Correlation between humic-like fluorescence (Raman Units, R.U. (*Lawaetz & Stedmon, 2008*)) and AOU ($\mu\text{mol O}_2 \text{ kg}^{-1}$). The linear regressions are computed without data from the North Atlantic (indicated as black circles). The other points correspond to the Equatorial and South Atlantic (red), Indian Ocean (green), Oceania Shelf (dark blue), Circumpolar Antarctic (light blue), Eastern South Pacific (pink) and Sargasso Sea (orange) (figure extracted from *Jørgensen et al., 2011*).

Most authors exclude the North Atlantic waters masses in their statistical analyses arguing that their humic-like FDOM content is not related with aging, because the North Atlantic area receives considerable amount of terrestrial organic matter (*Hernes & Benner, 2006*).

Jørgensen et al. (2011) hypothesized that a major fraction of the humic-like FDOM signal that is carried into the deep ocean by North Atlantic waters (i.e, NADW) should have terrestrial origin and they linked one fluorescing component (C – peak) found in their study to terrestrial lignin-like materials. However, the North Atlantic area also displays a relatively high productivity. Earlier studies suggest that the C-peak, traditionally assigned with a terrestrial origin (*Coble, 2007*), is also produced by marine bacterial activity (*Romera-Castillo et al., 2011b, Shimotori et al., 2012*). Further, it has been shown that marine bacteria cultivated in artificial sea water with glucose and inorganic nutrients can produce a C-peak (*Kramer and Herndl, 2004*), indicating that a terrestrial material is not needed to generate C-peak compounds. Therefore, a proper assessment of the biogeochemical processes regulating RDOC in the global deep ocean should include the analysis of all water masses.

3. RDOC and the glacial-interglacial atmospheric CO_2 variability

The large cyclic variations in climate that have occurred in the Earth's planet for the past two million years are statistically linked with cyclic variations in the orbital parameters of the Earth (*Hays, 1976*). The astronomic forcing drives most of the temporal and spatial distribution

of solar radiation incident on the Earth's surface, known as Milankovitch cycles (*Milankovitch, 1930*). But these orbital driven variations in the direct energy budget are insufficient to explain the observed amplitude and timing of these climate cycles, therefore positive feedbacks within the Earth's climate system must amplify orbital forcing (*Sigman & Boyle, 2000; Sigman et al., 2010*).

3.1. CO_2 cyclicity

The concentration of carbon dioxide in the atmosphere, which has varied during glacial/interglacial cycles (*Petit et al., 1999*), may have triggered subsequent feedbacks (*Sigman et al., 2010*). For the last 420 kyr, the atmospheric CO_2 oscillated between about 180 ppmv (peak glacial periods) and 280 ppmv (peak interglacial periods) in 100 kyr cycles (*Petit et al., 1999; Sigman & Boyle, 2000; Falkowsky, 2000*). The regularity of the CO_2 variations, like a “rhythmic breathing” of the planet (*Steffen, 2000; Pelegrí, 2008*), and the remarkable consistency for the upper and lower limits of the pre – industrial atmospheric CO_2 domain are suggestive of a well-ordered set of dominant internal mechanisms, intertwined loop of forcing and feedbacks, that constrains the amount of carbon held by the different reservoirs of the Earth system (*Sigman & Boyle, 2000; Falkowsky, 2000*). Currently, the cause of these glacial interglacial variations in CO_2 is not yet fully identified.

A variety of reconstruction proxies and models of different complexity conclude that there is no single mechanism to explain the entire CO_2 change. Rather, it is likely due to a non-linear combination of different processes acting during different stages of glacial-interglacial transitions (*Sigman & Boyle, 2000; Doney & Schimmel, 2007; Khofeld & Ridwell, 2009; Ciais et al., 2013*). As it was mentioned in the first part of the introduction, the dominant mechanisms responsible for the long-term variability in the concentration of atmospheric CO_2 rely on the ocean (*Broecker, 1982; Kohfeld & Ridwell, 2009*). The mechanisms occurring in the oceans that have been mostly proposed to explain glacial-interglacial variations for the glacial terminations involves (a) changes in the export rate of organic carbon to the deep ocean through differences in the availability and efficiency use of nutrients and shifts in plankton community structure (*Martin, 1990; Broecker & Henderson, 1998; Matsumoto et al., 2002; Boop et al., 2003; Khofeld et al., 2005; Matsumoto, 2007; Khofeld & Ridwell, 2009*), (b) changes in ocean chemistry and carbonate flows to the deep ocean (*Archer & Maier-Reimer, 1994; Sigman & Boyle, 2000; Matsumoto et al., 2002; Marchito et al., 2005; Peacock et al., 2006*) and (c) changes in ocean mixing/ventilation (*François et al., 1997; Sarmiento & Toggweiler, 1984*;

Siegenthaler & Wenk, 1984; Watson & Naveira-Garabato, 2006; Khofeld & Ridwell, 2009). All of them imply variations in the size and timescale of the carbon storage into the deep ocean.

Studies from paleo records highlight the possibility that the sequestration of carbon into long-lived DOC may have also played an important role in the global carbon budget and climate through Earth's history (*Logan et al., 1995; Rothman et al., 2003; Swanson-Hysell et al., 2010; Sexton et al., 2011; Sarnthei et al., 2013; Wang et al., 2014; Ma et al., 2017*). Despite that, few studies have used ocean carbon models that explore the role of the MCP on the long-lived dissolved organic matter pool size and their effect on the past Earth's climate system (*Paillard, 1993; Peltier et al., 2007; Pelegrí et al., 2011; Ma & Tian., 2014; Ma et al., 2017*). It is clear that further research is needed to determine the RDOC production rates and how small changes to these rates imply variations in the RDOC pool size and how would impact on atmospheric CO_2 at geological time-scales.

3.2. Ocean physiology

Complex systems are composed of many subsystems in homeostatic equilibrium, which interact non-linearly at different scales in response to small changes of the external forcing (or, in physiological terms, small changes of potential action). These patterns of interaction between subsystems give rise to a macroscopic structure or organization of the complex system that allows "self-regulating" the energy flows through different processes. The consequence is that the macroscopic complex system reaches certain stable states or attractors (in dynamic equilibrium) where the thermodynamic optimum occurs (*Haken, 1983*). The macroscopic organization of a complex system can be described by different global properties and mechanisms, with fewer degrees of freedom than its subsystems (*Haken, 1983*).

Ideas from eminent scientists such as *James Hutton (1726-1797)*, *Alfred Lotka (1882-1949)* and *James Lovelock (Lovelock, 1988)* have led to a holistic view of the Earth system as a complex system that operates as a "super-organism". The self-regulation (the dynamic balance) of planet Earth is obtained through the macroscopic organization resulting from the interaction, a combination of positive and negative feedbacks, between optimized pulsatile global systems (biosphere, hydrosphere and atmosphere) at different spatial and temporal scales as a response to the annual pulse of insolation (*Falkowsky, 2000; Steffen et al., 2004*).

Pelegrí (2008) suggested that the homeostatic equilibrium of the Earth's climate depends largely on the capacity of the oceanic system to capture and transform incident solar radiation through marine organisms and transport it in various forms through ocean circulation. The

mechanisms involved are similar to those in complex livings, whose internal environment is maintained through a series of homeostatic regulatory mechanisms that give rise to an adequate cellular metabolism (*Pelegri, 2008*). In mammals, for example, cells receive an adequate supply of nutrients and oxygen that allows the generation of energy in the form of adenosine triphosphate (ATP) through the oxidation of biomass. This energy allows the metabolic state or maintenance of the energy expenditure necessary to maintain vital functions, in either a state of rest or activity.

Following the physiological analogy, the energetic variables should be the marine dissolved inorganic carbon and inorganic nutrients. Firstly, the efficiency of the marine autotrophic system in the formation of organic matter in the upper ocean depends mostly on these variables and, secondly, the metabolic expenditure of the ocean or internal energy available to the system depends on the transformation of such organic matter (*Pelegri et al., 2011*). Also, from a physiological perspective the organizational spatial ocean pattern is tree-like, with the branching of currents down to scales where diffusion becomes more effective; this is analogous to what happens with the arteries and veins of our body, with the spatial branching of major arteries (veins) until the arterioles (venules), making an efficient delivery of blood to all major organs of the body, although the actual exchange of oxygen and carbon dioxide with cells occurs through diffusion from the interstitial fluid. Currents would have the same role in terms of energy transfer (carbon and nutrients) in our planet as arteries and veins do for organisms with a circulatory system (*Pelegri, 2005, 2008, Pelegri & Duró 2013*). The physiological approach - named Ocean Physiology (*Pelegri 2005, 2008*) - was already intuited in the early sixteenth century by *Leonardo Da Vinci* who compared ocean currents with the blood flow of a human body. *James Hutton* in 1785 also proposed that the study of the Earth should be done through physiological concepts, and compared the circulation of blood with the recycling of the elements.

The existence of pulsatile frequencies is another fundamental characteristic of all living systems. On planet Earth, a seasonal rhythmic frequency is clearly distinguishable, imposed externally by the irradiation of solar energy. The annual pulse of solar energy input modulates all the main biological processes (primary production and respiration) and physical processes (surface evolution of the mixing layer and recirculation of surface water through the permanent thermocline and the deep ocean). The changes in the spatial distribution and the amplitude of the cycle of annual insolation are, in turn, driven by the natural orbital oscillations of the Earth. On the last ca. 800 kyrs, the astronomically induced variations in the seasonal contrast, especially the variation in the amplitude of the seasonal change in the southern gradients of insolation (precession), may have caused a potential-action cycle of 100

ka, establishing two macroscopic organizations or homeostatic states: the glacial and interglacial states (*Milankovitch, 1930; Paillard, 2001; Rahmstorf, 2002*).

The process by which the Planet Earth reaches this temporal structure can be described also using Ocean Physiology, which positions the upper ocean in two different energetic states. The switch between two states is analogous to the variations experienced by the metabolism of a living being, changing between states of rest (basal energy) and exercise (high energy). Both states are perfectly sustainable but in the latter there is a much higher flux of energy among the different compartments of the system, leading to a higher metabolic rate in the upper ocean (the productive part of the system, where organic carbon is mostly oxidized and nutrients are used to maintain the metabolic functions of the organisms of the euphotic layer) (*Pelegri, 2008*).

In the context of Ocean Physiology, the ocean would have oscillated between these two metabolic states, characterized by (1) quite different thermohaline recirculation rates (slow/rapid during the glacial/interglacial periods) (*Imbrie et al., 1992; Labeyrie et al., 1992*), which result in different DIC and deep inorganic nutrient concentrations reaching the upper ocean, and (2) differences in the activity and respiratory efficiency of microorganisms in the recycling of organic matter (*Del Giorgio & Duarte, 2002*).

These ideas were exemplified in *Pelegri (2008)* by an idealized model of two boxes, for the balance of organic and inorganic nutrients and carbon in the oceans. In this model, the ocean is separated between an upper compartment (upper thermocline) and a deep one. The exchange of properties between these two compartments is determined by the intensity of the MOC, the concentration of DIC/nutrients in the deep waters that reach the surface region, and the upper-ocean remineralization rate. The predicted upper-ocean DIC reproduces the atmospheric CO_2 glacial-interglacial pattern with correlations between the modelled DIC for the upper ocean and the CO_2 observations about 0.8 (*Pelegri et al., 2011*).

The above considerations suggest that Ocean Physiology could be a good approach for evaluate the consequence in variations in the intensity of the MCP and the RDOC pool size on the glacial-interglacial Earth's system response.

4. Aim of the thesis

The general objective of this thesis is to contribute to an improved understanding of the connections between RDOC production and the metabolism of the ocean, with special attention to the way the MCP may have contributed to the glacial-interglacial abrupt climatic transitions of the Earth system. To this end, two specific objectives have been developed:

Objective 1: To evaluate the relative influence of water-mass mixing and microbial activity in the spatial variability of RDOC in the deep ocean.

Objective 2: To develop a “two-box” ocean model that helps understanding the role of the RDOC, via the microbial carbon pump, in the glacial-interglacial transitions.

To answer objective 1, a novel statistical modelling approximation was developed and published under the title “*A simple nonlinear and end-member-free approach for obtaining ocean remineralization patterns*” (De La Fuente et al., 2017). The purpose of this work was to render an objective and simple methodology for resolving the non-conservative fraction of biogeochemical variables. An application of the statistical method was carried out in “*Does a general relationship exist between fluorescent dissolved organic matter and microbial respiration?*” (De La Fuente et al., 2014) where the RDOC microbial production is explored through FDOM-AOU relationships in the dark Atlantic equatorial ocean and the relative importance of the biogeochemical and mixing processes is clarified.

To answer objective 2, a simple two-box ocean model was developed based on the Ocean physiology approach (Pelegri et al, 2008). The model solves the time-dependent equation for DIC, constraining the intensity of the MOC and the interglacial concentration level, in order to explain the general seesaw pattern for atmospheric CO_2 over the last 420 kyr. This work was published as “*Global constraints on net primary production and inorganic carbon supply during glacial and interglacial cycles*” (Pelegri et al., 2013).

References

- Álvarez-Salgado, X. A, Nieto-Cid, M., Álvarez, M., Pérez, F. F., Morín, P., Mercier, H., (2013). New insights on the mineralization of dissolved organic matter in central, intermediate, and deep water masses of the northeast North Atlantic. *Limnol. Oceanogr.* 58, 681–696.
- Archer, D., Maier-Reimer, E., (1994). Effect of deep-sea sedimentary calcite preservation on atmospheric CO_2 concentration. *Nature.* 367(6460), 260–263.
- Arístegui, J., Duarte, C.M., Agustí, S., Doval, M., Álvarez-Salgado, X.A., Hansell, D.A., (2002). Dissolved Organic Carbon Support of Respiration in the Dark Ocean. *Science.* 298, 1967.
- Arístegui, J., Agustí, S., Middelburg, J. J., and Duarte, C. M., (2005). Respiration in the mesopelagic and bathypelagic zones of the ocean. In *Respiration in Aquatic Ecosystems*, Ed P. Del Giorgio and P. Williams (New York, NY: Oxford University Press), 181–205.
- Arístegui, J., Gasol, J. M., Duarte, C. M., and Herndl, G. J., (2009). Microbial oceanography of the dark ocean’s pelagic realm. *Limnol. Oceanogr.* 54, 1501–1529
- Arrhenius, S., (1896). On the Influence of Carbonic Acid in the Air upon the Temperature of the Ground. *Philos. Mag. and Journal of Science.* 5(41), pages 237-276.

- Azam, F., Fenchel, T., Field, J., Gray, J., Meyer-Reil, L., Thingstad, F., (1983). The Ecological Role of Water-Column Microbes in the Sea. *Mar. Ecol. Prog. Ser.* 10, 257–263.
- Benner, R., Biddanda, B., (1998). Photochemical transformations of surface and deep marine dissolved organic matter : Effects on bacterial growth. *Limnol.Oceanogr.* 1373–1378.
- Benner, R. and Herndl, G. J., (2011). Bacterially derived dissolved organic matter in the microbial carbon pump, in: *Microbial Carbon Pump in the Ocean*, edited by: Jiao, N., Azam, F., and Sanders, S., Science/AAAS, Washington, DC 46–48.
- Bereiter, B., Eggleston, S., Schmitt, J., Nehrbass-Ahles, C., Stocker, T. F., Fischer, H., Kipfstuhl, S., and Chappellaz, J., (2015). Revision of the EPICA Dome C CO₂ record from 800 to 600 kyr before present, *Geophys. Res. Lett.*, 42, 542– 549
- Berger, A., Loutre, M., (1991). Insolation values for the climate of the last 10 million years. *Quat. Sci. Rev.* 10, 297-317.
- Bopp, L., Kohfeld, K. E., Le Quéré, C., and Aumont, O., (2003) Dust impact on marine biota and atmospheric CO₂ during glacial periods. *Paleoceanography.* 18, 1046.
- Bricaud, A., Morel, A., and Prieur, L., (1981). Absorption by dissolved organic matter of the sea (yellow substance) in the UV and visible domains. *Limnol. Oceanogr.*, 26, 43–53.
- Broecker, W.S., (1982). Glacial to interglacial changes in ocean chemistry. *Prog. Oceanogr.* 11, 151–197.
- Broecker, W.S., Henderson, G.M., (1998). The sequence of events surrounding Termination II and their implications for the cause of glacial interglacial CO₂ changes. *Paleoceanography*, 13, 352–364.
- Carlson, C.A., Hansell, D.A., Nelson, N.B., Siegel, D.A., Smethie, W.M., Khatiwala, S., Meyers, M.M., Halewood, E., (2010). Dissolved organic carbon export and subsequent remineralization in the mesopelagic and bathypelagic realms of the North Atlantic basin. *Deep-Sea Res. Pt II*, 57 (16), 1433-1445.
- Castro, C.G., Nieto-Cid, M., Álvarez-Salgado, X. a., Pérez, F.F., (2006). Local remineralization patterns in the mesopelagic zone of the Eastern North Atlantic, off the NW Iberian Peninsula. *Deep-Sea Res. Pt I*, 53(12), 1925–1940.
- Carlson, T., Hansell, D. A., (2015). DOM Sources, Sinks, Reactivity, and Budgets. In *Biogeochemistry of Marine Dissolved Organic Matter (Eds Hansell, D. A. & Carlson, C. A.)* 369–388 (Academic Press, 2015).
- Catalá, T.S., et al., (2015) .Turnover time of fluorescent dissolved organic Matter in the Dark Global Ocean. *Nat. Commun.* 6, 5986.
- Catalá, T.S., et al., (2016). Drivers of fluorescent dissolved organic matter in the global epipelagic ocean. *Limnol. Oceanogr.* 61, 1101–1119.
- Ciais, P., Sabine, C., Bala, G., Bopp, L., Brovkin, V., et al., House, J.I., (2014). *Carbon and Other Biogeochemical Cycles*. In: *Edenhofer, O., Pichs-Madruga, R., Sokona, Y., Farahani, E., Kadner, S., Seyboth, K., Adler, A., Baum, I., Brunner, S., Eickemeier, P., Kriemann, B., Savolainen, J., Schlömer, S., von Stechow, C., T., Z., J.C., M. (Eds.), Climate Change 2013. Cambridge University Press, United Kingdom, pp. 465–570.*
- Coble, P.G., Schultz, C.A., Mopper, K., (1993). Fluorescence contouring analysis of DOC Inter-calibration Experiment samples : a comparison of techniques. *Mar. Chem.*, 41 (1–3), 173-178.
- Coble, P.G., (1996). Characterization of marine and terrestrial DOM in seawater using excitation-emission matrix spectroscopy. *Mar. Chem.* 51, 325–346.
- Coble, P.G., (2007). Marine Optical Biogeochemistry : The Chemistry of Ocean Color. *Chem. Rev.* 402–418.
- Coble, P.G., Lead, J., Baker, A., Reynolds, D.M., Spencer, R.G.M., (2014). Aquatic Organic Matter Fluorescence. *Cambridge Environmental Chemistry Series. Cambridge University Press, Cambridge.*
- Chen, R.F., Bada, J.L., (1992). The fluorescence of dissolved organic matter in seawater. *Mar.Chem.* 37 (3–4), pp. 191-221.

- De La Fuente, P., Marrasé, C., Canepa, A., Álvarez-Salgado, X.A., Gasser, M., Fajar, N.M., Romera-Castillo, C., Pelegrí, J.L., (2014). Does a general relationship exist between fluorescent dissolved organic matter and microbial respiration?—The case of the dark equatorial Atlantic Ocean. *Deep Sea Res. Part I Oceanogr. Res. Pap.* 89, 44–55.
- De La Fuente, P., J.L. Pelegrí, A. Canepa, M. Gasser, F. Domínguez and Marrasé, C., (2017). A simple Nonlinear and End-member-Free Approach for Obtaining Remineralization Patterns. *J. Atmos. Oceanic Technol.* 34, 2443 – 2455
- Del Giorgio, P. A, Duarte, C.M., (2002). Respiration in the open ocean. *Nature* 420, 379–384.
- Del Vecchio, R., Blough, N.V., (2004). Spatial and seasonal distribution of chromophoric dissolved organic matter and dissolved organic carbon in the Middle Atlantic Bight. *Mar. Chem.* 89, 169–187.
- Determann, S., Reuter, R., Willkomm, R., (1996). Fluorescent matter in the eastern Atlantic Ocean. Part 2 : vertical profiles and relation to water masses. *Deep-Sea Res. Pt I*, 43, 345–360.
- Doney, S.C., Schimel, D.S., (2007). Carbon and Climate System Coupling on Timescales from the Precambrian to the Anthropocene. *Annu. Rev. Environ. Resour.* 32, 31–66.
- Ducklow, H.W., Steinberg, D.K., Buesseler, K.O., (2001). Upper Ocean Carbon Export and the Biological Pump. *Oceanography*, 14,50–58.
- Dunne, J.P., Sarmiento, J.L., Gnanadesikan, A., (2007). A synthesis of global particle export from the surface ocean and cycling through the ocean interior and on the seafloor. *Global Biogeochem. Cy.* 21: GB4006.
- EPICA Community Members, (2004). Eight glacial cycles from an Antarctic ice core. *Nature* 429, 623–628.
- Falkowski, P., et al., (2000) .The Global Carbon Cycle : A Test of Our Knowledge of Earth as a System. *Science. New Series*, 290(5490) 291–296.
- Feely, R.A., Sabine, C.L., Takahashi, T., Wanninkhof, R., (2001). Uptake and storage of carbon dioxide in the ocean: The global CO₂ survey. *Oceanography* 14(4), 18–32.
- François, R., Altabet, M.A., Yu, E., Sigman, D.M., Bacon, M.P., Frank, M., Bohrmann, G., Bareille, G., Labeyrie, L.D., (1997). Contribution of Southern Ocean surface-water stratification to low atmospheric CO₂ concentrations during the last glacial period. *Nature*, 389, 929–935.
- Ganachaud, A., Wunsch, C., (2000). Improved estimates of global ocean circulation, heat transport and mixing from hydrographic data. *Nature* 408, 453–457.
- Gouriou, Y., Reverdin, G., (1992). Isopycnal and diapycnal circulation of the upper equatorial Atlantic Ocean in 1983–1984. *J. Geophys. Res.* 97, 3543.
- Green, S.A., Blough, N. V, (2014). Natural Waters Optical absorption and fluorescence of chromophoric properties dissolved organic matter in natural waters. *Limnol. Oceanogr.* 39, 1903–1916.
- Gruber, N., Sarmiento, J.L., (2002). Large-scale biogeochemical-physical interactions in elemental cycles. *In The Sea*, edited by A.R. Robinson et al., pp. 337-399, John Wiley & Sons, Inc., New York.
- Hansell, D., Carlson, C., (1998). Deep-ocean gradients in the concentration of dissolved organic carbon. *Nature*, 263–266.
- Hansell, D. A., Carlson, C. A., Repeta, D.J., Schlitzer, R., (2009). Dissolved Organic Matter in the Ocean A Controversy Stimulates New Insights. *Oceanography* 22, 202–211.
- Hansell, D. A., Carlson, C. a., Schlitzer, R., (2012). Net removal of major marine dissolved organic carbon fractions in the subsurface ocean. *Global Biogeochem. Cy.* 26, 1–9.
- Hansell, D.A., Carlson, C.A., (2013a). Localized refractory dissolved organic carbon sinks in the deep ocean. *Global Biogeochem. Cy.* 27, 705–710.
- Hansell, D. A., (2013b). Recalcitrant Dissolved Organic Carbon Fractions. *Ann. Rev. Mar. Sci.* 5, 421 – 445.
- Haken, H. (1983). Synergetics: An Introduction. Non-equilibrium phase transitions and self-organization. *In Physics, Chemistry, and Biology*, Springer-Verlag, Berlin.

- Hayase, K., Tsubota, H., Sunada, I., (1989). Relationships of fluorescence and AOU in the three north pacific water samples. *Sci. Total Environ.* 82, 315–318.
- Hayase, K., Shinozuka, N., (1995). Vertical distribution of fluorescent organic matter along with AOU and nutrients in the equatorial Central Pacific. *Mar. Chem.* 48, 283–290.
- Hays, J. D., Imbrie, J., Shackleton, N. J., (1976). Variations in the Earth 's Orbit : Pacemaker of the Ice Ages . *Science*, 194(4270), 1121–1132.
- Heinze, C., et al., (2015). The ocean carbon sink - Impacts, vulnerabilities and challenges. *Earth Syst. Dyn.* 6, 327–358.
- Helms, J.R., Stubbins, A., Ritchie, J.D., Minor, E.C., Kieber, D.J., Mopper, K., (2008). Absorption spectral slopes and slope ratios as indicators of molecular weight, source, and photobleaching of chromophoric dissolved organic matter. *Limnol. Oceanogr.* 53,955–969.
- Hernes, P.J., Benner, R., (2006). Terrigenous organic matter sources and reactivity in the North Atlantic Ocean and a comparison to the Arctic and Pacific oceans. *Mar. Chem.* 100 (1-2), 66–79.
- Hopkinson, C.S., Vallino, J.J., (2005). Efficient export of carbon to the deep ocean through dissolved organic matter. *Nature* 433, 142–145.
- Imbrie, J., et al., (1992). On the structure and origin of major glaciation cycles 1. Linear responses to Milankovitch forcing. *Paleoceanography*, 7 (6), 701–738, 607.
- Imbrie, J., et al., (1993). On the structure and origin of major glaciation cycles 2, the 1000,000 year cycle. *Paleoceanography* 8, 35–42.
- Jiao, N., et al., (2010). Microbial production of recalcitrant dissolved organic matter: long-term carbon storage in the global ocean. *Nat. Rev. Microbiol.* 8, 593–599.
- Jiao, N., Azam, F., (2011). Microbial carbon pump and its significance for carbon sequestration in the ocean. In *Microbial Carbon Pump in the Oceans*, eds Jiao, N., Azam, F., Sanders, S., *Science Booklet, Supplement to Science*, PP. 43 – 45.
- Jiao, N., Robinson, C., Azam, F., Thomas, H., Baltar, F., Dang, H., Johnson, M., (2014). Mechanisms of microbial carbon sequestration in the ocean – future research directions. *Biogeosciences.* 11, 5285-5306.
- Jiao N, et al., (2018). Unveiling the enigma of refractory carbon in the ocean. *Natl Sci Rev.*5, 459–63.
- Jørgensen, L., Stedmon, C.A., Kragh, T., Markager, S., Middelboe, M., Søndergaard, M., (2011). Global trends in the fluorescence characteristics and distribution of marine dissolved organic matter. *Mar. Chem.* 126, 139–148.
- Jørgensen, L., Stedmon, C., (2014). Tracing the long-term microbial production of recalcitrant fluorescent dissolved organic matter in seawater. *Geophys. Res. Lett.* 41, 2481–2488.
- Kaiser, K., Benner, R., (2008). Major bacterial contribution to the ocean reservoir of detrital organic carbon and nitrogen. *Limnol. Oceanogr.* 53, 99–112.
- Kalle, K., (1966).The Problem of the Gelbstoff in the Sea. *Oceanogr. Mar. Biol. An Annual Review*, 4 91-104.
- Kanwisher, J., (1960). pCO₂ in Sea Water and its Effect on the Movement of CO₂ in Nature. *Tellus* 12, 209–215.
- Kohfeld, K. E., (2005). Role of Marine Biology in Glacial-Interglacial CO₂ Cycles. *Science*, 308(5718), 74-78.
- Kohfeld, K.E., Ridgwell, A., (2009). Glacial-Interglacial Variability in Atmospheric CO₂. In: *Le Quéré C, Saltzman ES, eds. Surface-ocean lower atmosphere processes*, pp. 251-86. *Geophysical monograph* 187. American Geophysical Union, Washington, DC.
- Kramer, G.D., Herndl, G.J., (2004). Photo- and bio-reactivity of chromophoric dissolved organic matter produced by marine bacterioplankton. *Aquat.Microb.Ecol.*, 36(3), 239–246.

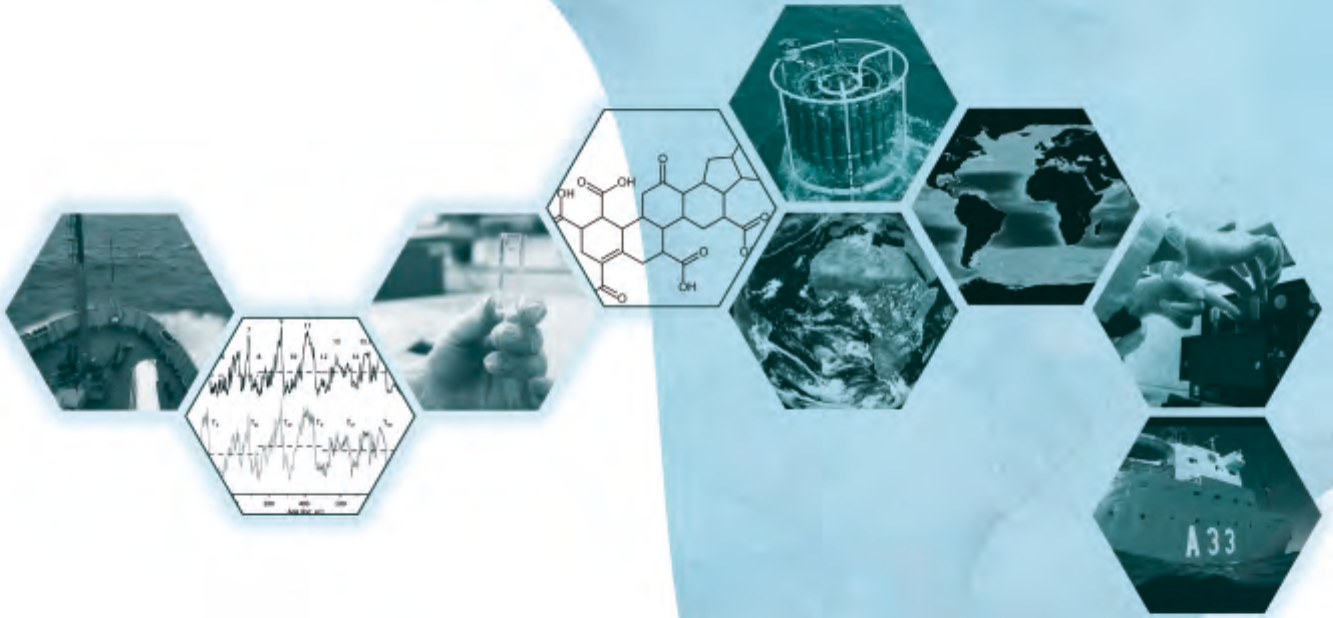
- Kwon, E.Y., Primeau, F., Sarmiento, J.L., (2009). The impact of remineralization depth on the air – sea carbon balance. *Nat. Geosci.* 2, 630–635.
- Labeyrie, L.D., Duplessy, J., Duprat, J., Juillet-Leclerc, A., Moyes, J., Michel, E., Kallel, N., Shackleton, N.J., (1992). Changes in the vertical structure of the North Atlantic Ocean between glacial and modern times. *Quat. Sci. Rev.* 11, 401–413.
- Lacis, A.A., G.A. Schmidt, D. Rind, and R.A. Ruedy, (2010). Atmospheric CO₂: Principal control knob governing Earth's temperature. *Science.* 330, 356-359.
- Lawaetz, A.J., Stedmon, C.A., Lawaetz, A.J., Stedmon, C.A., (2008). Fluorescence Intensity Calibration Using the Raman Scatter Peak of Water. *Appl. Spectrosc.* 63, 936-940.
- Lechtenfeld, O.J., Hertkorn, N., Shen, Y., Witt, M., Benner, R., (2015). Marine sequestration of carbon in bacterial metabolites. *Nat. Commun.* 6, 6711.
- Legendre, L., Rivkin, R.B., Weinbauer, M.G., Guidi, L., Uitz, J., (2015). The microbial carbon pump concept: Potential biogeochemical significance in the globally changing ocean. *Prog. Oceanogr.* 134, 432–450
- Le Quéré, C., & Metzl, N. (2004). Natural Processes Regulating the Ocean Uptake of CO₂. In: *Field, C.B. and Raupach, M.R (Eds).The global carbon cycle: Integrating Humans, Climate, and the natural World. Scope 62, Island Press, Washington, DC, pp. 243-255.*
- Logan, G. A., Hayes, J. M., Hieshima, G. B., and Summons, R. E., (1995). Terminal Proterozoic reorganization of biogeochemical cycles. *Nature.* 376(6535), 53–56.
- Lovelock J.E., (1988). The ages of Gaia: A biography of our living earth. *W.W. Norton & Co., New York, USA.*
- Lüthi, D., et al.,(2008). High-resolution carbon dioxide concentration record 650,000-800,000 years before present. *Nature.* 453, 379–382.
- Ma, W., Tian, J., (2014). Modelling the contribution of dissolved organic carbon to carbon sequestration during the last glacial maximum. *Geo-Mar. Lett.* 34, 471–482.
- Ma, W., Wang, P., Tian, J., (2017). Modelling 400–500-kyr Pleistocene carbon isotope cyclicity through variations in the dissolved organic carbon pool. *Global and Planet. Change.* 152, 187–198.
- Machín, F., Pelegrí, J.L., (2006). Effect of the Canary Islands in the blockage and mixing of the North Atlantic eastern water masses. *Geophys. Res. Lett.* 33, 1–5.
- Marchitto, T.M., Lynch-stieglitz, J., Hemming, S.R., (2005). Deep Pacific CaCO₃ compensation and glacial – interglacial atmospheric CO₂. *Earth Planet. Sc. Lett.* 231(3-4),317-336
- Marinov, I., Sarmiento, J.L., (2004). The role of the oceans in the global carbon cycle: an overview. In: *Follows M, Oguz T (eds) Ocean carbon cycle and climate, NATO ASI. Kluwer Academic Publishers, Ankara, p 251–295.*
- Martin, J., (1990). Glacial-interglacial CO₂ change: the iron hypothesis. *Paleoceanography* 5, 1–13.
- Matsumoto, K., Sarmiento, J.L., Brzezinski, M.A., (2002). Silicic acid leakage from the Southern Ocean : A possible explanation for glacial atmospheric pCO₂. *Global biogeochem. Cy.* 16(3).
- Matsumoto, K., (2007). Biology-mediated temperature control on atmospheric pCO₂ and ocean biogeochemistry. *Geophys.Res. Lett.* 34, 1-5.
- Milankovitch, M.(1930). Mathematische Klimalehre und Astronomische Theorie der Klimaschwankungen. In: *Handbuch der Klimatologie. Band 1: Allgemeine Klimalehre, Teil (Eds. W. Köppen and R. Geiger), Gebrüder Borntraeger, Berlin, p. 1-76.*
- Myhre, G., et al., (2013). Anthropogenic and Natural Radiative Forcing. In Stocker TF et al. (eds) *Climate Change 2013: The Physical Science Basis. Contribution of Working Group I to the Fifth Assessment Report of the Intergovernmental Panel on Climate Change. Cambridge University Press, Cambridge/New York.*

- Mopper, K., Schultz, C. A., (1993). Fluorescence as a possible tool for studying the nature and water column distribution of DOC components. *Mar. Chem.* 41, 229–238.
- Nelson, N.B., Siegel, D. A., Carlson, C. A., Swan, C., Smethie, W.M., Khatiwala, S., (2007). Hydrography of chromophoric dissolved organic matter in the North Atlantic. *Deep Sea Res. Pt I.* 54, 710–731.
- Nelson, N.B., Coble, P.G., (2010). Optical Analysis of Chromophoric Dissolved Organic matter. In practical guidelines for the analysis of seawater, (eds) O. Wurl. (Boca Raton, FL:CRC), pp. 79–96.
- Nelson, N.B., Siegel, D. A., Carlson, C. A., Swan, C.M., (2010). Tracing global biogeochemical cycles and meridional overturning circulation using chromophoric dissolved organic matter. *Geophys. Res. Lett.* 37. L03610.
- Nelson, N.B., Siegel, D.A., (2013). The Global Distribution and Dynamics of Chromophoric Dissolved Organic Matter. *Annu. Rev. Mar. Sci.* 5, 447-476.
- Nieto-Cid, M., Álvarez-Salgado, X., Gago, J., Pérez, F.F., (2005). DOM fluorescence, a tracer for biogeochemical processes in a coastal upwelling system (NW Iberian Peninsula). *Mar. Ecol. Prog. Ser.* 297, 33–50.
- Nieto-Cid, M., Álvarez-Salgado, X., Pérez, F.F., (2006). Microbial and photochemical reactivity of fluorescent dissolved organic matter in a coastal upwelling system. *Limnol. Oceanogr.*, 51(3), 1391–1400.
- Ogawa, H., Tanoue, E., (2003). Dissolved Organic Matter in Oceanic Waters. *J. Oceanogr.* 59, 129–147.
- Orsi, A. H., Johnson, G.C., Bullister, J.L., (1999). Circulation, mixing, and production of Antarctic Bottom Water. *Prog. Oceanogr.* 43, 55–109.
- Paillard, D., (1993). Dissolved organic matter and the glacial-interglacial pCO₂ problem. *Global Biogeochem. Cycles* 7, 901–914.
- Paillard, D. (2001). Glacial cycles: Toward a new paradigm. *Reviews of Geophysics.* 39, 325 – 346.
- Peacock, S., Lane, E., Restrepo, J. M., (2006). A possible sequence of events for the generalized glacial-interglacial cycle. *Global Biogeochem. Cycles.* 20, GB2010.
- Pelegrí, J. L., Csanady, G. T., (1991). Nutrient transport and mixing in the Gulf Stream. *J. Geophys. Res.* 96(C2), 2577–2583.
- Pelegrí, J.L., (2005). Les artèries de Gaia. *Omni Cellula.* 8, 11–17
- Pelegrí, J.L., Marrero-Díaz, A., Ratsimandresy, A. W., (2006). Nutrient irrigation of the North Atlantic. *Prog. Oceanogr.* 70, 366–406.
- Pelegrí, J.L., (2008). A physiological approach to oceanic processes and glacial-interglacial changes in atmospheric CO₂. *Sci. Mar.* 72, 185.
- Pelegrí, J.L., Olivella, R., García-Olivares, A., (2011). A simple metabolic model of glacial-interglacial energy supply to the upper ocean. *Earth Syst. Dyn. Discuss.* 2, 271–313.
- Pelegrí, J.L., Duró, A., (2013). La memòria oceànica del clima: El sistema circulatori d'un planeta viu. *Mètode* 77, 36–43.
- Pelegrí, J.L., De La Fuente, P., Olivella, R. and García-Olivares, A., (2013), Global constraints on net primary production and inorganic carbon supply during glacial and interglacial cycles. *Paleoceanography.* 28, 713 - 725
- Peltier, W.R., Liu, Y., Crowley, J.W., (2007). Snowball Earth prevention by dissolved organic carbon remineralization. *Nature.* 450, 813–818.
- Perez, F. F., Mouriño, C., Fraga, F., and Rios, A. F. (1993). Displacement of water masses and remineralization rates off the Iberian Peninsula by nutrient anomalies. *J. Mar. Res.* 51, 869–892.
- Petit, J.R. et al., (1999). Climate and atmospheric history of the past 420,000 years from the Vostok ice core, Antarctica. *Nature.* 399, 429–436.

- Prentice, I.C., et al., (2001). The carbon cycle and atmospheric carbon dioxide. *Clim. Chang. Sci. Basis. Contrib. Work. Gr. I to Third Assess. Rep. Intergov. Panel Clim. Chang.* 183–237.
- Rahmstorf, S., (2002). Ocean circulation and climate during the past 120,000 years. *Nature.* 419, 207–214.
- Rahmstorf, S.,(2006). Thermohaline ocean circulation. In *Encyclopedia of Quaternary Sciences, Edited by S. A. Elias. Elsevier, 1-10.*
- Reinthal, T., Salgado, X.A., Álvarez, Á., Aken, M., Van, H.M., Herndl, G.J., (2013). Impact of water mass mixing on the biogeochemistry and microbiology of the Northeast Atlantic Deep Water. *Global Biogeochem. Cy., 27, 1151–1162.*
- Ridgwell, A., Arndt, S., (2015). Why Dissolved Organics Matter: DOC in Ancient Oceans and Past Climate Change. In *Biogeochemistry of Marine Dissolved Organic Matter (2 ed., pp. 1). AP.*
- Romera-Castillo, C., Sarmiento, H., Marrase, C., (2010). Production of chromophoric dissolved organic matter by marine phytoplankton. *Limnol. Oceanogr.* 55(1), 446–454.
- Romera-Castillo, C., Nieto-Cid, M., Castro, C.G., Marrasé, C., Largier, J., (2011a). Fluorescence : Absorption coefficient ratio — Tracing photochemical and microbial degradation processes affecting coloured dissolved organic matter in a coastal system. *Mar. Chem.* 125, 26–38.
- Romera-Castillo, C., Sarmiento, H., Gasol, J.M., Marrase, C., (2011b). Net Production and Consumption of Fluorescent Colored Dissolved Organic Matter by Natural Bacterial Assemblages Growing on Marine Phytoplankton Exudates. *Appl. Environ. Microb.* 77 (21), 7490–7498.
- Romera-Castillo, C., Álvarez-Salgado, X.A., Galí, M., Gasol, J.M., Marrasé, C., (2013). Combined effect of light exposure and microbial activity on distinct dissolved organic matter pools . A seasonal field study in an oligotrophic coastal system (Blanes Bay , NW Mediterranean). *Mar. Chem.* 148, 44–51.
- Rothman, D.H., Hayes, J.M., Summons, R.E., (2003). Dynamics of the Neoproterozoic carbon cycle. *Proc. Natl. Acad. Sci. USA.* 100, 8124–8129.
- Royer, D.L., (2006). CO₂-forced climate thresholds during the Phanerozoic. *Geochim. Cosmochim. Acta.* 70, 5665–5675.
- Royer, D.L., Berner, R.A., Park, J., (2007). Climate sensitivity constrained by CO₂ concentrations over the past 420 million years. *Nature.* 446, 530–532.
- Sarmiento, J., Toggweiler, J., (1984). A new model for the role of the oceans in determining atmospheric pCO₂. *Nat. Publ. Gr.* 312, 237–242.
- Sarmiento, J. L., Gruber, N., Brzezinski, M., Dunne, J.P., (2004) High-latitude controls of thermocline nutrients and low latitude biological productivity. *Nature.* 427, 56-60.
- Sarnthein, M., Schneider, B., Grootes, P.M., (2013). Peak glacial ¹⁴C ventilation ages suggest major draw-down of carbon into the abyssal ocean. *Clim. Past,* 9, 2595–2614.
- Schneider, B., Karstensen, J., Oeschies, A., (2005). Model-based evaluation of methods to determine C : N and N : P regeneration ratios from dissolved nutrients. *Global Biogeochem. Cy.* 19, GB2009.
- Sexton, P.F., Norris, R.D., Wilson, P. a, Pälike, H., Westerhold, T., Röhl, U., Bolton, C.T., Gibbs, S., (2011). Eocene global warming events driven by ventilation of oceanic dissolved organic carbon. *Nature.* 471, 349–352.
- Shimotori, K., Watanabe, K., Hama, T., (2012). Fluorescence characteristics of humic-like fluorescent dissolved organic matter produced by various taxa of marine bacteria. *Aquat. Microb. Ecol.* 65, 249–260.
- Siegel, D. A., (2016). Prediction of the Export and Fate of Global Ocean Net Primary Production: The EXPORTS Science Plan. *Front. Mar. Sci.* 3, 22.
- Siegenthaler, U., Wenk, T., (1984). Rapid atmospheric CO₂ variations and ocean circulation. *Nat. Publ. Gr.* 312, 237–242.

- Siegenthaler, U., Sarmiento, J., (1993). Atmospheric carbon dioxide and the ocean. *Nature*. 365, 119 – 125.
- Sigman, D.M., Boyle, E.A., (2000). Glacial/Interglacial variations in atmospheric CO₂. *Nature* 407, 859–869.
- Sigman, D.M., Hain, M.P., Haug, G.H., (2010). The polar ocean and glacial cycles in atmospheric CO₂ concentration. *Nature*. 466, 47–55.
- Stedmon, C.A., Nelson, N.B., (2015). Chapter 10 - The Optical Properties of DOM in the Ocean, in: Hansell, D.A., Carlson, C.A. (Eds.), *Biogeochemistry of Marine Dissolved Organic Matter* (Second Edition). *Academic Press, Boston*, pp. 481–508.
- Steffen. W., (2000). An integrated approach to understanding Earth's metabolism. In *Global Change Newsletter, n°41 The International Geosphere–Biosphere Programme (IGBP): A Study of Global Change of the International Council for Science (ICSU)*.
- Steffen, W., et al., (2004). Global change and the earth system: a planet under pressure. *The IGBP global change series. Springer-Verlag, Berlin*.
- Swan, C.M., Siegel, D.A., Nelson, N.B., Carlson, C.A., Nasir, E., (2009). Biogeochemical and hydrographic controls on chromophoric dissolved organic matter distribution in the Pacific Ocean. *Deep-Sea Res. Pt I*. 56, 2175–2192.
- Swanson-Hysell, N.L., Rose, C. V, Calmet, C.C., Halverson, G.P., Hurtgen, M.T., Maloof, A.C., (2010). Cryogenian glaciation and the onset of Carbon-Isotope Decoupling. *Science*. 328 (5978), 608-611.
- Talley, L.D., Pickard, G.E., Emery, W.J., Swift., J.H., (2011). Descriptive Physical Oceanography: An Introduction. 6th ed. *Elsevier, Burlington, MA*, 560 pp.
- Turner, J.T., (2014). Zooplankton Fecal Pellets, Marine Snow, Phytodetritus and the Ocean 's Biological Pump. *Progr. Oceanogr.* 130, 205-248.
- Volk, T., Hoffert, M.I., (1985). Ocean carbon pumps: Analysis of relative strengths and efficiencies in ocean driven atmospheric CO₂ changes. In *The Carbon Cycle and Atmospheric CO₂: Natural variations Archaean to present*, ed. by E.T. Sundquist and W.S. Broecker, *Geophys. Monogr.Ser.*, 32, 99-110, AGU, Washington, D.C., 1985.
- Wang, P., Li, Q., Tian, J., Jian, Z., Liu, C., Li, L., Ma, W., (2014). Long-term cycles in the carbon reservoir of the Quaternary ocean: a perspective from the South China Sea. *Natl Sci Rev.* 1, 119–143.
- Wanninkhof, R., (1992). Relationship between wind speed and gas exchange over the ocean. *J. Geophys. Res.*, 97(C5), 7373– 7382.
- Wanninkhof, R., (2014). Relationship between wind speed and gas exchange over the ocean revisited. *Limnol. Oceanogr. Methods*, 12.
- Watson, A. J., Naveira Garabato, A. C., (2006). The role of Southern Ocean mixing and upwelling in glacial-interglacial atmospheric CO₂ change. *Tellus B*. 58(1), 73–87.
- Williams, R.G., Roussenov, V., Follows, M.J., (2006). Nutrient streams and their induction into the mixed layer. *Global Biogeochem. Cy.* 20, 1–18.
- Yamashita, Y., Tanoue, E., (2008). Production of bio-refractory fluorescent dissolved organic matter in the ocean interior. *Nat. Geosci.* 1, 579–582.
- Yamashita, Y., Cory, R.M., Nishioka, J., Kuma, K., Tanoue, E., Jaffe, R., (2010). Fluorescence characteristics of dissolved organic matter in the deep waters of the Okhotsk Sea and the north western North Pacific Ocean. *Deep-Sea Res. Pt II*. 57, 1478–1485.
- Zeebe, R., Wolf-Gladrow, D., (2001): CO₂ in Seawater: Equilibrium, Kinetics, Isotopes. *Elsevier Oceanography Book Series*, 65, 346 pp, Amsterdam.
- Zhang, C., Dang, H., Azam, F., Benner, R., (2018). Evolving Paradigms in Biological Carbon Cycling in the Ocean. *Natl. Sci. Rev.* 5, 481–499.

INFLUENCE OF MIXING OF WATER MASSES AND MICROBIAL ACTIVITY ON THE SPATIAL VARIABILITY OF REFRACTORY DISSOLVED ORGANIC MATTER (RDOC) IN THE DEEP OCEAN



A simple nonlinear and end-member-free approach for obtaining ocean remineralization patterns

De La Fuente, P., Pelegrí, J.L., Canepa, A., Gasser, M., Domínguez, F., and Marrasé, C., (2017). A simple Nonlinear and End-member-Free Approach for Obtaining Remineralization Patterns. *J. Atmos. Oceanic Technol.* 34, 2443 – 2455, <https://doi.org/10.1175/JTECHD-17-0090.1> ©American Meteorological Society. Used with permission.

Does a general relationship exist between dissolved organic matter and microbial respiration? – The case of the dark equatorial Atlantic Ocean

De La Fuente, P., Marrasé, C., Canepa, A., Álvarez-Salgado, X.A., Gasser, M., Fajar, N.M., Romera-Castillo, C., Pelegrí, J.L., (2014). Does a general relationship exist between fluorescent dissolved organic matter and microbial respiration?—The case of the dark equatorial Atlantic Ocean. *Deep Sea Res. Part I Oceanogr. Res. Pap.* 89, 44–55. doi: <https://doi.org/10.1016/j.dsr.2014.03.007> Elsevier. Used with permission.

A Simple Nonlinear and End-Member-Free Approach for Obtaining Ocean Remineralization Patterns

PATRICIA DE LA FUENTE AND JOSEP L. PELEGRÍ

Institut de Ciències del Mar, Consejo Superior de Investigaciones Científicas, Barcelona, Spain

ANTONIO CANEPA

Escuela de Ciencias del Mar, Pontificia Universidad Católica de Valparaíso, Valparaíso, Chile

MARC GASSER

Institut de Ciències del Mar, Consejo Superior de Investigaciones Científicas, Barcelona, Spain

FRANCISCO DOMÍNGUEZ

DC Servicios Ambientales, Santa Cruz de Tenerife, Spain

CÈLIA MARRASÉ

Institut de Ciències del Mar, Consejo Superior de Investigaciones Científicas, Barcelona, Spain

(Manuscript received 13 May 2017, in final form 22 August 2017)

ABSTRACT

The variability of a biogeochemical property in the ocean is the outcome of both nonconservative (such as respiration and photosynthesis) and conservative (mixing of water masses with distinct concentrations at origin) processes. One method to separate both contributions is based on a multiple regression of the biogeochemical property in terms of temperature θ and salinity S as conservative proxies of water masses. This regression delivers the variability related to the conservative fraction and hence allows for identifying the residual as the biogeochemical anomaly. Here, the standard multiple linear regression (MLR) method, which assumes that water masses mix locally and linearly, is compared with a nonlinear polynomial regression (PR) over the entire (θ, S) space. The PR method has two important advantages over MLR: allows for simultaneous nonlinear mixing of all water masses and does not require knowing the end-member water types. Both approaches are applied to data along 7.5°N in the equatorial Atlantic Ocean, and the biogeochemical anomalies are calculated for humic-like fluorescent dissolved organic matter, apparent oxygen utilization, and nitrate—all of them related through in situ remineralization processes. The goodness of both approaches is assessed by analyzing the linear dependence and the coefficient of correlation between the anomalies. The results show that the PR method can be applied over the entire water column and yet retains the local variability associated with nonconservative processes. The potential of the PR approach is also illustrated by calculating the oxygen–nitrate stoichiometric ratio for the entire 7.5°N transatlantic section.

1. Introduction

The dissolved organic matter (DOM) in the ocean is represented by diverse pools with different biological

Supplemental information related to this paper is available at the Journals Online website: <https://doi.org/10.1175/JTECH-D-17-0090.s1>.

Corresponding author: J. L. Pelegrí, pelegri@icm.csic.es

lability, which can be conceptually divided into labile (residence time of minutes to days), semilabile (days to months), semirefractory (years to decades), and refractory (centuries to millennia) (Carlson et al. 2010; Catala et al. 2015; Hansell 2013 and references therein; Yamashita and Tanoue 2008). Marine DOM is the largest active reservoir of reduced carbon on Earth's surface (Hedges et al. 1997), and most of the DOM in the dark ocean (waters deeper than 200 m) is refractory DOM (RDOM), with a pool of about 630 PgC (Hansell 2013).

DOI: 10.1175/JTECH-D-17-0090.1

© 2017 American Meteorological Society. For information regarding reuse of this content and general copyright information, consult the [AMS Copyright Policy](#) (www.ametsoc.org/PUBSReuseLicenses).

A fraction of the RDOM is spectroscopically characterized through the emission of fluorescence at the excitation/emission wavelengths that distinguish humic substances when irradiated with ultraviolet; this RDOM fraction is named humic-like fluorescent DOM (FDOM) (Coble 2007, 1996). In situ FDOM production is a key process for maintaining the oceanic pool of optically active RDOM at centennial and millennia time scales (Catala et al. 2015; Yamashita and Tanoue 2008). Further insight into FDOM production will help advance our knowledge on RDOM cycling and its role in carbon sequestration into the deep ocean.

A number of studies have endorsed the idea that FDOM is mostly produced in situ via heterotrophic oxidation of organic matter in the dark ocean: this is based on a significant and positive association between FDOM and both apparent oxygen utilization (AOU) and nutrient salts (nitrate NO_3 and phosphate PO_4) that changes with water mass (Álvarez-Salgado et al. 2013; Catala et al. 2015; Chen and Bada 1992; De La Fuente et al. 2014; Hayase and Shinozuka 1995; Hayase et al. 1989; Jørgensen et al. 2011; Yamashita and Tanoue 2008; Yamashita et al. 2007).

Different statistical approaches are commonly used to obtain the ratios of FDOM production to oxygen depletion and inorganic-nutrients generation. The most usual is through simple regression models between the biogeochemical variables (Chen and Bada 1992; Hayase and Shinozuka 1995; Hayase et al. 1989; Jørgensen et al. 2011; Yamashita and Tanoue 2008; Yamashita et al. 2007). However, an important bias in the calculation of the biogeochemical ratios is introduced in those water masses with a high initial content of FDOM, acquired through river input of terrestrial humic compounds in the area of source water formation. For instance, a high amount of terrestrial organic matter is released from the continents to those regions where North Atlantic Deep Water (NADW) is formed. Jørgensen et al. (2011) found a significant and high correlation between FDOM and AOU for the dark global ocean but only when omitting the NADW from the linear regression model. In contrast, Yamashita and Tanoue (2008) found a high and significant relationship between FDOM and AOU for the deep Pacific Ocean (depths over 1000 m), where mixing is small and the initial content of FDOM in the source water is low.

The abovementioned simple regression models assume that all of the data variability is only due to biological controls, neglecting any effect associated with the mixing of water masses with distinct contents at origin (Carlson et al. 2010; Reinthaler et al. 2013; Schneider et al. 2005). However, the relationship between any pair of non-conservative parameters indeed depends upon 1) the conservative mixing of source waters with different contents and 2) the nonconservative biological processes that take

place since the water mass formation region (Álvarez-Salgado et al. 2013; Castro et al. 1998, 2006; De La Fuente et al. 2014; Pérez et al. 1993, 1998, 2001; Reinthaler et al. 2013).

Statistical methods may be used to isolate the variability associated with both mixing and nonconservative biological processes. These methods are based on the idea that mixing of water masses has the same effect on both conservative and nonconservative properties. Hence, the evolution of the conservative fraction of a biogeochemical property may be inferred from the covariance between these biogeochemical data and both salinity S and potential temperature θ as conservative proxies of water mass; that is, the conservative fraction is determined from a regression model as a function of (θ, S) . The resultant anomalies, calculated as the observed values minus the modeled values, should reflect the variability associated with biological processes.

The challenge is to use the best-possible regression model; that is, a data-fit model that can properly track the conservative evolution of the water masses without removing the biogeochemical anomalies. One simple approach is to assume that the water parcel results from the linear mixing of two or more source water types (SWT; called end-members) in a conservative θ - S space, a physical process that should equally transform the conservative and nonconservative properties. In particular, since any water sample in the conservative θ - S space can be expressed as the linear combination of three (θ, S) end-members, the corresponding biogeochemical concentration should emerge from a multiple linear correlation with S and θ (e.g., Álvarez-Salgado et al. 2013). The linear mixing approach has been extensively used for determining the distribution of water masses in the World Ocean, either using the classical method of mixing triangles when only temperature and salinity are involved (Mamayev 1975) or employing different varieties of the optimum multiparameter method when other properties are also considered (e.g., Mackas et al. 1987; Llanillo et al. 2012, 2013).

Despite the extensive application of the classical mixing method to infer the conservative fraction of the biogeochemical variables, the assumption of conservative local and lineal mixing in the θ - S space is not necessarily true. There is no justification behind the assumption that only three water types participate in the composition of any given water parcel, and there is no unique solution for the linear mixing of three conservative properties (temperature, salinity, and mass) with more than three end-members. Further, ocean mixing is not isotropic in the θ - S space as, in the absence of convective processes, it takes place preferentially along isopycnals. Therefore, the conservative fraction of any biogeochemical variable may as well be proportional

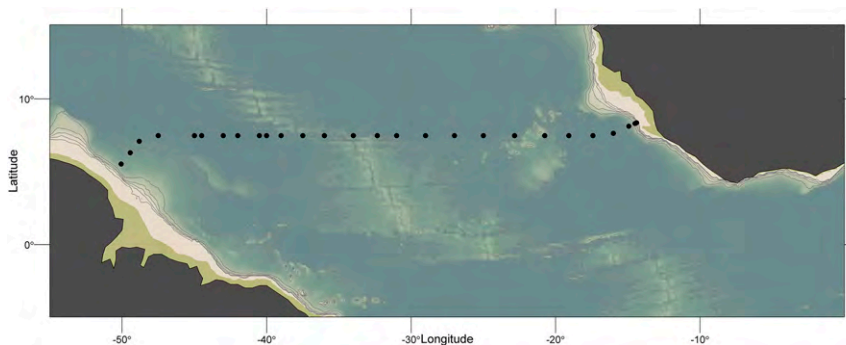


FIG. 1. Study area showing the biogeochemical stations along 7.5°N during the MOC2-Equatorial cruise.

to a nonlinear function of θ and S . Recently, through a multiple nonlinear regression for both FDOM and AOU as a function of temperature and salinity over the entire (θ, S) space, De La Fuente et al. (2014) found a significant correlation between the FDOM and AOU anomalies for the dark equatorial Atlantic Ocean.

In this study we explore the goodness of linear-local and nonlinear-global methods to obtain the nonconservative anomalies. All these approaches remove the information associated with conservative mixing of source water types through a multiple regression of the nonconservative property with S and θ . However, while one approach is based on the local linear mixing of a maximum of three source water masses (Carlson et al. 2010; Castro et al. 2006; Li and Peng 2002; Nieto-Cid et al. 2005; Schneider et al. 2005), the other one focuses on fitting high-order polynomial models over the entire θ - S space (De La Fuente et al. 2014).

For our analysis we use the dataset obtained during a cruise carried out in the equatorial Atlantic Ocean in April–May 2010. The slopes, coefficients of correlation, and the significance of the relationships between the anomalies obtained from both approaches are evaluated. The differences in these relationships are then examined, and the strengths and weaknesses of both methods are discussed. Finally, the potential of the nonlinear-global method is also illustrated, calculating the stoichiometric ratio between oxygen and nitrate.

2. Measurements

Measurements were obtained from 26 full-depth hydrographic stations during the MOC2-Equatorial cruise, carried out along 7.5°N in the equatorial Atlantic Ocean on board R/V *Hespérides* between 20 April and 13 May 2010 (Fig. 1); data are available at the Carbon Hydrographic Data Office (<https://cchdo.ucsd.edu/cruise/29HE20100405>). Continuous salinity and temperature profiles were recorded with a Sea-Bird 911plus CTD

system attached to a 24 Niskin rosette sampler. Water samples at 24 levels were used to determine the concentrations of dissolved oxygen (DO), nitrate (NO_3), and FDOM. For this study we have considered only those levels deeper than 200 m (ocean interior).

DO water samples were taken in sealed flasks (250 mL) and kept in the dark for 24 h until their analysis. DO was determined using an automated potentiometric modification of the original Winkler method following WOCE standards (Culbertson 1994) with a precision of $\pm 0.5 \mu\text{mol kg}^{-1}$. AOU is defined as the deficit of oxygen concentration relative to its atmospheric saturation value under equal physical conditions (Benson and Krause 1984; Weiss 1970).

NO_3 water samples were collected in stoppered polypropylene conical centrifuge tubes (15 mL). The samples were fitted directly onto the AutoSampler of a four-channel Technicon Bran+Luebbe AutoAnalyzer II (AAII) for determining nitrates and nitrites by continuous flow analysis (Tréguer and Le Corre 1975).

FDOM water samples were collected in acidclean glass bottles of 250 mL and analyzed on board within 2 h after sampling at the ship laboratory temperature (ca. 20°C) with a PerkinElmer LS spectrometer equipped with a xenon discharge lamp. Slit widths were 10 nm for the excitation and emission wavelengths. Measurements were performed in a 1-cm quartz cell, and Milli-Q water was used as a reference blank. The fluorescence intensity was measured at fixed excitation/emission wavelengths of 340/440 nm, F(340/440), characteristic of humic-like substances (Coble 1996), and normalized to Raman units (RU) according to Lawaetz and Stedmon (2009).

3. Methods

As exposed in the introduction, almost all previous studies on regeneration ratios assume that the conservative fraction of a biogeochemical variable arises as a linear combination of three end-members. The essence

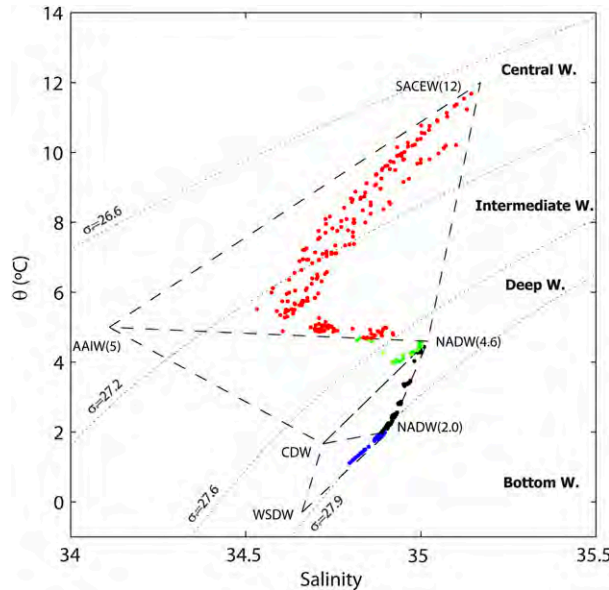


FIG. 2. The θ - S diagram with the biogeochemical stations data, split in mixing triangles as follows: NADW(2.0)-CDW-WSDW (blue dots), NADW(4.6)-NADW(2.0)-CDW (black dots), AAIW(5)-NADW(4.6)-CDW (green dots), and SACEW(12)-AAIW(5)-NADW(4.6) (red dots). The isopycnals (σ_θ) 26.6, 27.2, 27.6, and 27.9 (gray lines), approximately corresponding to the isoneutrals (γ^n) 26.65, 27.3, 27.8, and 28.12, are used to divide the water column into the following isoneutral strata: central (26.65–27.3), intermediate (27.3–27.8), deep (27.8–28.12), and bottom (>28.12).

of the approach may be understood by considering the closed system of equations that represents any data point as the conservative combination of three water types:

$$\begin{aligned}\theta &= x_a \theta_a + x_b \theta_b + x_c \theta_c, \\ S &= x_a S_a + x_b S_b + x_c S_c, \\ 1 &= x_a + x_b + x_c.\end{aligned}\quad (1)$$

For any data point in the (θ, S) space that falls inside a triangle closed by the end-members (θ_a, S_a) , (θ_b, S_b) , and (θ_c, S_c) , there is one unique solution for the end-member fractions x_a, x_b, x_c ; for example, $x_a = x_a(\theta, S, \theta_a, \theta_b, \theta_c, S_a, S_b, S_c)$. For fixed properties of the end-members, this expression turns into a linear functional dependence $x_a = x_a(\theta, S)$. Hence, the conservative fraction of any property with concentration Y that follows a linear combination of the values of the three end-members can be expressed as

$$Y = x_a(\theta, S)Y_a + x_b(\theta, S)Y_b + x_c(\theta, S)Y_c. \quad (2)$$

This is a linear expression of θ and S that relies on the mixing of three end-members in the (θ, S) space, commonly calculated by adjusting the predictions to the data points in a least squares sense (sometimes including a

TABLE 1. Thermohaline characteristics of the SWTs from [Álvarez et al. \(2014\)](#).

| SWT, full name | SWT, abbreviated | θ ($^{\circ}\text{C}$) | S |
|--|------------------|---------------------------------|-------|
| South Atlantic Central Subequatorial Water | SACEW(12) | 12.00 | 35.17 |
| Antarctic Intermediate Water | AAIW(5) | 5.00 | 34.11 |
| Upper and Middle North Atlantic Deep Water | NADW(4.6) | 4.60 | 35.02 |
| Lower North Atlantic Deep Water | NADW(2.0) | 2.02 | 34.91 |
| Upper and Lower Circumpolar Deep Water | CDW | 1.66 | 34.72 |
| Weddell Sea Deep Water | WSDW | -0.30 | 34.66 |

regeneration or consumption term). However, mixing of more than three end-members or the existence of preferential mixing pathways, such as along isopycnals, will lead to nonlinear relations.

a. MLR

For each nonconservative response variable Y —such as $F(340/440)$, AOU, or NO_3 —a multiple linear regression (MLR) model is applied in terms of the conservative thermohaline predictor variables— S and θ ([Carlson et al. 2010](#); [Castro et al. 2006](#); [Nieto-Cid et al. 2005](#); [Schneider et al. 2005](#)). All data in the θ - S plane are made to correspond to three end-member mixing triangles ([Fig. 2](#)), with the source water types as defined in [Álvarez et al. \(2014\)](#) ([Table 1](#)), ensuring that each observation is explained as a mixture of up to three source waters.

The biogeochemical variables are modeled as follows:

$$\hat{Y}_{ik} = \alpha_{0k} + \alpha_{1k}S_{ik} + \alpha_{2k}\theta_{ik}, \quad (3)$$

where ik is the i sample observation out of a total of nk observations in the respective k mixing triangle. For each ik (θ, S) pair, the anomaly from the model ΔY_{ik} is obtained by subtracting the value estimated through the optimal model (\hat{Y}_{ik}) from the observed value (Y_{ik}):

$$\Delta Y_{ik} = Y_{ik} - \hat{Y}_{ik}. \quad (4)$$

The unknown parameters (α_{0k} , α_{1k} , and α_{2k}) are determined using an ordinary least squares (OLS) fitting, that is, minimizing the summed square of ΔY_{ik} .

For each mixing triangle and variable [$F(340/440)$, AOU, or NO_3], the significance of the model is tested through the F statistic [$\text{Pr}(>|F|)$ with p value < 0.01]; the variance captured by the model is evaluated through the adjusted coefficient of determination, adjusted r squared ($\text{adj-}r^2$) ([Table S1](#), supplemental materials); and the significance of the estimated coefficients is tested through a Student's t statistic [$\text{Pr}(>|t|)$ with p value < 0.05].

b. PR

An alternative approach consists of a multiple non-linear polynomial regression (PR) between each non-conservative response variable Y and the conservative thermohaline predictor variables for the entire (θ, S) space. De La Fuente et al. (2014) used a quadratic polynomial (PR2) to model the biogeochemical variable. It includes all linear and quadratic terms in θ and S , as well as a nonlinear dependence on the product of θ and S :

$$\hat{Y}_i = \alpha_0 + \alpha_1 S_i + \alpha_2 \theta_i + \alpha_3 S_i^2 + \alpha_4 \theta_i^2 + \alpha_5 \theta_i S_i. \quad (5)$$

where i is the sample observation out of a total of n observations in the dataset. The anomalies are obtained through an expression analogous to Eq. (4):

$$\Delta Y_i = Y_i - \hat{Y}_i. \quad (6)$$

We expect that the higher the order of the polynomial, the better the data fit and the lower the anomalies. However, a high-order polynomial is not necessarily a good solution because each additional term may lead to a minimal improvement in the solution. A useful tool to ensure that these new high-order terms are meaningful is the Akaike information criterion (AIC), which rewards the goodness of fit (as assessed by the likelihood function) but penalizes the excess of parameters; so, the lower the AIC, the better the model (Zuur et al. 2009). Through a stepwise selection process that uses the AIC, we increase the complexity of the polynomial and come up with two new PR models; these models are particular cases of the full cubic polynomial (Table S2, supplemental materials) as explained next.

The second PR model (PR3) is similar to PR2 but with the cubic term in θ replacing the quadratic term in S :

$$\hat{Y}_i = \alpha_0 + \alpha_1 S_i + \alpha_2 \theta_i + \alpha_4 \theta_i^2 + \alpha_5 \theta_i S_i + \alpha_7 \theta_i^3. \quad (7)$$

The third PR model (PRcub) includes all quadratic and three cubic terms (this is the full cubic polynomial except for the S^3 term):

$$\begin{aligned} \hat{Y}_i = & \alpha_0 + \alpha_1 S_i + \alpha_2 \theta_i + \alpha_3 S_i^2 + \alpha_4 \theta_i^2 + \alpha_5 \theta_i S_i \\ & + \alpha_7 \theta_i^3 + \alpha_8 S_i \theta_i^2 + \alpha_9 S_i^2 \theta_i. \end{aligned} \quad (8)$$

For each of the abovementioned models, the unknown parameters (α_i) are determined using an OLS fitting, that is, minimizing the anomalies [Eq. (6)]. The significance of the model is tested through the F statistic [$\Pr(>|F|)$ with p value < 0.01], the variance captured by the model is evaluated through the $\text{adj-}r^2$ (Table S3, supplemental materials), and the significance of the estimated coefficients is tested through the Student's t test [$\Pr(>|t|)$ with p value < 0.05].

c. Anomaly analysis

1) DEFINITION OF WATER STRATA

To compare the behavior of all four models (MLR, PR2, PR3, and PRcub), the water column (depths greater than 200 m) in the region of study is divided in four water strata (central, intermediate, deep, and bottom) that correspond to different isoneutral (γ^n) ranges (San Antolín Plaza et al. 2012) (Fig. 2; see Table 1 for the nomenclature of the different water types). The mixing triangle defined by SACEW(12)–AAIW(5)–NADW(4.6) corresponds to central ($26.65 > \gamma^n < 27.3$) and intermediate ($27.3 > \gamma^n < 27.8$) waters (Álvarez et al. 2014; Arhan et al. 1998; San Antolín Plaza et al. 2012; Stramma and Schott 1999). The mixing triangles defined by AAIW(5)–NADW(4.6)–CDW and NADW(4.6)–CDW–NADW(2.0) conform to deep waters, approximately delimited by the $27.8 > \gamma^n < 28.12$ isoneutral range, with a major contribution from NADW (Álvarez et al. 2014; San Antolín Plaza et al. 2012; Stramma and Schott 1999). The mixing triangle defined by WSDW–CDW–NADW(2.0) includes bottom waters ($\gamma^n > 28.12$), with a predominance of AABW (Álvarez et al. 2014; San Antolín Plaza et al. 2012; Stramma and Schott 1999). Computation of γ^n is performed following McDougall and Barker (2011).

2) BIOGEOCHEMICAL SIGNIFICANCE OF THE ANOMALIES

The biogeochemical anomalies— $\Delta\text{F}(340/440)$, ΔAOU , and ΔNO_3 —are determined using the MLR and PR approaches for the entire ocean, as well as for each water stratum. For each model, the relationships between each pair of anomalies are then calculated by means of a simple linear regression II [standard major axis (SMA)] that takes into account the variability of both variables. This includes the slope of the linear regression together with the corresponding adjusted correlation coefficient ($\text{adj-}r^2$) and the significance of the test (p value < 0.05).

In this study we use the $\text{adj-}r^2$ for the biogeochemical anomalies in order to identify which model (MLR, PR2, PR3, and PRcub) best removes the conservative contributions. Under the assumption that all anomalies respond to related nonconservative processes (Álvarez-Salgado et al. 2013; Catala et al. 2015; Chen and Bada 1992; De La Fuente et al. 2014; Hayase and Shinozuka 1995; Hayase et al. 1989; Jørgensen et al. 2011; Yamashita and Tanoue 2008; Yamashita et al. 2007), we expect that the model that best captures the conservative behavior will lead to anomalies that retain most of the variability associated with the biogeochemical processes, that is, will lead to the highest correlation among the anomalies.

All statistical analyses are carried out with the statistical programming software R, version 0.97.551, using the package “smatr” (Warton et al. 2012; <https://cran.r-project.org/web/packages/smatr/index.html>).

4. Results

a. Model analysis

The MLR approach proposes that the physicochemical variability of a biogeochemical variable (Y) is the outcome of the linear mixing of up to three water masses. For each mixing triangle and variable, Eq. (3) defines a plane in the three-dimensional space (θ – S – Y); in contrast, the PR methods predict a single and continuous surface for each variable, $Y = Y(\theta, S)$ (Figs. 3 and S1 in supplemental materials).

The MLR and the three PR models (PR2, PR3, and PRcub) are applied to $F(340/440)$, AOU, and NO_3 . The projection of the triangular planes on the θ – S domain leads to the three-end-member mixing triangles concept, where any θ – S point belongs to one single triangle. However, the projection of the data to the other two planes, either $S = S(\theta, Y)$ or $\theta = \theta(S, Y)$, shows substantial overlapping between mixing triangles, particularly in the S – Y plane (Figs. 3 and S1 in supplemental materials). This may be interpreted as indicative of a nonconservative contribution to the Y variable, but it may also reflect the intrinsic limitations when choosing a maximum of three end-members for conservative mixing.

The model statistics—AIC, $\text{adj-}r^2$, and Fisher’s p value—are presented in Tables S1 and S3 (supplemental materials). These statistics show that all models are highly significant (p value < 0.001), yet PR3 and particularly PRcub provide the highest $\text{adj-}r^2$ values.

b. Anomaly analysis: Remineralization ratios

Applying the MLR method to each individual stratum and applying the PR2, PR3, and PRcub methods to the entire ocean interior (Table S2, supplemental materials), we find the anomaly ratios to always be significant (p value < 0.05), except for the $\Delta F(340/440)$ – ΔNO_3 relationship in bottom waters when using the PR2 method (Tables 2–4). When considering the entire water column (depths greater than 200 m), all methods except PRcub give similar slopes and $\text{adj-}r^2$ coefficients. When looking at the results of MLR, PR2, and PR3 per water stratum, all slopes and $\text{adj-}r^2$ are very much alike in the central and intermediate strata but show some significant differences in the deep and bottom strata (Tables 2–4). In these deep and bottom waters, PR3 gives the highest correlation coefficients and the values closest to the mean-depth values, except for ΔAOU – ΔNO_3 in bottom waters. In contrast, for most water strata PRcub leads to

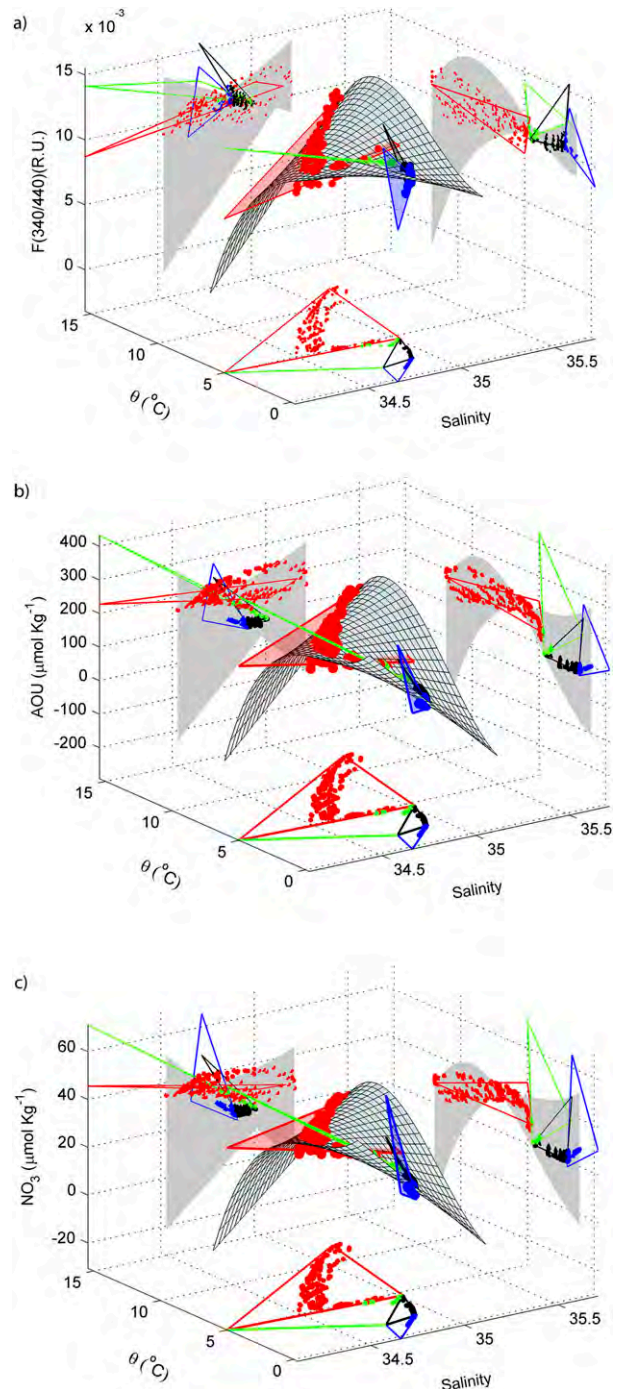


FIG. 3. (a) Three-dimensional representation of the PR3 (surface) and MLR (planes) predictions for $F(340/440)$ as a function of S and θ ; the colors of the lines and dots define the different planes used by MLR as follows: NADW(2.0)–CDW–WSDW (blue), NADW(4.6)–NADW(2.0)–CDW (black), AAIW(5)–NADW(4.6)–CDW (green), and SACEW(12)–AAIW(5)–NADW(4.6) (red). The θ – S diagram corresponds to the projection onto the bottom plane; similar projections are drawn on the $F(340/440)$ – S and θ – $F(340/440)$ planes with the shaded area corresponding to the 2D projection on the respective surface. (b) As in (a), but using AOU rather than $F(340/440)$. (c) As in (a), but using NO_3 rather than $F(340/440)$.

TABLE 2. Relationship of $\Delta F(340/440)$ with ΔAOU for the MLR, PR2, PR3, and PRcub methods, as deduced using an SMA regression. The slope of the linear regression (slope), the adjusted correlation coefficient ($\text{adj-}r^2$), the significance of the test (p value with $\alpha = 0.05$), and the total sampling points (n) are shown for the ocean interior and each water strata (central, intermediate, deep, and bottom). The slope is shown only for significant relationships (p value < 0.05).

| $\Delta F(340/440)-\Delta AOU$ | | | | | |
|--------------------------------|----------|----------------------------|------------------|-----------|-----|
| Water strata | Approach | Slope ($\times 10^{-5}$) | $\text{adj-}r^2$ | p value | n |
| Ocean interior | MLR | 2.9 ± 0.1 | 0.82 | <0.001 | 355 |
| | PR2 | 3.1 ± 0.1 | 0.79 | <0.001 | 355 |
| | PR3 | 3.5 ± 0.1 | 0.78 | <0.001 | 355 |
| | PRcub | 4.1 ± 0.1 | 0.59 | <0.001 | 355 |
| Central | MLR | 2.8 ± 0.1 | 0.92 | <0.001 | 96 |
| | PR2 | 2.9 ± 0.1 | 0.92 | <0.001 | 96 |
| | PR3 | 3.3 ± 0.1 | 0.90 | <0.001 | 96 |
| | PRcub | 3.8 ± 0.2 | 0.81 | <0.001 | 96 |
| Intermediate | MLR | 3.0 ± 0.1 | 0.80 | <0.001 | 102 |
| | PR2 | 3.1 ± 0.1 | 0.79 | <0.001 | 102 |
| | PR3 | 3.2 ± 0.1 | 0.76 | <0.001 | 102 |
| | PRcub | 4.7 ± 0.3 | 0.52 | <0.001 | 102 |
| Deep | MLR | 5.5 ± 0.0 | 0.31 | <0.001 | 127 |
| | PR2 | 4.8 ± 0.0 | 0.57 | <0.001 | 127 |
| | PR3 | 3.6 ± 0.2 | 0.60 | <0.001 | 127 |
| | PRcub | 4.3 ± 0.3 | 0.47 | <0.001 | 127 |
| Bottom | MLR | 9.7 ± 0.1 | 0.61 | <0.001 | 30 |
| | PR2 | 9.5 ± 0.0 | 0.20 | <0.001 | 30 |
| | PR3 | 6.4 ± 0.4 | 0.80 | <0.001 | 30 |
| | PRcub | 3.9 ± 0.7 | 0.26 | <0.01 | 30 |

slopes that are quite different from the other methods, with much lower $\text{adj-}r^2$.

The scattered plots of the biogeochemical anomalies help visualize the high correlation achieved by MLR, PR2, and PR3 (Figs. 4–6). The data points for the original variables appear clustered by water stratum; in contrast, the anomalies closely fall into one single regression line. Despite the similarity between all the methods, it is ostensible that the anomalies calculated by both MLR and PR3 remain closer to the regression line. It is worthwhile pointing out the high correlation between ΔAOU and ΔNO_3 —in excess of 0.9 for MLR, PR2, and PR3—which provides a mean slope for the entire ocean interior of 8.0 ± 0.1 . This value is in fairly good agreement with the global-average 138:16 stoichiometric $-O_2:N$ ratio reported by Takahashi et al. (1985).

The abovementioned results confirm that PRcub is inadequate to retain the nonconservative signature. This model provides the best adjustment to the data, but the fit is so good that it gets rid of the variability caused by nonconservative processes. For this reason in the forthcoming discussion we have considered only the MLR, PR2, and PR3 models.

TABLE 3. As in Table 2, but for $\Delta F(340/440)$ with ΔNO_3 .

| $\Delta F(340/440)-\Delta NO_3$ | | | | | |
|---------------------------------|----------|----------------------------|------------------|-----------|-----|
| Water strata | Approach | Slope ($\times 10^{-4}$) | $\text{adj-}r^2$ | p value | n |
| Ocean interior | MLR | 2.3 ± 0.1 | 0.79 | <0.001 | 338 |
| | PR2 | 2.6 ± 0.1 | 0.73 | <0.001 | 338 |
| | PR3 | 2.8 ± 0.1 | 0.71 | <0.001 | 338 |
| | PRcub | 2.9 ± 0.1 | 0.48 | <0.001 | 338 |
| Central | MLR | 2.3 ± 0.1 | 0.92 | <0.001 | 91 |
| | PR2 | 2.4 ± 0.1 | 0.92 | <0.001 | 91 |
| | PR3 | 2.7 ± 0.1 | 0.92 | <0.001 | 91 |
| | PRcub | 2.9 ± 0.1 | 0.75 | <0.001 | 91 |
| Intermediate | MLR | 2.2 ± 0.1 | 0.77 | <0.001 | 98 |
| | PR2 | 2.3 ± 0.1 | 0.76 | <0.001 | 98 |
| | PR3 | 2.4 ± 0.1 | 0.70 | <0.001 | 98 |
| | PRcub | 3.1 ± 0.2 | 0.39 | <0.001 | 98 |
| Deep | MLR | 3.7 ± 0.3 | 0.14 | <0.001 | 119 |
| | PR2 | 3.6 ± 0.3 | 0.40 | <0.001 | 119 |
| | PR3 | 3.0 ± 0.2 | 0.50 | <0.001 | 119 |
| | PRcub | 3.0 ± 0.2 | 0.36 | <0.001 | 119 |
| Bottom | MLR | 8.7 ± 2.0 | 0.30 | <0.01 | 30 |
| | PR2 | — | — | 0.92 | 30 |
| | PR3 | 5.8 ± 0.8 | 0.40 | <0.001 | 30 |
| | PRcub | 2.3 ± 0.5 | 0.17 | <0.05 | 30 |

5. Discussion

In this study we have used the MLR and PR approaches to assess what portion of the distribution of a biogeochemical variable is related to the conservative

TABLE 4. As in Table 2, but for ΔAOU with ΔNO_3 .

| $\Delta AOU-\Delta NO_3$ | | | | | |
|--------------------------|----------|---------------|------------------|-----------|-----|
| Water strata | Approach | Slope | $\text{adj-}r^2$ | p value | n |
| Ocean interior | MLR | 8.0 ± 0.1 | 0.95 | <0.001 | 376 |
| | PR2 | 8.0 ± 0.1 | 0.94 | <0.001 | 376 |
| | PR3 | 8.0 ± 0.1 | 0.92 | <0.001 | 376 |
| | PRcub | 7.0 ± 0.1 | 0.84 | <0.001 | 376 |
| Central | MLR | 8.1 ± 0.1 | 0.97 | <0.001 | 100 |
| | PR2 | 8.4 ± 0.1 | 0.97 | <0.001 | 100 |
| | PR3 | 8.3 ± 0.2 | 0.94 | <0.001 | 100 |
| | PRcub | 7.7 ± 0.2 | 0.87 | <0.001 | 100 |
| Intermediate | MLR | 7.4 ± 0.1 | 0.96 | <0.001 | 107 |
| | PR2 | 7.4 ± 0.1 | 0.95 | <0.001 | 107 |
| | PR3 | 7.4 ± 0.1 | 0.94 | <0.001 | 107 |
| | PRcub | 6.5 ± 0.3 | 0.77 | <0.001 | 107 |
| Deep | MLR | 6.5 ± 0.3 | 0.61 | <0.001 | 133 |
| | PR2 | 7.5 ± 0.3 | 0.75 | <0.001 | 133 |
| | PR3 | 8.0 ± 0.2 | 0.88 | <0.001 | 133 |
| | PRcub | 6.7 ± 0.2 | 0.83 | <0.001 | 133 |
| Bottom | MLR | 9.0 ± 1.3 | 0.36 | <0.001 | 36 |
| | PR2 | 4.7 ± 0.5 | 0.63 | <0.001 | 36 |
| | PR3 | 9.0 ± 0.8 | 0.70 | <0.001 | 36 |
| | PRcub | 6.0 ± 0.2 | 0.94 | <0.001 | 36 |

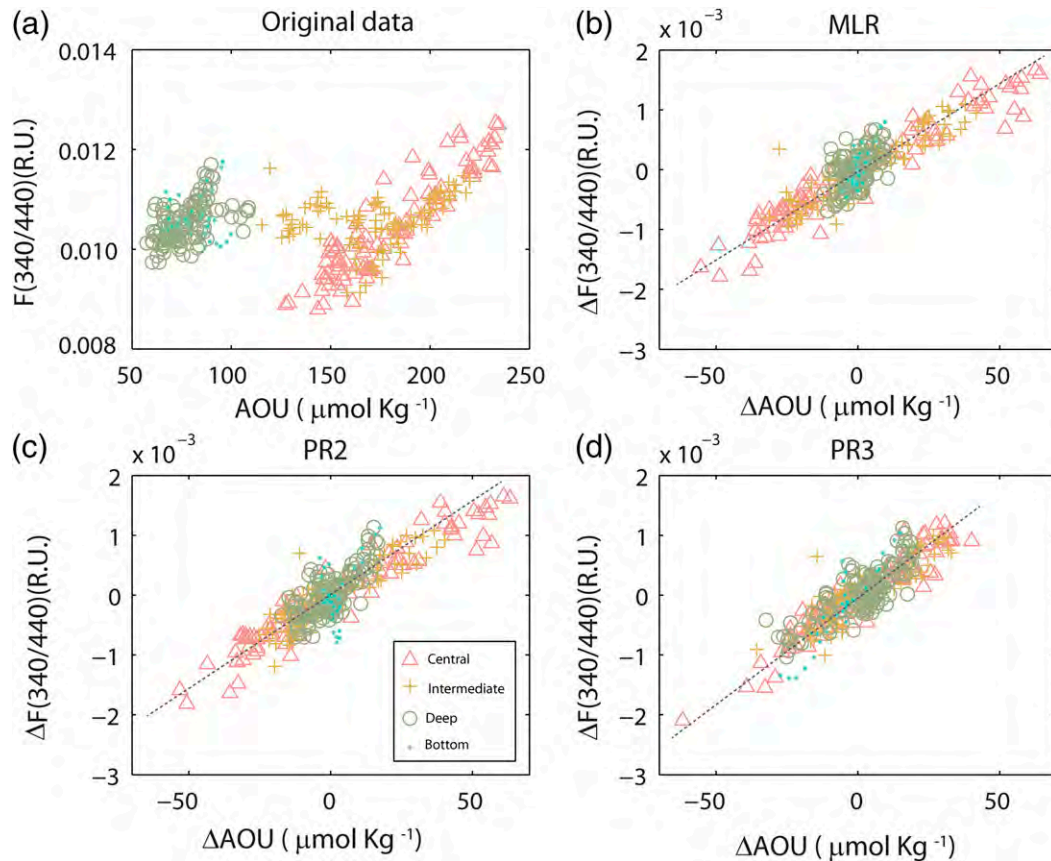


FIG. 4. Scattered plots for the biogeochemical variables: (a) $F(340/440)$ – AOU using the original data; $\Delta F(340/440)$ – ΔAOU after using the (b) MLR, (c) PR2, and (d) PR3 approaches, with the regression lines (p value < 0.05 ; dotted gray lines). The different water strata are indicated: central waters (red triangles), intermediate waters (orange crosses), deep waters (gray circles), and bottom waters (blue dots).

thermohaline properties, that is, to examine what fraction corresponds to the water properties at origin. The differences between the modeled values and the observations are hence identified as biogeochemical anomalies. Both the MLR and PR approaches involve regressions for the nonconservative variables as a function of θ and S over the entire (θ, S) space. However, the MLR method uses a linear regression over a confined three-end-member mixing domain, while the PR method uses a nonlinear and global regression.

The general good agreement between the MLR and PR models is an important result, showing that the PR models may replace the classical MLR methods. Its relevance arises because the PR method has no constraint or subjective criterion in the selection of the water masses involved in the conservative mixing. Further, the behavior of PR3 for the deep and bottom strata represents a substantial improvement in the quality of the results.

The MLR method requires identifying the water masses involved in the conservative mixing (i.e., end-member

water mass definition and mixing triangles), which is often a difficult task (Carlson et al. 2010; Castro et al. 2006; Li and Peng 2002; Nieto-Cid et al. 2005). Further, in the MLR approach, the thermohaline characteristics arise from a set of vertically ordered mixing triangles, where any data point has to be inside a triangle delimited by three end-members in the (θ, S) plane. These assumptions cause two principal limitations in the MLR predictive skill of a biogeochemical variable Y that directly affect the anomalies. First, any forecast is a linear combination of three water types, with the outcome depending heavily on the end-member definitions that set the data clusters. Second, the predictions are segmented into distinct subgroups, with artificial ocean boundaries or discontinuities in the (θ, S, Y) space (Mamayev 1975; Tomczak 1981; Pérez et al. 1998; You 2002).

In contrast with the MLR method, the PR approaches allow high-order (nonlinear) dependences of the biogeochemical variables on both θ and S . One should keep in mind that water masses have preferential oceanic pathways along constant density surfaces. Therefore,

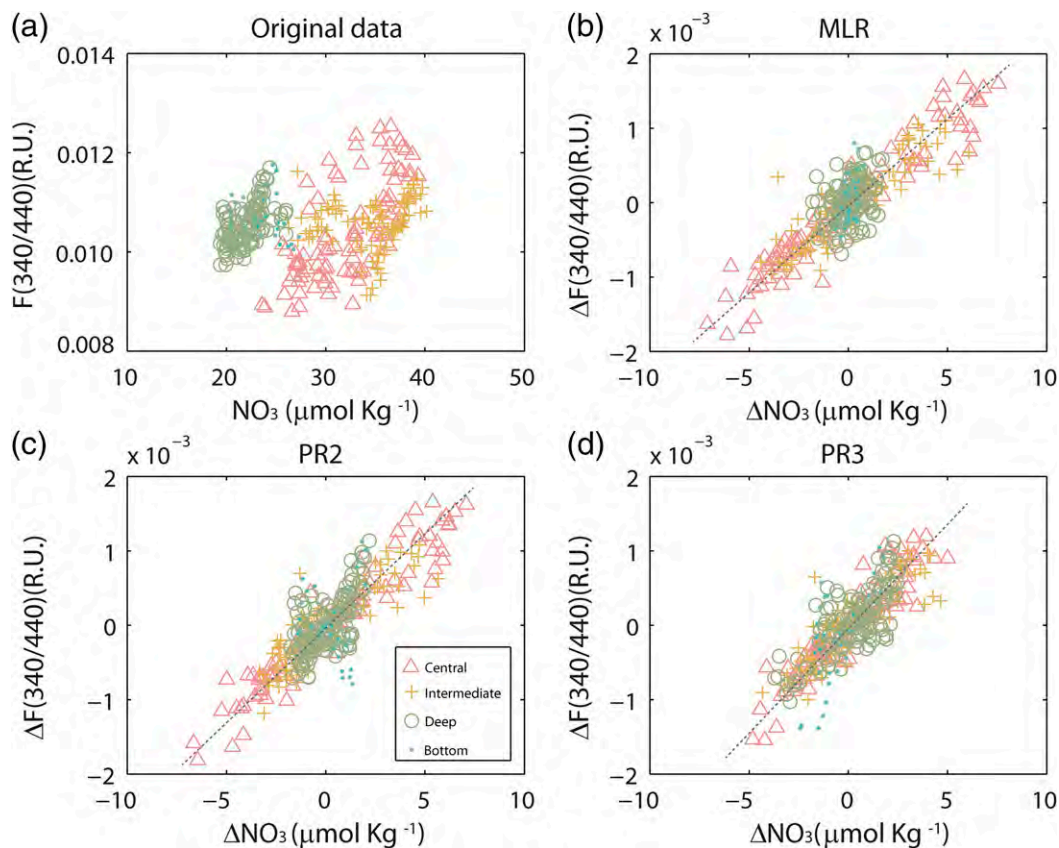


FIG. 5. Scattered plots as in Fig. 4, but for $F(340/440)$ – NO_3 .

since density displays a nonlinear dependence with temperature and salinity (the equation of state), we may expect that the water masses will not mix linearly in the θ – S space, in contrast to the mixing triangle concept. Actually, it is remarkable that the PR3 method has terms with the same temperature and salinity dependences as the leading terms in the equation of state, in consonance with the idea that the predominant mixing of biogeochemical variables occurs along isopycnal surfaces. Recently, several works have pointed out the importance of these nonlinear dependences in the context of the global overturning circulation (Klocker and McDougall 2010; Nycander et al. 2015).

In terms of the anomaly correlation slopes and coefficients, the MLR, PR2, and PR3 methods give similar results for either the entire or the surface/intermediate fractions of the water column (Figs. 4–6), but PR3 provides higher correlation coefficients for the deep and bottom waters (Tables 2–4). The largest differences among the methods correspond to the bottom waters: PR2 leads to anomaly scattered plots that have the same pattern as the original data [especially for $\Delta F(340/440)$ – ΔNO_3 where the correlation is nonsignificant], while both MLR and PR3

show significant correlations among anomalies, although the range of values is smaller for MLR than for PR3 (Figs. 7 and S2 in supplemental materials).

We have also explored another polynomial model—PRcub—which retains all terms up to third order except the S^3 term. This model shows high skill replicating the biogeochemical variables. However, the associated anomalies bear relatively low linear correlation, hence indicating that the model removes most of the nonconservative signal. This particular instance points to the importance of the second methodological step—the analysis of the anomalies—when selecting the most adequate polynomial regression model.

These results strongly suggest that MLR, PR2, and PR3 do equally well for the surface and intermediate strata, and they indicate that PR3 does better in the deep and bottom waters, identifying the conservative fraction much better than PR2 and yet conserving the biogeochemical signal better than MLR (i.e., a local mixing triangle can fit the predictions very well to the data so the anomalies lose their nonconservative signal). Further, the PR3 method appears capable of unraveling the eastern and western bottom water masses (separated by the

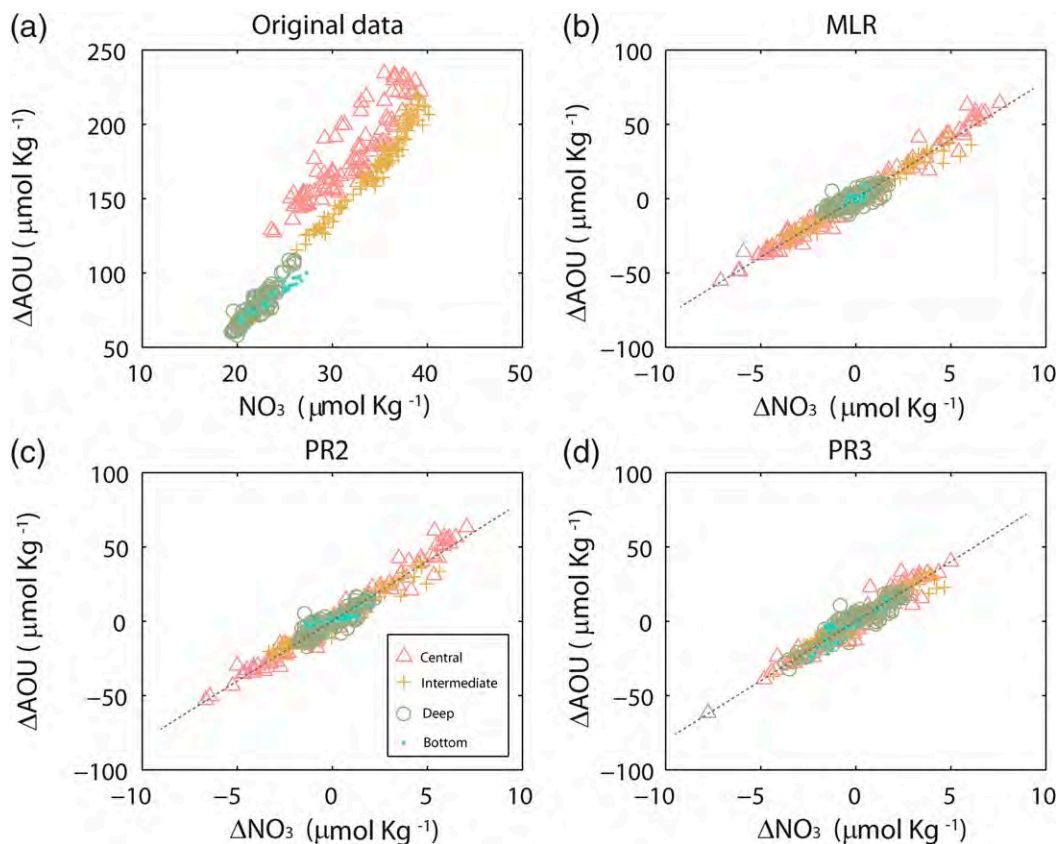


FIG. 6. Scattered plots as in Fig. 4, but for AOU–NO₃.

Mid-Atlantic Ridge) (Figs. 7 and S2 in supplemental materials). The anomaly linear regression is set predominantly by the data in the eastern basin, influenced by the African upwelling where major remineralization processes take place (Peña-Izquierdo et al. 2015). The data from the western basin shows little dependence of the F(340/440) anomalies on NO₃ and AOU, probably as a consequence of input of humic-organic-matter sediments.

Our results have shown that the humic-organic-matter PR method, originally used to study the FDOM distributions in the deep ocean (De La Fuente et al. 2014), has good skill at distinguishing between the conservative and nonconservative contributions to biogeochemical variables. The method has two main advantages: conceptual (as nonlinear mixing is allowed) and operative (as it does not require identifying mixing triangles). The potential of the method has also been illustrated with the AOU and NO₃ concentrations, rendering an oxygen–nitrogen Redfield ratio close to values reported in the literature. It is important to note that the biogeochemical properties mix as temperature and salinity (this is why we can make the regression), but their values at origin ought to be independent [see the discussion at the beginning of the

methods section (section 3)]; if these water type properties depend on temperature and salinity, then the method may not work. This is precisely what happens (not shown) if we apply the PR method directly to dissolved oxygen, as this quantity has a complex nonlinear dependence on both θ and S . This limitation is removed when we work with the AOU, simply because we are removing the oxygen saturation at origin.

6. Conclusions

We have presented a simple objective methodology for resolving the nonconservative fraction of biogeochemical variables. Briefly, it first models the data with a nonlinear temperature and salinity polynomial and then calculates the anomalies as the difference between observation and prediction. Our main contribution has been to show that the polynomial regression can produce a fit to data in the entire domain that is as good as or better than a classical local linear mixing approach, and to illustrate that the best polynomial is not one that produces the best data fit but one that leads to anomalies that are highly correlated. This is based on the idea that

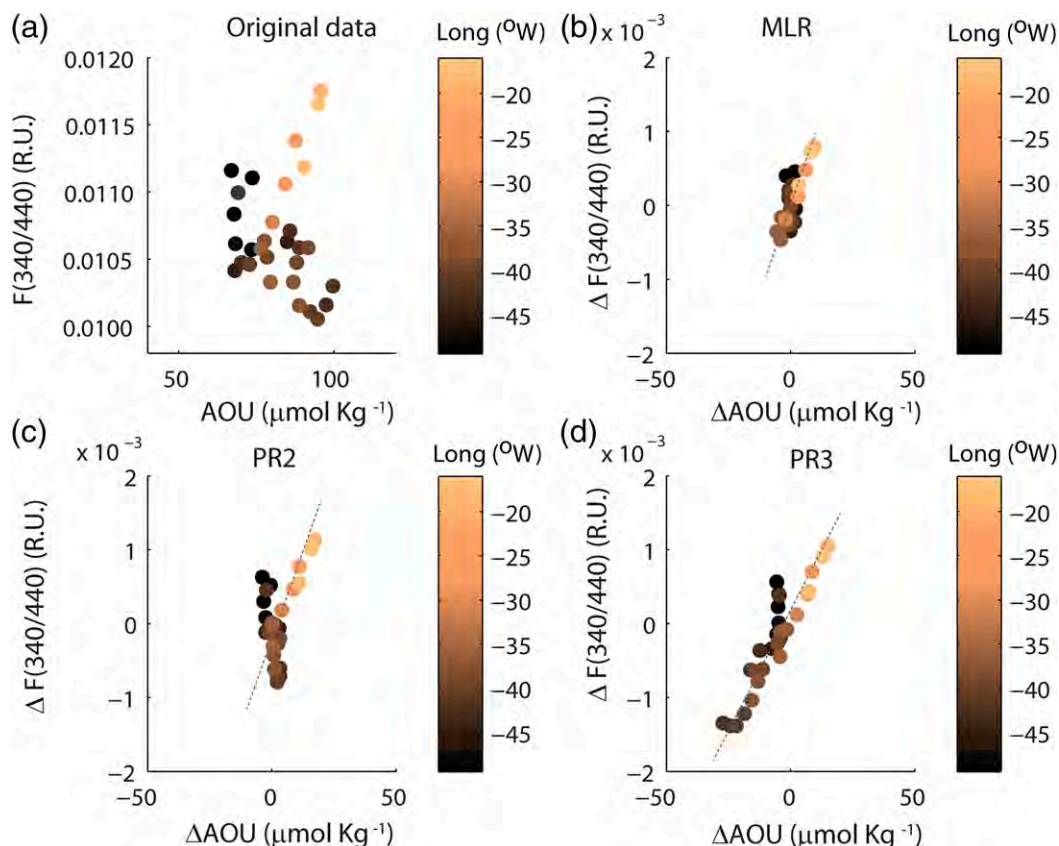


FIG. 7. Scattered plots for $F(340/440)$ – AOU as in Fig. 4, but only for the data points within the bottom water stratum and the color code indicating the longitude of the water sample.

a high correlation between different property anomalies is the outcome of one or several biogeochemical processes simultaneously acting on all properties.

The traditional multiple linear regression (MLR) approach assumes that any water parcel results from the linear combination of up to three water types and hence the conservative fraction of its biogeochemical properties retains this same linear combination. Here, instead, we have assumed that a water parcel results from the nonlinear mixing of an undefined number of water masses, which is expressed through a polynomial function in terms of both (θ, S) , what we have named the polynomial regression (PR) approach.

We have explored the behavior of the MLR as well as several versions of the PR. A high-order polynomial (PRcub) produces the best fit (in terms of statistical criteria and AIC) to the observations. However, the adjustment is so good that the anomalies lose their nonconservative signal, as shown by the low correlation between related biogeochemical properties. Contrarily, MLR and two polynomials of relatively low order (PR2 and PR3) have lower adjustment to the biogeochemical

data but lead to anomalies that bear much higher correlation.

Considering the entire water column of the equatorial North Atlantic, we find that the PR3 biogeochemical anomalies are well correlated, as good as for MLR and better than for a quadratic polynomial (PR2). For each individual stratum, the major discrepancy between the results from the MLR and PR approaches occurs in deep waters and particularly in bottom waters, where PR3 does substantially better than either PR2 or MLR; further, within each of these water strata, PR3 retains a larger range of variations than MLR, suggesting that the latter approach removes some of the nonconservative fraction.

The PR3 methodology also shows good potential for complementary calculations. One example is its ability to identify differences in behavior within the western and eastern Atlantic basins, which may be related to the resuspension of sedimentary organic matter to the west versus the intense biogeochemical processes to the east. Another remarkable instance is its good skill in calculating Redfield regeneration ratios.

The proposed methodology renders a simple and objective way to identify the nonconservative anomalies for any ocean biogeochemical variable. For our transoceanic cruise in the equatorial North Atlantic, the optimum predictor of the conservative fraction of a biogeochemical variable corresponds to a PR cubic in temperature, linear in salinity, and with one single nonlinear term, but this may change for other regions. Once the particular polynomial is obtained, the spatial and/or temporal distribution of both physical and biogeochemical contributions can be easily calculated, lending information not only on the biogeochemical processes and stoichiometric ratios but also on the patterns of connectivity within a certain region.

Acknowledgments. We thank the assistance from the crew and technicians of the R/V *Hespérides* during the MOC2-Equatorial cruise. We are grateful to Fiz Pérez and Noelia Fajar for the oxygen calculations on board the vessel, and Xosé Anton Álvarez-Salgado for the methodological and scientific advice. This research was supported by the Spanish government through projects MOC2 (CTM2008-06438-CO2) and VA-DE-RETRO (CTM2014-56987-P). Patricia De La Fuente would like to thank the Agència de Gestió d'Ajuts Universitaris i de Recerca de la Generalitat de Catalunya (AGAUR) for its financial support through an FI-AGAUR fellowship.

REFERENCES

- Álvarez, M., S. Brea, H. Mercier, and X. A. Álvarez-Salgado, 2014: Mineralization of biogenic materials in the water masses of the South Atlantic Ocean. I: Assessment and results of an optimum multiparameter analysis. *Prog. Oceanogr.*, **123**, 1–23, <https://doi.org/10.1016/j.poccean.2013.12.007>.
- Álvarez-Salgado, X. A., M. Nieto-Cid, M. Álvarez, F. F. Pérez, P. Morin, and H. Mercier, 2013: New insights on the mineralization of dissolved organic matter in central, intermediate, and deep water masses of the northeast North Atlantic. *Limnol. Oceanogr.*, **58**, 681–696, <https://doi.org/10.4319/lo.2013.58.2.0681>.
- Arhan, M., H. Mercier, B. Bourle, and Y. Gouriou, 1998: Hydrographic sections across the Atlantic at 7°30N and 4°30S. *Deep-Sea Res. I*, **45**, 829–872, [https://doi.org/10.1016/S0967-0637\(98\)00001-6](https://doi.org/10.1016/S0967-0637(98)00001-6).
- Benson, B. B., and D. Krause, 1984: The concentration and isotopic fractionation of oxygen dissolved in freshwater and seawater in equilibrium with the atmosphere. *Limnol. Oceanogr.*, **29**, 620–632, <https://doi.org/10.4319/lo.1984.29.3.0620>.
- Carlson, C. A., D. A. Hansell, N. B. Nelson, D. A. Siegel, W. M. Smethie, S. Khatiwala, M. M. Meyers, and E. Halewood, 2010: Dissolved organic carbon export and subsequent remineralization in the mesopelagic and bathypelagic realms of the North Atlantic basin. *Deep-Sea Res. II*, **57**, 1433–1445, <https://doi.org/10.1016/j.dsr2.2010.02.013>.
- Castro, C. G., F. F. Pérez, S. E. Holley, and A. F. Ríos, 1998: Chemical characterisation and modelling of water masses in the Northeast Atlantic. *Prog. Oceanogr.*, **41**, 249–279, [https://doi.org/10.1016/S0079-6611\(98\)00021-4](https://doi.org/10.1016/S0079-6611(98)00021-4).
- , M. Nieto-Cid, X. A. Álvarez-Salgado, and F. F. Pérez, 2006: Local remineralization patterns in the mesopelagic zone of the Eastern North Atlantic, off the NW Iberian Peninsula. *Deep-Sea Res. I*, **53**, 1925–1940, <https://doi.org/10.1016/j.dsr.2006.09.002>.
- Catalá, T. S., and Coauthors, 2015: Turnover time of fluorescent dissolved organic matter in the dark global ocean. *Nat. Commun.*, **6**, 5986, <https://doi.org/10.1038/ncomms6986>.
- Chen, R. F., and J. L. Bada, 1992: The fluorescence of dissolved organic matter in seawater. *Mar. Chem.*, **37**, 191–221, [https://doi.org/10.1016/0304-4203\(92\)90078-O](https://doi.org/10.1016/0304-4203(92)90078-O).
- Coble, P. G., 1996: Characterization of marine and terrestrial DOM in seawater using excitation-emission matrix spectroscopy. *Mar. Chem.*, **51**, 325–346, [https://doi.org/10.1016/0304-4203\(95\)00062-3](https://doi.org/10.1016/0304-4203(95)00062-3).
- , 2007: Marine optical biogeochemistry: The chemistry of ocean color. *Chem. Rev.*, **107**, 402–418, <https://doi.org/10.1021/cr050350+>.
- Culbertson, C. H., 1994: Dissolved oxygen. WOCE operations manual, Vol. 3, Section 3.1, Part 3.1.3, Revision 1, WOCE Hydrographic Programme Office Rep. WHPO 91-1, WOCE Rep. 68/91, 15 pp., https://www.nodc.noaa.gov/woce/woce_v3/wocedata_1/whp/manuals/pdf/91_1/culber2.pdf.
- De La Fuente, P., C. Marrasé, A. Canepa, X. A. Álvarez-Salgado, M. Gasser, N. M. Fajar, C. Romera-Castillo, and J. L. Pelegrí, 2014: Does a general relationship exist between fluorescent dissolved organic matter and microbial respiration? The case of the dark equatorial Atlantic Ocean. *Deep-Sea Res. I*, **89**, 44–55, <https://doi.org/10.1016/j.dsr.2014.03.007>.
- Hansell, D. A., 2013: Recalcitrant dissolved organic carbon fractions. *Annu. Rev. Mar. Sci.*, **5**, 421–445, <https://doi.org/10.1146/annurev-marine-120710-100757>.
- Hayase, K., and N. Shinozuka, 1995: Vertical distribution of fluorescent organic matter along with AOU and nutrients in the equatorial Central Pacific. *Mar. Chem.*, **48**, 283–290, [https://doi.org/10.1016/0304-4203\(94\)00051-E](https://doi.org/10.1016/0304-4203(94)00051-E).
- , H. Tsubota, and I. Sunada, 1989: Relationships of fluorescence and AOU in three North Pacific water samples. *Sci. Total Environ.*, **81–82**, 315–318, [https://doi.org/10.1016/0048-9697\(89\)90138-1](https://doi.org/10.1016/0048-9697(89)90138-1).
- Hedges, J. I., R. G. Keil, and R. Benner, 1997: What happens to terrestrial organic matter in the ocean? *Org. Geochem.*, **27**, 195–212, [https://doi.org/10.1016/S0146-6380\(97\)00066-1](https://doi.org/10.1016/S0146-6380(97)00066-1).
- Jørgensen, L., C. A. Stedmon, T. Kragh, S. Markager, M. Middelboe, and M. Søndergaard, 2011: Global trends in the fluorescence characteristics and distribution of marine dissolved organic matter. *Mar. Chem.*, **126**, 139–148, <https://doi.org/10.1016/j.marchem.2011.05.002>.
- Klocker, A., and T. J. McDougall, 2010: Influence of the nonlinear equation of state on global estimates of diapycnal advection and diffusion. *J. Phys. Oceanogr.*, **40**, 1690–1709, <https://doi.org/10.1175/2010JPO4303.1>.
- Lawaetz, A. J., and C. A. Stedmon, 2009: Fluorescence intensity calibration using the Raman scatter peak of water. *Appl. Spectrosc.*, **63**, 936–940, <https://doi.org/10.1366/000370209788964548>.
- Li, Y.-H., and T.-H. Peng, 2002: Latitudinal change of remineralization ratios in the oceans and its implication for nutrient cycles. *Global Biogeochem. Cycles*, **16**, 1130, <https://doi.org/10.1029/2001gb001828>.
- Llanillo, P. J., J. Pelegrí, C. Duarte, M. Emelianov, M. Gasser, J. Gourrion, and A. Rodríguez-Santana, 2012: Meridional and zonal changes in water properties along the continental slope off central and northern Chile. *Cienc. Mar.*, **38**, 307–332, <https://doi.org/10.7773/cm.v38i1B.1814>.
- , J. Karstensen, J. L. Pelegrí, and L. Stramma, 2013: Physical and biogeochemical forcing of oxygen and nitrate changes

- during El Niño/El Viejo and La Niña/La Vieja upper-ocean phases in the tropical eastern South Pacific along 86°W. *Biogeosciences*, **10**, 6339–6355, <https://doi.org/10.5194/bg-10-6339-2013>.
- Mackas, D. L., K. L. Denman, and A. F. Bennett, 1987: Least-square multiple tracer analysis of water mass composition. *J. Geophys. Res.*, **92**, 2907–2918, <https://doi.org/10.1029/JC092iC03p02907>.
- Mamayev, O. I., 1975: *Temperature–Salinity Analysis of World Ocean Waters*. Elsevier Scientific, 374 pp.
- McDougall, T. J., and P. M. Barker, 2011: Getting started with TEOS-10 and the Gibbs Seawater (GSW) Oceanographic Toolbox. SCOR/IAPSO Working Group 127, 28 pp.
- Nieto-Cid, M., J. Gago, and F. F. Pérez, 2005: DOM fluorescence, a tracer for biogeochemical processes in a coastal upwelling system (NW Iberian Peninsula). *Mar. Ecol. Prog. Ser.*, **297**, 33–50, <https://doi.org/10.3354/meps297033>.
- Nycander, J., M. Hieronymus, and F. Roquet, 2015: The nonlinear equation of state of sea water and the global water mass distribution. *Geophys. Res. Lett.*, **42**, 7714–7721, <https://doi.org/10.1002/2015GL065525>.
- Peña-Izquierdo, J., E. van Sebille, J. L. Pelegrí, J. Sprintall, E. Mason, P. J. Llanillo, and F. Machín, 2015: Water mass pathways to the North Atlantic oxygen minimum zone. *J. Geophys. Res. Oceans*, **120**, 3350–3372, <https://doi.org/10.1002/2014JC010557>.
- Pérez, F. F., C. Mouriño, F. Fraga, and A. F. Rios, 1993: Displacement of water masses and remineralization rates off the Iberian Peninsula by nutrient anomalies. *J. Mar. Res.*, **51**, 869–892, <https://doi.org/10.1357/0022240933223891>.
- , A. F. Rios, C. G. Castro, and F. Fraga, 1998: Mixing analysis of nutrients, oxygen and dissolved inorganic carbon in the upper and middle North Atlantic ocean east of the Azores. *J. Mar. Syst.*, **16**, 219–233, [https://doi.org/10.1016/S0924-7963\(97\)00108-5](https://doi.org/10.1016/S0924-7963(97)00108-5).
- , and Coauthors, 2001: Mixing analysis of nutrients, oxygen and inorganic carbon in the Canary Islands region. *J. Mar. Syst.*, **28**, 183–201, [https://doi.org/10.1016/S0924-7963\(01\)00003-3](https://doi.org/10.1016/S0924-7963(01)00003-3).
- Reinthal, T., X. A. Álvarez Salgado, M. Álvarez, H. M. Van Aken, and G. J. Herndl, 2013: Impact of water mass mixing on the biogeochemistry and microbiology of the Northeast Atlantic Deep Water. *Global Biogeochem. Cycles*, **27**, 1151–1162, <https://doi.org/10.1002/2013GB004634>.
- San Antolín Plaza, M. Á., J. L. Pelegrí, F. J. Machín, and V. Benítez Barrios, 2012: Inter-decadal changes in stratification and double diffusion in a transatlantic section along 7.5°N. *Sci. Mar.*, **76**, 189–207, <https://doi.org/10.3989/scimar.03616.19G>.
- Schneider, B., J. Karstensen, A. Oschlies, and R. Schlitzer, 2005: Model-based evaluation of methods to determine C:N and N:P regeneration ratios from dissolved nutrients. *Global Biogeochem. Cycles*, **19**, GB2009, <https://doi.org/10.1029/2004GB002256>.
- Stramma, L., and F. Schott, 1999: The mean flow field of the tropical Atlantic Ocean. *Deep-Sea Res. II*, **46**, 279–303, [https://doi.org/10.1016/S0967-0645\(98\)00109-X](https://doi.org/10.1016/S0967-0645(98)00109-X).
- Takahashi, T., W. S. Broecker, and S. Langer, 1985: Redfield ratio based on chemical data from isopycnal surfaces. *J. Geophys. Res.*, **90**, 6907–6924, <https://doi.org/10.1029/JC090iC04p06907>.
- Tomczak, M., Jr., 1981: An analysis of mixing in the frontal zone of South and North Atlantic Central Water off North-West Africa. *Prog. Oceanogr.*, **10**, 173–192, [https://doi.org/10.1016/0079-6611\(81\)90011-2](https://doi.org/10.1016/0079-6611(81)90011-2).
- Tréguer, P., and P. Le Corre, 1975. *Manuel d'Analyse des Sels Nutritifs dans l'Eau de Mer*. Université de Bretagne Occidentale, 110 pp.
- Warton, D. I., R. A. Duursma, D. S. Falster, and S. Taskinen, 2012: Smatr 3—An R package for estimation and inference about allometric lines. *Methods Ecol. Evol.*, **3**, 257–259, <https://doi.org/10.1111/j.2041-210x.2011.00153.x>.
- Weiss, R. F., 1970: The solubility of nitrogen, oxygen and argon in water and seawater. *Deep-Sea Res. Oceanogr. Abstr.*, **17**, 721–735, [https://doi.org/10.1016/0011-7471\(70\)90037-9](https://doi.org/10.1016/0011-7471(70)90037-9).
- Yamashita, Y., and E. Tanoue, 2008: Production of bio-refractory fluorescent dissolved organic matter in the ocean interior. *Nat. Geosci.*, **1**, 579–582, <https://doi.org/10.1038/ngeo279>.
- , A. Tsukasaki, T. Nishida, and E. Tanoue, 2007: Vertical and horizontal distribution of fluorescent dissolved organic matter in the Southern Ocean. *Mar. Chem.*, **106**, 498–509, <https://doi.org/10.1016/j.marchem.2007.05.004>.
- You, Y., 2002: Dianeutral exchange between intermediate and deep water in the tropical Atlantic. *J. Geophys. Res.*, **107**, 3023, <https://doi.org/10.1029/2000JC000520>.
- Zuur, A. F., E. N. Ieno, N. J. Walker, A. A. Saveliev, and G. M. Smith, 2009: *Mixed Effects Models and Extensions in Ecology with R*. Statistics for Biology and Health, Springer, 574 pp., <https://doi.org/10.1007/978-0-387-87458-6>.

Supplemental materials for “A simple nonlinear and endmember-free approach for obtaining ocean remineralization patterns” by P. De La Fuente, J. L. Pelegrí, A. Canepa, M. Gasser, F. Domínguez and C. Marrasé.

Supplemental tables

Table S1. Model statistics (adj-r^2 and Fisher’s p-value) from the MLR approach for each mixing triangle and biogeochemical variable.

Table S2. Coefficients for the three PR models, according to the following cubic polynomial (with potential temperature in °C and no units for salinity): $\hat{Y}_i = \alpha_0 + \alpha_1 S_i + \alpha_2 \theta_i + \alpha_3 S_i^2 + \alpha_4 \theta_i^2 + \alpha_5 \theta_i S_i + \alpha_6 S_i^3 + \alpha_7 \theta_i^3 + \alpha_8 S_i^2 \theta_i + \alpha_9 S_i \theta_i^2$.

Table S3. Model statistics (AIC, adj-r^2 , residual standard error (RSE) and Fischer’s p-value) from the polynomial regressions PR2, PR3 and PRcub.

Supplemental figures

Figure S1. (a) Three-dimensional representation of the PR2 (surface) and MLR (planes) predictions for F(340/440) as a function of salinity (S) and potential temperature (θ); the colors of the lines and dots define the different planes used by MLR as follows: NADW(2.0) - CDW - WSDW (blue), NADW(4.6) - NADW(2.0) - CDW (black), AAIW(5) - NADW(4.6) - CDW (green), and SACEW(12) - AAIW(5) - NADW(4.6) (red). The θ -S diagram corresponds to the projection on the bottom plane; similar projections are drawn on the S - F(340/440) and θ - F(340/440) planes with the shaded area corresponding to the 2D projection on the respective surface. (b) As in panel (a) but using AOU rather than F(340/440). (c) As in panel (a) but using NO_3 rather than F(340/440).

Figure S2. Scattered plots for F(340/440) – NO_3 as in Figure 4, but only for the data points within the bottom water stratum.

Table S1. Model statistics (adj-r^2 and Fisher's p-value) from the MLR approach for each mixing triangle and biogeochemical variable.

| Three endmember | Y(θ ,S) | adj-r ² | p-value |
|-----------------------------|-----------------|--------------------|---------|
| SACEW(12)-AAIW(5)-NADW(4.6) | F(340/440) | 0.13 | < 0.001 |
| | AOU | 0.13 | < 0.001 |
| | NO ₃ | 0.33 | < 0.001 |
| AAIW(5)- NADW(4.6)-CDW | F(340/440) | 0.60 | < 0.001 |
| | AOU | 0.98 | < 0.001 |
| | NO ₃ | 0.98 | < 0.001 |
| NADW(4.6)- NADW(2.0)-CDW | F(340/440) | 0.46 | < 0.001 |
| | AOU | 0.55 | < 0.001 |
| | NO ₃ | 0.62 | < 0.001 |
| NADW(2.0)-CDW-WSDW | F(340/440) | 0.33 | < 0.001 |
| | AOU | 0.87 | < 0.001 |
| | NO ₃ | 0.96 | < 0.001 |

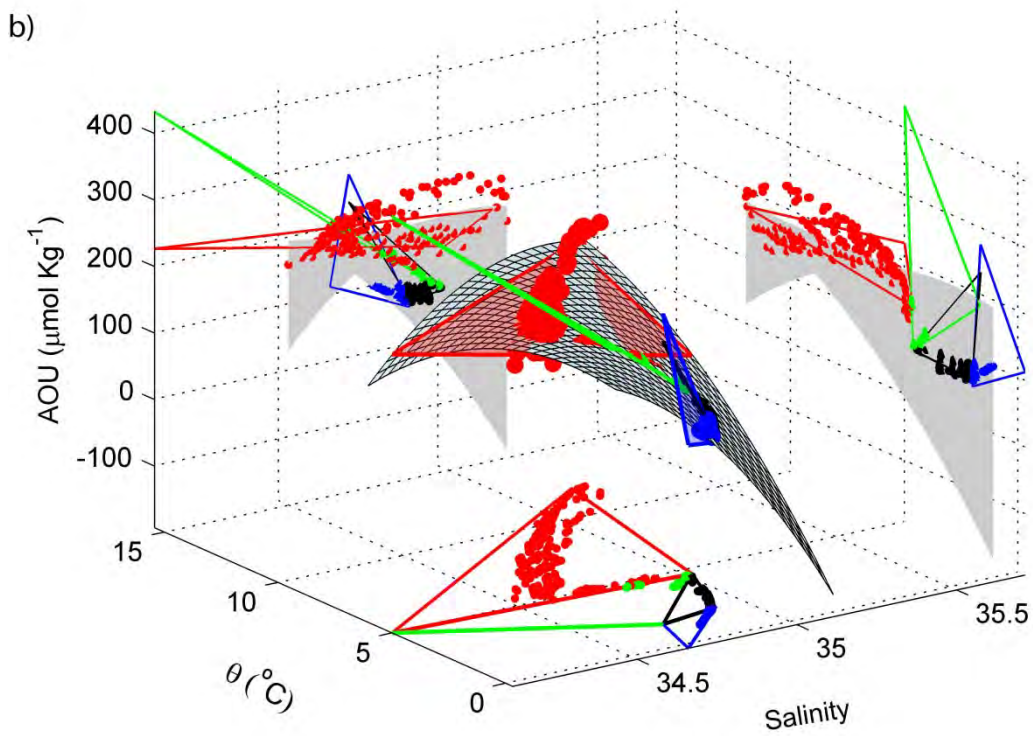
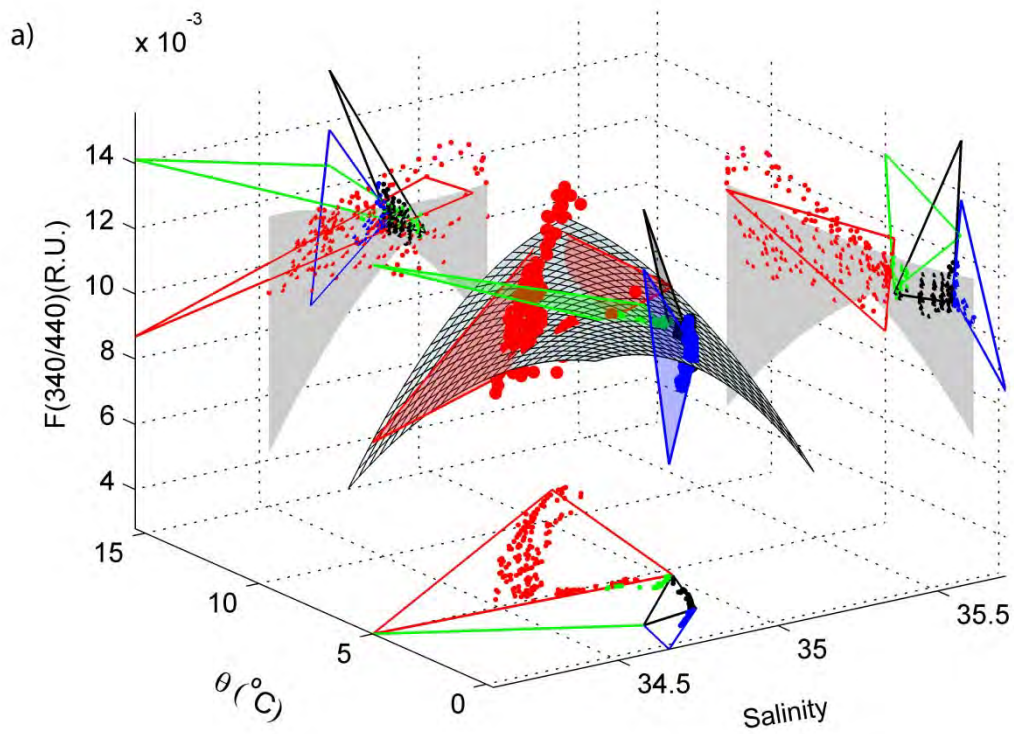
Table S2. Coefficients for the three PR models, according to the following cubic polynomial (with potential temperature in °C and no units for

salinity): $\hat{Y}_i = \alpha_0 + \alpha_1 S_i + \alpha_2 \theta_i + \alpha_3 S_i^2 + \alpha_4 \theta_i^2 + \alpha_5 \theta_i S_i + \alpha_6 S_i^3 + \alpha_7 \theta_i^3 + \alpha_8 S_i^2 \theta_i + \alpha_9 S_i \theta_i^2$.

| \hat{Y}_i | Model | α_0 | α_1 | α_2 | α_3 | α_4 | α_5 | α_6 | α_7 | α_8 | α_9 |
|-----------------|-------|------------------------|------------------------|------------------------|--------------------|------------------------|------------------------|------------|------------------------|------------------------|-----------------------|
| F(340/440) | PR2 | -14 | 0.82 | 0.05 | -0.01 | -4.04×10^{-5} | -1.57×10^{-3} | - | - | - | - |
| | PR3 | 0.35 | -9.68×10^{-3} | -0.082 | - | -3.38×10^{-4} | -2.32×10^{-3} | - | -2.31×10^{-5} | - | - |
| | PRcub | 22.93 | -1.35 | -9.41 | 0.020 | -0.055 | -0.55 | - | -6.49×10^{-5} | -8.21×10^{-3} | 1.61×10^{-3} |
| AOU | PR2 | -5.82×10^{-5} | 3.40×10^{-4} | -2.44×10^{-3} | -497 | 1.99 | 71 | - | - | - | - |
| | PR3 | 2.36×10^4 | -6.73×10^2 | -3.68×10^3 | - | 14.4 | 1.04×10^2 | - | -1.01 | - | - |
| | PRcub | 5.31×10^5 | -3.13×10^4 | -2.61×10^5 | 4.61×10^2 | -1.66×10^3 | 1.54×10^4 | - | -2.37 | -2.28×10^2 | 48.79 |
| NO ₃ | PR2 | -7.75×10^4 | 4.54×10^3 | -3.50×10^2 | -66.4 | -0.31 | 10.17 | - | - | - | - |
| | PR3 | 3.37×10^3 | -96.10 | -4.92×10^2 | - | 1.74 | 13.99 | - | -0.126 | - | - |
| | PRcub | 4.50×10^4 | -2.65×10^3 | -2.82×10^4 | 39.14 | -1.85×10^2 | 1.66×10^3 | - | -0.27 | -24.61 | 5.43 |

Table S3. Model statistics (AIC, adj-r², residual standard error (RSE) and Fischer's p-value) from the polynomial regressions PR2, PR3 and PRcub.

| F(340/440) (θ,S) | AIC | adj-r² | RSE | p-value |
|-----------------------------|------------|--------------------------|------------|----------------|
| PR2 | -4355 | 0.17 | 0.00058 | < 0.001 |
| PR3 | -4417 | 0.30 | 0.00053 | < 0.001 |
| PRcub | -4649 | 0.63 | 0.00038 | < 0.001 |
| AOU (θ,S) | AIC | adj-r² | RSE | p-value |
| PR2 | 3396 | 0.88 | 18 | < 0.001 |
| PR3 | 3246 | 0.92 | 14 | < 0.001 |
| PRcub | 2874 | 0.96 | 10 | < 0.001 |
| NO₃ (θ,S) | AIC | adj-r² | RSE | p-value |
| PR2 | 1686 | 0.87 | 2.25 | < 0.001 |
| PR3 | 1554 | 0.91 | 1.89 | < 0.001 |
| PRcub | 1299 | 0.95 | 1.34 | < 0.001 |



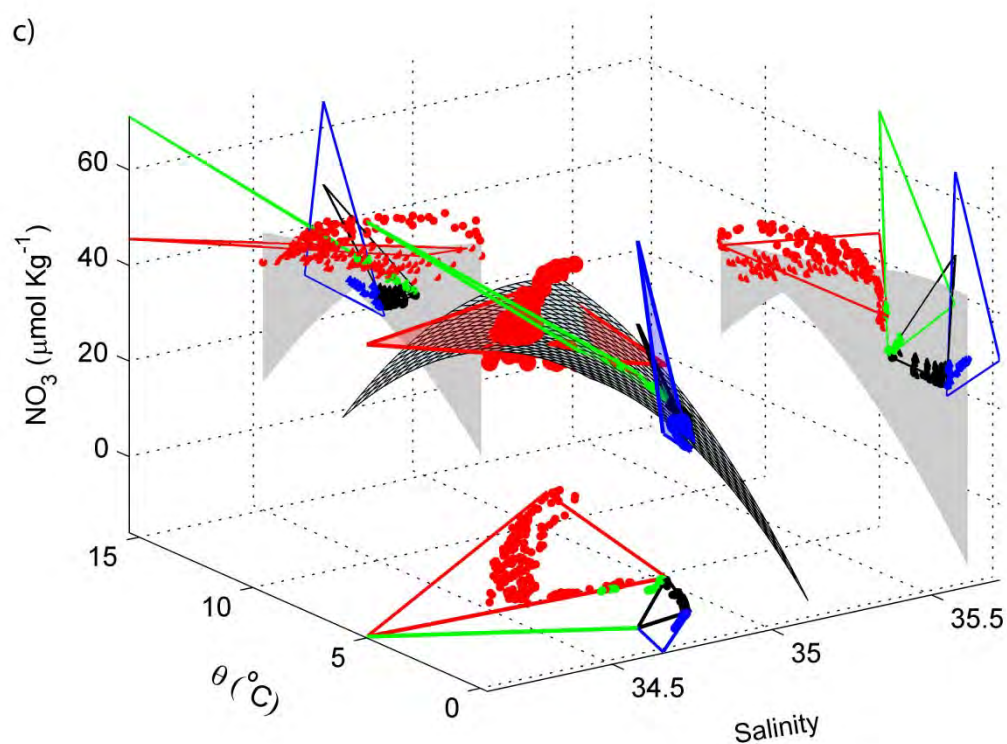


Figure S1. (a) Three-dimensional representation of the PR2 (surface) and MLR (planes) predictions for F(340/440) as a function of salinity (S) and potential temperature (θ); the colors of the lines and dots define the different planes used by MLR as follows: NADW(2.0) - CDW - WSDW (blue), NADW(4.6) - NADW(2.0) - CDW (black), AAIW(5) - NADW(4.6) - CDW (green), and SACEW(12) - AAIW(5) - NADW(4.6) (red). The θ -S diagram corresponds to the projection on the bottom plane; similar projections are drawn on the S - F(340/440) and θ - F(340/440) planes with the shaded area corresponding to the 2D projection on the respective surface. (b) As in panel (a) but using AOU rather than F(340/440). (c) As in panel (a) but using NO_3 rather than F(340/440).

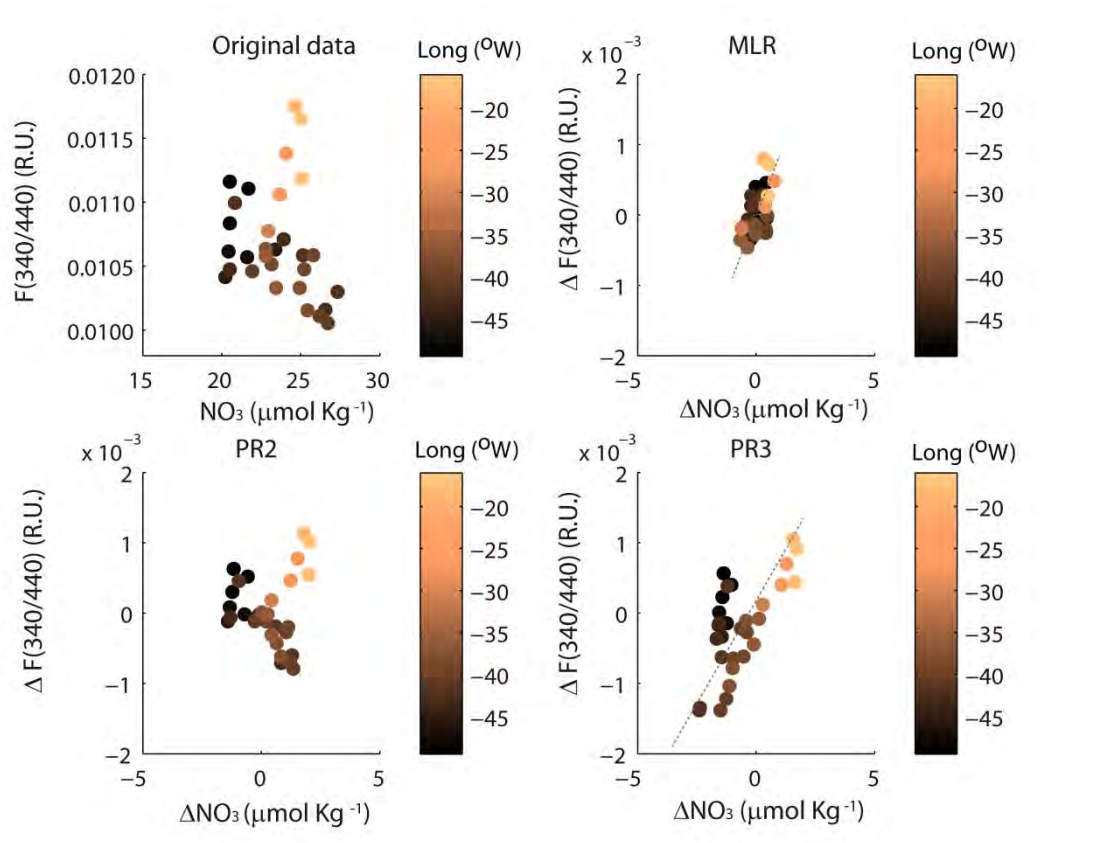


Figure S2. Scattered plots for F(340/440) – NO₃ as in Figure 4, but only for the data points within the bottom water stratum.



Does a general relationship exist between fluorescent dissolved organic matter and microbial respiration?—The case of the dark equatorial Atlantic Ocean

Patricia De La Fuente^a, Celia Marrasé^{a,*}, Antonio Canepa^a, X. Antón Álvarez-Salgado^b, Marc Gasser^a, Noelia M. Fajar^b, Cristina Romera-Castillo^c, Josep L. Pelegrí^a

^a Institut de Ciències del Mar, CSIC, Passeig Marítim de la Barceloneta 37-49, 08003 Barcelona, Spain

^b Instituto de Investigaciones Mariñas, CSIC, Eduardo Cabello, 6, 36208 Vigo, Spain

^c Department of Chemistry and Biochemistry, Florida International University, Miami, FL 33199, USA

ARTICLE INFO

Article history:

Received 25 November 2013

Received in revised form

18 March 2014

Accepted 21 March 2014

Available online 13 April 2014

Keywords:

Water masses

Fluorescent dissolved organic matter

AOU

Equatorial Atlantic Ocean

ABSTRACT

The distributions of humic-like fluorescent dissolved organic matter (at excitation/emission wavelengths of 340 nm/440 nm, $F(340/440)$) and apparent oxygen utilization (AOU) are determined from water samples taken at 27 stations along 7.5°N, in the equatorial Atlantic Ocean. The relationship between $F(340/440)$ and AOU is evaluated. The influence of water mass mixing is removed through multiple regressions of both $F(340/440)$ and AOU with salinity and temperature for the ocean interior. A general and significant relationship between the residuals of $F(340/440)$ and AOU is found for the entire water column deeper than 200 m ($R^2=0.79$, $n=360$, p -value <0.001), endorsing the idea that changes in fluorescence intensity are directly related to in situ oxidation of organic matter by microbial activity in the dark equatorial Atlantic Ocean. In addition, we analyse and discuss the relationships between the residuals of $F(340/440)$ and AOU for all individual water masses.

© 2014 Elsevier Ltd. All rights reserved.

1. Introduction

The major source of marine dissolved organic matter (DOM) in the epipelagic ocean is the photosynthesis of phytoplankton (Hansell et al., 2009; Hansell, 2013; Nelson and Siegel, 2013). DOM and organic particles that escape rapid mineralization by heterotrophic microbes in the epipelagic ocean are transformed by either biotic (Microbial Carbon Pump, Jiao et al., 2010) or abiotic processes into recalcitrant material. Such material accumulates in the mesopelagic and bathypelagic layers to form the largest reservoir of reduced carbon on Earth (Hansell et al., 2009; Hansell, 2013; Nelson and Siegel, 2013).

A variable fraction of this recalcitrant material fluoresces at the excitation/emission (Ex/Em) wavelengths characteristic of humic substances (Coble et al., 1990; Coble, 1996, 2007) when irradiated with ultraviolet (UV) light, the so called fluorescent DOM (FDOM). In oceanic waters, the profile of humic-like FDOM is typically low at the sea surface and increases with depth (Chen and Bada, 1992;

Yamashita and Tanoue, 2008; Yamashita et al., 2010; Jørgensen et al., 2011). However, the fluorescence intensity is relatively high in surface waters of upwelling regions because of the enhanced biological activity and the upward flux of FDOM-rich mesopelagic waters (Determann et al., 1996; Nieto-Cid et al., 2005, 2006; Romera-Castillo et al., 2011a; Jørgensen et al., 2011; Nelson and Siegel, 2013), and in areas with large inputs of terrestrial organic matter (Del Castillo et al., 1999; Nelson and Siegel, 2013).

In the dark open ocean (waters deeper than 200 m, hereafter named ocean interior), because of the significant association between humic-like DOM fluorescence and apparent oxygen utilization (AOU) (Hayase et al., 1989; Chen and Bada, 1992; Hayase and Shinozuka, 1995; Yamashita et al., 2007; Yamashita and Tanoue, 2008; Yamashita et al., 2010; Jørgensen et al., 2011; Nelson and Siegel, 2013; Álvarez-Salgado et al., 2013), the humic-like FDOM serves as a tracer for the generation of recalcitrant DOM as a by-product of microbial respiration. However, it seems likely that the observed distributions of humic-like FDOM and AOU, and hence their relationship, will depend on their content at origin, typically within surface waters before they escape to the deep ocean (Yamashita and Tanoue, 2008; Nelson and Siegel, 2013; Álvarez-Salgado et al., 2013).

The MOC2-Equatorial cruise occupied a transatlantic line along 7.5°N in April–May 2010 on board the R/V *Hespérides*. The meridional transport of properties across the 7.5°N line (i.e. heat, fresh water,

* Corresponding Author. Tel.: +34 93 230 9591; fax: +34 93 230 95 55.

E-mail addresses: patriciadlf@icm.csic.es (P. De La Fuente), celia@icm.csic.es (C. Marrasé), canepa@icm.csic.es (A. Canepa), xsalgado@iim.csic.es (X. Antón Álvarez-Salgado), gasser@icm.csic.es (M. Gasser), nfajar@iim.csic.es (N.M. Fajar), cromerac@fu.edu (C. Romera-Castillo), pelegr@icm.csic.es (J.L. Pelegrí).

carbon and nutrients among others) has been previously studied by several authors (Flugister, 1960; Oudot, 1993; Arhan et al., 1998; Lappo et al., 2001; Sarafanov et al., 2007). This transect constitutes a meeting zone for waters of northern and southern origin at all levels. Western boundary currents are responsible for inter-hemispheric exchange, most of the time after substantial recirculations within the equatorial and tropical regions. The net flow in the epipelagic (0–200 m) and mesopelagic (200–1000 m) layers is northward, being compensated by a net southward transport in the abyssal ocean, from 1000 m to the bottom (Arhan et al., 1998; Stramma and Schott, 1999).

The mesopelagic layer is formed by central (upper thermocline) and intermediate waters, while the abyssal ocean (here defined as waters deeper than 1000 m) is dominated by deep and bottom waters. In the central waters domain we find a combination of North Atlantic Central Water (NACW) and South Atlantic Central Water (SACW), with a predominance of relatively aged SACW. At the intermediate levels the northward extension of Antarctic Intermediate Water (AAIW) occurs and at depth the North Atlantic Deep Water (NADW) overlays the Antarctic Bottom Water (AABW).

Field observations of humic-like FDOM in the equatorial Atlantic Ocean are scarce, predominantly sampled along meridional transects close to the African coast (Deterrmann et al., 1996; Jørgensen et al., 2011; Nelson and Siegel, 2013; Andrew et al., 2013). Therefore, the humic-like FDOM data obtained during the MOC2-Equatorial cruise, with good spatial resolution across the under-sampled equatorial Atlantic Ocean, provides an excellent opportunity to evaluate the relative influence of both FDOM-concentration at origin and in situ microbial activity on the observed humic-like FDOM distribution. Specifically, the spatial distribution of FDOM (with Ex/Em wavelengths of 340 nm/440 nm) is used as a proxy for recalcitrant dissolved organic matter within the equatorial Atlantic Ocean, and the dependence of this variable with AOU (as a proxy for microbial respiration) is examined. We indeed find that the relationship between humic-like FDOM and AOU changes among the different water strata. Therefore, we use salinity and temperature, which are characteristic of each water mass, to remove the effect of the different initial concentrations. After applying the best fit-model to explain the dependence of FDOM and AOU on temperature and salinity, we examine the behaviour of both FDOM and AOU residuals. These residuals display a general significant relationship for the ocean interior, which endorses the very important role of in situ microbial processes in relation to the Microbial Carbon Pump (MCP) and the recalcitrant DOM storage in the dark equatorial Atlantic Ocean (Jiao et al., 2010).

2. Material and methods

2.1. Measurements

The second phase of the MOC2-Equatorial cruise crossed the equatorial Atlantic Ocean from South America to West Africa along 7.5°N, between 20 April and 13 May 2010, with a total of 62 hydrographic stations. Measurements for this study were obtained from 27 stations along this track (Fig. 1), using water samples from the whole water column (except for stations 63, 72, 108 and 109 where the deepest samples were taken at 99 m, 153 m, 1570 m and 181 m, respectively). Vertical profiles of temperature and conductivity were obtained with a SeaBird 911 Plus CTD system mounted in a 24 Niskin bottle rosette that collected water samples at standard depths; Chl-a fluorescence was determined with a Seapoint Fluorometer sensor.

Seawater samples for the O₂ analysis were taken from Niskin bottles in sealed flasks (~250 mL) with a PVC pipe, avoiding bubble formation, and stored in darkness for 24 h. Dissolved oxygen concentration was measured using an automated potentiometric modification of the original Winkler method following WOCE standards (WOCE, 1994). The accuracy of the method is $\pm 0.5 \mu\text{mol kg}^{-1}$.

Water samples for the FDOM measurements were collected from each Niskin bottle in acid cleaned glass bottles of 250 mL, previously rinsed three times with the corresponding seawater. In order to avoid sample contamination, several precautions were taken during collection of the water sample: gloves were used, contact with the spigot of the Niskin bottle was avoided, and the formation of air bubbles was minimized. Each sample was stored in darkness and far away from the presence of volatile organic compounds. They were allowed to stand until reaching room temperature. Fluorescence measurements were conducted within 2 h after sampling; samples were not filtered.

Fluorescence measurements were performed using a Perkin Elmer LS spectrometer with a 150 W Xenon lamp, and the sensitivity mode was set at 10-nm slit widths for both excitation and emission wavelengths. Milli-Q water was used as a reference blank for fluorescence analysis. An acid-cleaned quartz cell of 1 cm was rinsed three times with the sample and then fluorescence intensity was measured at fixed Ex/Em wavelengths of 340 nm/440 nm ($F(340/440)$), which is characteristic of humic-like substances (Coble et al., 1990; Coble, 1996). $F(340/440)$ data was normalized to Raman Units (R.U.) according to Lawaetz and Stedmon (2009).

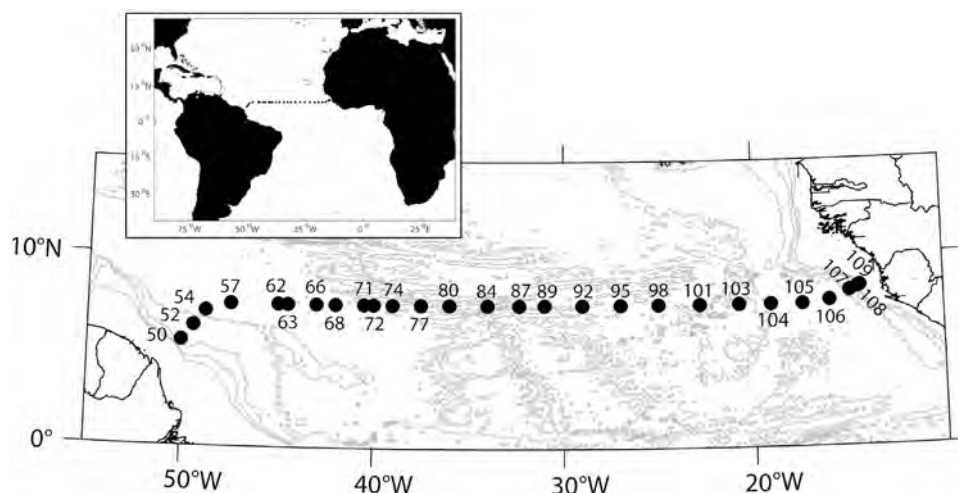


Fig. 1. Study area showing the stations used in this study along 7.5°N, occupied during the MOC2-Equatorial cruise.

AOU is defined as the difference between saturation O_2 concentration ($O_{2,sat}$), which depends on in situ temperature and salinity, and the observed O_2 concentration, i.e. $AOU = O_{2,sat} - O_2$ (Weiss, 1970; Ito et al., 2004); $O_{2,sat}$ was calculated following Benson and Krause (1984).

2.2. Water regions and water masses

The water column is divided into surface (0–200 m) and ocean interior (deeper than 200 m). Furthermore, the ocean interior is separated in two depth-layers: mesopelagic (200–1000 m) and abyssal (1000 m to the sea bottom). It is also classified into different water masses using neutral density levels, following the study of San Antolín et al. (2012) for the same section. Neutral density, γ^n , is computed following Jackett and McDougall (1997) using the code available at the Gibbs-SeaWater (GSW) Oceanographic Toolbox (McDougall and Barker, 2011) with the anomaly

values defined as neutral density $= (1000 + \gamma^n) \text{ kg m}^{-3}$. In the mesopelagic layer we find central waters (NACW and SACW), with a neutral density range of $26.65 < \gamma^n < 27.3$, and intermediate waters (AAIW), with a neutral density range of $27.3 < \gamma^n < 27.8$. The abyssal layer is occupied by deep waters (NADW), with neutral densities of $27.8 < \gamma^n < 28.12$, and bottom waters (AABW), with neutral densities of $\gamma^n > 28.12$.

Water masses in the equatorial Atlantic Ocean are characterized on the basis of potential temperature (θ), salinity (S), and dissolved oxygen (O_2) (Figs. 2 and 3). The predominant central water along 7.5°N is SACW, having its origin in the southern hemisphere (Stramma and Schott, 1999). Below 200 m, SACW is characterized by θ and S values that define a straight line in the (θ , S) space, which passes through points (6 °C, 34.6) and (14 °C, 35.4) (Fig. 3d). SACW shows an oxygen minimum at 300–500 m in the eastern region which is indicative of slow water renewal near the Guinea Dome region (Stramma and Schott, 1999) (Figs. 2 and 3). AAIW appears as a cold and low-salinity tongue at depths 500–1100 m, most pronounced in the western half of

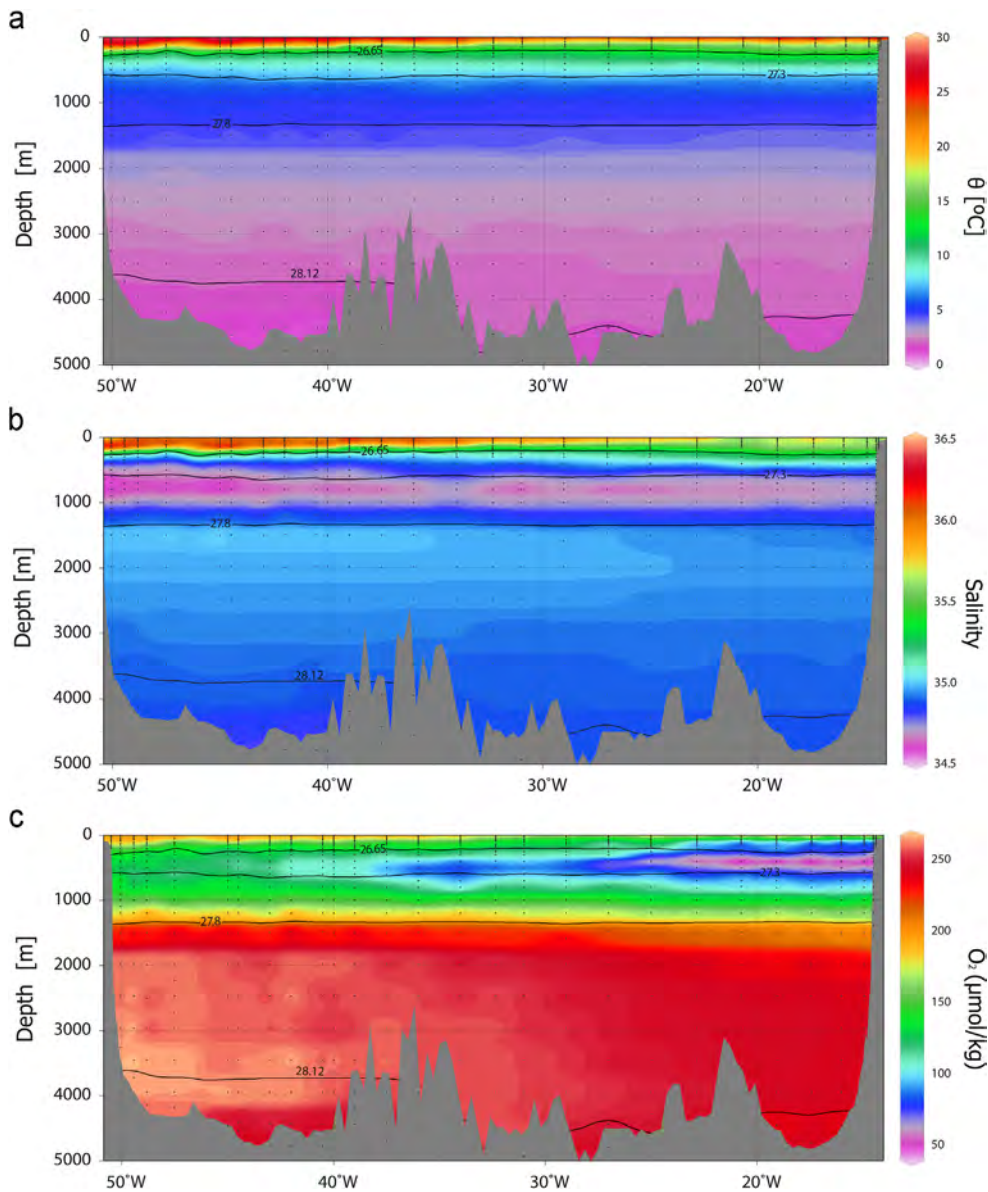


Fig. 2. Colour contour maps for (a) potential temperature, θ (°C), (b) salinity and (c) dissolved oxygen, O_2 ($\mu\text{mol kg}^{-1}$), for the 7.5°N line. Black lines represent neutral density, γ^n , isolines separating the water strata: central waters (SACW and NACW, $26.65 < \gamma^n < 27.3$), intermediate waters (AAIW, $27.3 < \gamma^n < 27.8$), deep waters (NADW, $27.8 < \gamma^n < 28.12$) and bottom waters (AABW, $\gamma^n > 28.12$). (For interpretation of the references to color in this figure legend, the reader is referred to the web version of this article.)

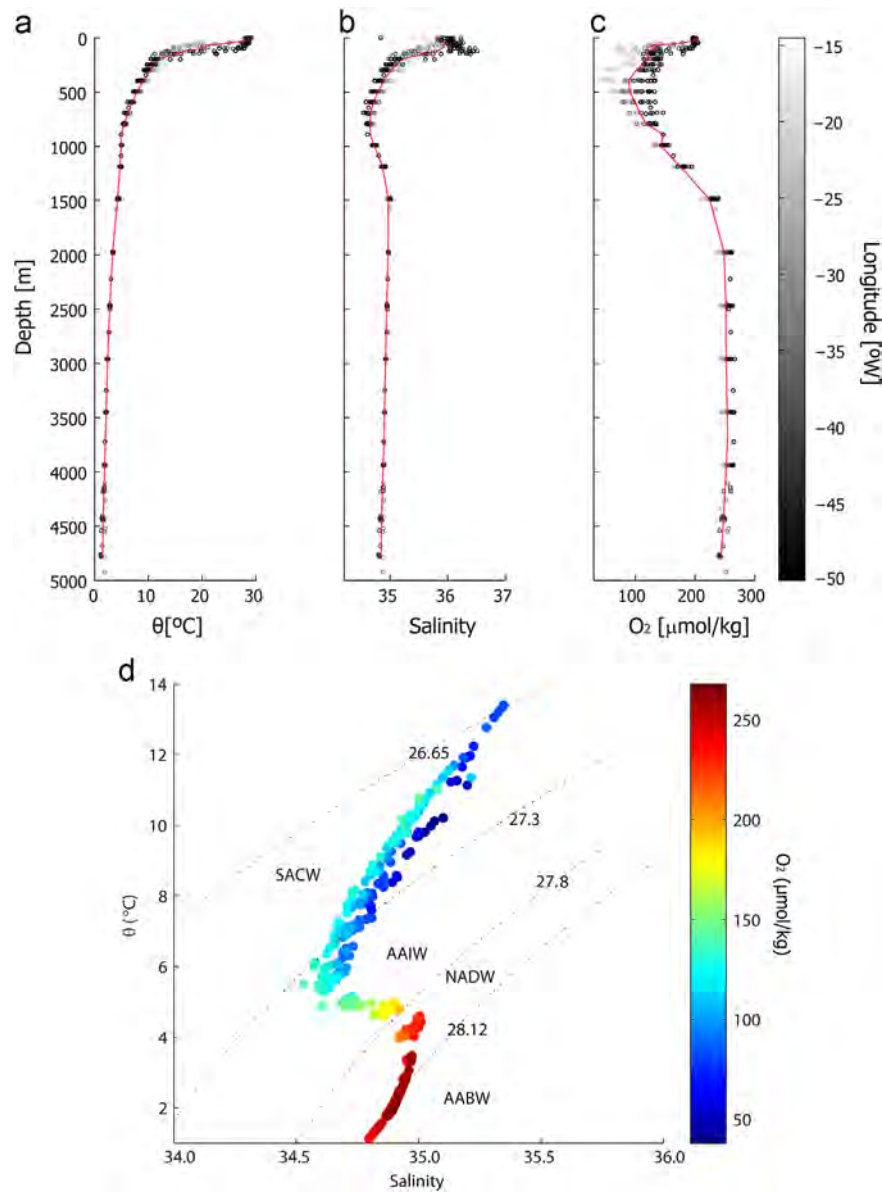


Fig. 3. Vertical profiles for (a) potential temperature, θ ($^{\circ}\text{C}$), (b) salinity and (c) dissolved oxygen, O_2 ($\mu\text{mol kg}^{-1}$). Vertical profiles are in different grey shades as a function of longitude ($^{\circ}\text{W}$). A reference profile (red curve) is calculated as a zonal average at each depth level. (d) θ/S diagram of 7.5°N line for the ocean interior (waters deeper than 200 m), color-coded for dissolved oxygen, O_2 ($\mu\text{mol kg}^{-1}$); dotted lines represent the isoneutrals separating the water strata: central waters (SACW and NACW, $26.65 < \gamma^{\sigma_t} < 27.3$), intermediate waters (AAIW, $27.3 < \gamma^{\sigma_t} < 27.8$), deep waters (NADW, $27.8 < \gamma^{\sigma_t} < 28.12$) and bottom waters (AABW, $\gamma^{\sigma_t} > 28.12$). (For interpretation of the references to color in this figure legend, the reader is referred to the web version of this article.)

the 7.5°N section (Stramma and Schott, 1999; Arhan et al., 1998; Sarafanov et al., 2007; Machín and Pelegrí, 2009) (Figs. 2 and 3). NADW stands out as a high-salinity and oxygen-rich domain; NADW is commonly divided into three components: upper NADW (UNADW), recognizable by a mid-depth salinity maximum, and middle and lower NADW (MNADW, LNADW), most distinguishable by oxygen maxima at 2000–2500 m and approximately 3700 m, respectively (Figs. 2 and 3) (Arhan et al., 1998; Sarafanov et al., 2007; Talley et al., 2011). The lowest temperature values are found in the AABW (Arhan et al., 1998; Sarafanov et al., 2007; Lappo et al., 2001) (Figs. 2 and 3). AABW is a mixture of unventilated Lower Circumpolar Deep Water (LCDW) and Weddell Sea Deep Water (WSDW), the latter being oxygen-rich cold waters recently formed in the Antarctic margins (Orsi et al., 1999); AABW presents salinity and oxygen concentrations lower than NADW (Figs. 2 and 3), characteristic of its southern origin (Arhan et al., 1998; Lappo et al., 2001).

2.3. Statistical analysis

The linear relationships between $F(340/440)$ and AOU are evaluated separately for the surface ocean (0–200 m) and for the ocean interior (> 200 m). For the ocean interior, individual linear relationships between $F(340/440)$ and AOU are also obtained for the four water strata (central, intermediate, deep and bottom). Model II linear regression is used to examine the relationship between $F(340/440)$ and AOU; model II regression refers to a family of model-fitting procedures that acknowledge the uncertainty of both response and predictor variables (Logan, 2010). Among different techniques, the Standard (Reduced) Major Axis (SMA) is selected. SMA arranges the variables in a dimensionally homogeneous way prior to the regression analysis (Legendre and Legendre, 1998). The uncertainty of response and predictor variables are incorporated through the minimization of the sum

Table 1
 $F(340/440)$ –AOU linear relationships as obtained from the model II regression (SMA technique, see Section 2). These relationships are determined for the ocean surface (0–200 m) and ocean interior (deeper than 200 m), and for the different water strata (central, intermediate, deep and bottom waters) of the ocean interior. The water strata are characterized using the neutral density criteria (see Section 2).

| Layer/water strata | Intercept ($\times 10^4$) | Slope ($\times 10^5$) | R^2 | n | p | SD $F(340/440)$ ($\times 10^4$) | SD AOU |
|--|-----------------------------|-------------------------|--------|-----|---------|-----------------------------------|------------|
| Surface (0–200 m) | 34 \pm 2 | 5.41 \pm 0.17 | 0.83 | 170 | < 0.001 | \pm 0.4 | \pm 68.2 |
| Ocean interior (> 200 m) | 89 \pm 1 | 1.20 \pm 0.01 | 0.05 | 360 | < 0.001 | \pm 6.4 | \pm 52.8 |
| Central w. (NACW/SACW) 26.65 < γ^n < 27.3 | 50 \pm 2 | 3.07 \pm 0.14 | 0.81 | 131 | < 0.001 | \pm 9.9 | \pm 27.5 |
| Intermediate w. (AAIW) 27.3 < γ^n < 27.8 | 73 \pm 4 | 1.85 \pm 0.22 | 0.07 | 102 | < 0.05 | \pm 4.9 | \pm 26.4 |
| Deep w. (NADW) 27.8 < γ^n < 28.12 | 78 \pm 2 | 3.60 \pm 0.31 | 0.27 | 126 | < 0.001 | \pm 3.9 | \pm 10.6 |
| Bottom w. (AAWB) γ^n > 28.12 | – | – | < 0.01 | 30 | 0.814 | \pm 4.3 | \pm 10.3 |

squares of the triangular areas defined by the observations and the regression line (Logan, 2010). The coefficients (intercept and slope) with their respective standard deviations obtained from the linear relationships, together with the corresponding correlation coefficient (R^2) and p -value ($\alpha=0.05$), are shown in Table 1.

To determine the relationship between $F(340/440)$ and AOU for the ocean interior without the influence of temperature and salinity, as a proxy of water masses, we follow two steps. The first step consists on performing multiple non-linear regressions for both $F(340/440)$ and AOU as a function of temperature and salinity over the whole (θ , S) space. A non-linear response is included in the models in the form of θ and S quadratic and interaction terms. The models turn out to have good skill capturing the variability associated to the (θ , S) pair of values, i.e. related to the source water masses. The optimal models are established based on the Akaike's Information Criterion (AIC) (data not shown). The AIC method penalizes in a negative way the excess of parameters, so it prevents an over-parameterization and allows evaluating which model gives the best fit: the lower the AIC value the better is the model (Zuur et al., 2009). For the optimal models, the regression coefficient (R^2) and the p -value ($\alpha=0.05$) are calculated.

The rationale behind searching for a relation between either $F(340/440)$ or AOU with temperature and salinity, is that these latter variables have proved to be a good proxy for different water masses (Mamayev, 1975). Water masses are often characterized by their conservative thermohaline properties. Non-conservative parameters are influenced not only by physical mixing and advection, but also by biological processes. Earlier studies have removed the physical variability (assumed to be associated with θ and S) through local linear regression models on salinity and temperature; these models are local in the sense that a (θ , S) pair is to be attained by the linear mixing in the (θ , S) space of up to a maximum of three end-member water types (Castro et al., 2006; Carlson et al., 2010). The non-linear method proposed here takes into account the possibility of non-isotropic mixing by incorporating the non-linear dependences with temperature and salinity.

The second step consists on subtracting the values estimated from the (θ , S) pair through the optimal model from the observed values. These residuals contain the FDOM and AOU variability not explained by (θ , S) and they are expected to mainly reflect the biological activity (Castro et al., 2006; Carlson et al., 2010). Henceforth we will refer to them as $F(340/440)$ and AOU biological anomalies, with the notation $\Delta F(340/440)$ and ΔAOU , respectively. For each water stratum, the relationship between $\Delta F(340/440)$ and ΔAOU is evaluated through a model II analysis of covariance (ANCOVA) using the package "smatr" (Warton et al., 2012) (Table 2). Finally, a simple model II (SMA) linear relationship between $\Delta F(340/440)$ and ΔAOU for the entire ocean interior is obtained. The calculated relationship is evaluated through the correlation coefficient (R^2) and the significance p -value ($\alpha=0.05$).

All statistical analyses are done using the free statistical software R, version 2.15.2 (Core Team, 2012), and the computing environment Matlab v.7.6.0.

Table 2

Result from the ANCOVA analysis. Slope for the linear relationship between $\Delta F(340/440)$ and ΔAOU among water strata using model II regression type SMA. The relationships are evaluated through the correlation coefficient, R^2 , and the significance p -value ($\alpha=0.05$). The existence of differences between the calculated slopes for each water strata with the general slope of $(3.14 \pm 0.08) \times 10^{-5}$ is evaluated using the statistic test of Likelihood ratio and the p -value.

| Water strata | Slope ($\times 10^5$) | R^2 | p | Likelihood statistic | p |
|--------------|-------------------------|-------|---------|----------------------|---------|
| General | 3.14 \pm 0.08 | 0.79 | < 0.001 | – | – |
| Central | 2.9 \pm 0.1 | 0.92 | < 0.001 | $r_{98} = -0.32$ | < 0.05 |
| Intermediate | 3.1 \pm 0.1 | 0.79 | < 0.001 | $r_{100} = -0.05$ | 0.58 |
| Deep | 4.7 \pm 0.3 | 0.57 | < 0.001 | $r_{124} = 0.55$ | < 0.001 |
| Bottom | 9.5 \pm 2.2 | 0.25 | < 0.05 | $r_{28} = 0.84$ | < 0.001 |

3. Results and discussion

3.1. $F(340/440)$ and AOU distributions

3.1.1. Surface (0–200 m)

$F(340/440)$ values are lowest in the first meters of the water column probably due to photobleaching by UV and blue light (Mopper et al., 1991; Chen and Bada, 1992; Stedmon and Markager, 2005). The intensity of sunlight, which is very high, and the stability of the near-surface layer at this latitude favour the photodegradation of FDOM (Determann et al., 1996; Chen and Bada, 1992; Mopper et al., 1991). The range of $F(340/440)$ values is very narrow through most of the 7.5°N section (2 to 3×10^{-3} R.U.). In surface waters the highest $F(340/440)$ values were found in stations 50 and 109 (7×10^{-3} R.U. and 5×10^{-3} R.U., respectively). The high surface $F(340/440)$ value at station 50 coincides with a low sea-surface salinity of 34.84, evidencing the influence of the Amazon plume (Salisbury et al., 2011). The high value observed in station 109 may indicate a terrestrial source (Del Castillo et al., 1999), as this is the station nearest to the African coast. The depth limit at which $F(340/440)$ values remain low ($< 5 \times 10^{-3}$ R.U.) decreases from West to East (54 ± 10 m to 6 ± 0.8 m) (Fig. 4) due to the eastward uplift of the seasonal thermocline. Below this depth, the $F(340/440)$ signal increases rapidly with depth (Figs. 4a and 5a).

$F(340/440)$ presents a subsurface maximum in the upper part of the main thermocline, close to the deep chlorophyll maximum (DCM) and coincident with a strong depth gradient in AOU (Figs. 4 and 5), therefore suggesting biological in situ FDOM production. The depths of $F(340/440)$ and Chl-a maxima in the westernmost stations vary from 120 m to 200 m (Fig. 4a) and from 70 m to 100 m (Fig. 4b), respectively. At the easternmost stations, maximum values take place at 40–50 m for both variables (Fig. 4). The sub-surface $F(340/440)$ maximum fluorescence intensities remain in a narrow range of 9 – 10×10^{-3} R.U. in the western part of the section, stations 50 to 98 (Fig. 4a). For stations 101 to 109, in the eastern end of the section, the $F(340/440)$ and DCM sub-surface maxima show the highest values, with mean values of $13 \pm 1.4 \times 10^{-3}$ R.U. for $F(340/440)$ and 0.90 ± 0.22 mg m^{-3} for Chl-a (Fig. 4), probably related to the influence of upwelling near the Guinea Dome (Siedler et al., 1992).

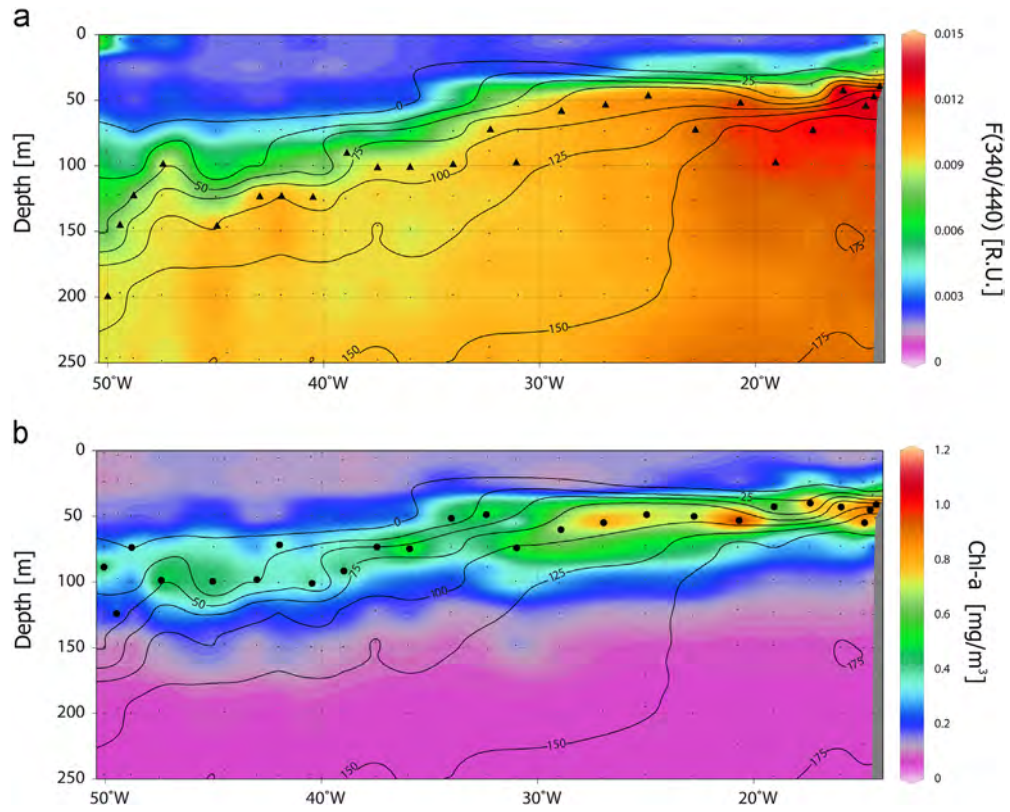


Fig. 4. Contour maps for (a) fluorescence intensity, $F(340/440)$ (R.U.) and (b) Chl-a (mg m^{-3}), from the sea surface down to 250 m depth. Black lines represent AOU isolines. Black triangles are sub-surface maximum values for $F(340/440)$ (R.U.). Black dots are sub-surface maximum values for Chl-a (mg m^{-3}).

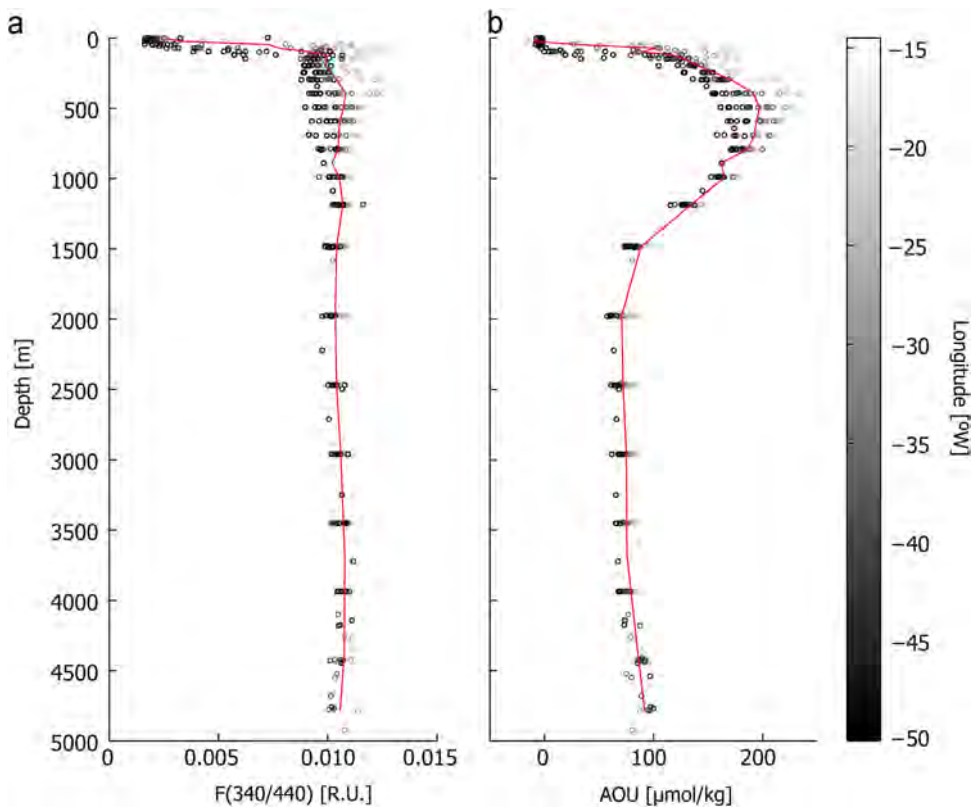


Fig. 5. Vertical profiles of (a) $F(340/440)$ (R.U.) and (b) AOU ($\mu\text{mol kg}^{-1}$), with different grey shading as a function of longitude ($^{\circ}\text{W}$). A reference profile (red curve) is calculated as a zonal average at each depth level. (For interpretation of the references to color in this figure legend, the reader is referred to the web version of this article.)

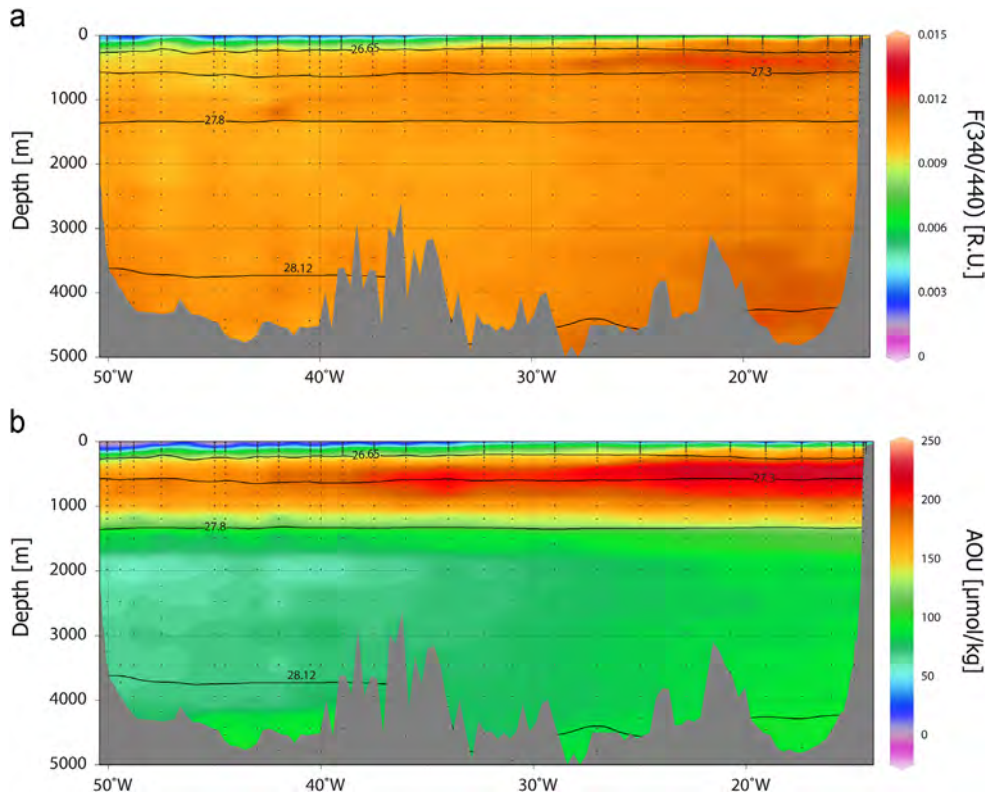


Fig. 6. Contour maps of (a) fluorescence intensity, $F(340/440)$ (R.U.) and (b) AOU ($\mu\text{mol kg}^{-1}$), along 7.5°N . Black lines represent neutral density, γ^t , isolines. Those isoneutrals delimiting the different water strata for the ocean interior are shown: central waters (SACW and NACW, $26.65 < \gamma^t < 27.3$), intermediate waters (AAIW, $27.3 < \gamma^t < 27.8$), deep waters (NADW, $27.8 < \gamma^t < 28.12$) and bottom waters (AABW, $\gamma^t > 28.12$).

3.1.2. Ocean interior (deeper than 200 m)

Through the mesopelagic layer (200–1000 m), $F(340/440)$ remains approximately constant but displays significant zonal changes, with maximum values in the eastern region. The distribution of AOU also shows a substantial zonal gradient and, most remarkably, typically displays a prominent depth maximum at 400–500 m (Figs. 5 and 6). The maximum $F(340/440)$ and AOU values correspond to the eastern part of the section (Figs. 5 and 6), where Guinea Dome upwelling takes place and the Oxygen Minimum Zone (OMZ) is found (Arhan et al., 1998; Karstensen et al., 2008; Stramma, 2008).

The $F(340/440)$ distribution at the mesopelagic layer displays some peaks of relatively high fluorescence intensity. The characteristic depth of these peaks ranges between 300 m and 800 m, coincident with the range where maximum AOU values are found for the ocean interior (Figs. 5 and 6). This suggests a link between $F(340/440)$ and biological activity, as other authors have pointed out (Yamashita et al., 2010; Jørgensen et al., 2011).

In the abyssal layer (1000 m to sea bottom), the vertical distribution of $F(340/440)$ remains quite constant (Figs. 5a and 6a). The highest values of fluorescence intensity are found again in the eastern part of the section probably due to the oxidation of the downward flux of organic matter caused by upwelling near the Guinea Dome. The AOU decreases progressively from maximum values at about 500 m to minimum levels at about 2000 m, and remains approximately constant further deep.

3.2. $F(340/440)$ –AOU relationship

3.2.1. Surface (0–200 m)

The significant linear relationship between $F(340/440)$ and AOU found for the top 200 m (slope = $(5.41 \pm 0.17) \times 10^{-5}$ R.U., $R^2 = 0.83$, $n = 170$, p -value < 0.001 , Table 1) suggests a biological in situ

production of $F(340/440)$, possibly related to the mineralization of organic matter by marine bacteria. However, this relationship should be taken with caution as there are other processes that may influence the observed values of fluorescence intensity, i.e. photo-degradation (Determann et al., 1996; Chen and Bada, 1992; Mopper et al., 1991) or the production of FDOM by marine phytoplankton (Romera-Castillo et al., 2010). Furthermore, the production of O_2 during primary production will also influence the $F(340/440)$ –AOU relationship.

3.2.2. Ocean interior (deeper than 200 m)

The linear relationship between AOU and $F(340/440)$ for the ocean interior is very weak although significant (slope = $(1.20 \pm 0.01) \times 10^{-5}$ R.U., $R^2 = 0.05$, $n = 360$, p -value < 0.001 , Table 1). This weak dependence is consistent with the observed different distributions of $F(340/440)$ and AOU across distinct water strata (Fig. 7). A scatter plot of $F(340/440)$ as a function of AOU indeed suggests a changing dependence for the different water strata (Fig. 8a). On the light of those results, we examine the dependence of $F(340/440)$ with AOU separately for different water strata.

3.2.2.1. Mesopelagic layer (200–1000 m); central and intermediate waters.

The relationship of $F(340/440)$ with AOU within the central waters is strong and significant (slope = $(3.07 \pm 0.14) \times 10^{-5}$ R.U., $R^2 = 0.81$, $n = 131$, p -value < 0.001 , Table 1) and intermediate waters present a very weak but significant linear relationship (slope = $(1.85 \pm 0.22) \times 10^{-5}$ R.U., $R^2 = 0.07$, $n = 102$, p -value < 0.05 , Table 1). In the boundary between the mesopelagic and abyssal layers (900–1200 m), the AOU decreases rapidly without an equivalent change in fluorescence intensity (Figs. 5 and 6), therefore the linearity in the relationship is lost (Fig. 8a). The sharp decrease in AOU values may be due to the presence of O_2 -rich upper deep waters (Fig. 7b). When we only consider data in the

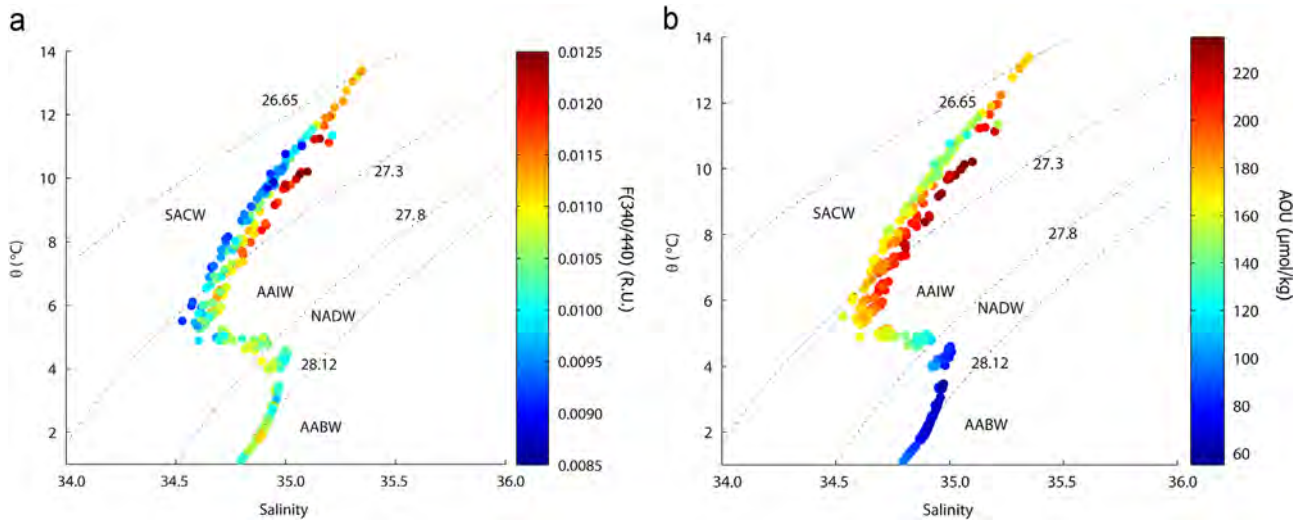


Fig. 7. θ/S diagram for the ocean interior, color-coded for (a) $F(340/440)$ and (b) AOU. Dotted lines represent the isoneutrals separating the water strata: central waters (SACW and NACW, $26.65 < \gamma^n < 27.3$), intermediate waters (AAIW, $27.3 < \gamma^n < 27.8$), deep waters (NADW, $27.8 < \gamma^n < 28.12$) and bottom waters (AABW, $\gamma^n > 28.12$). (For interpretation of the references to color in this figure legend, the reader is referred to the web version of this article.)

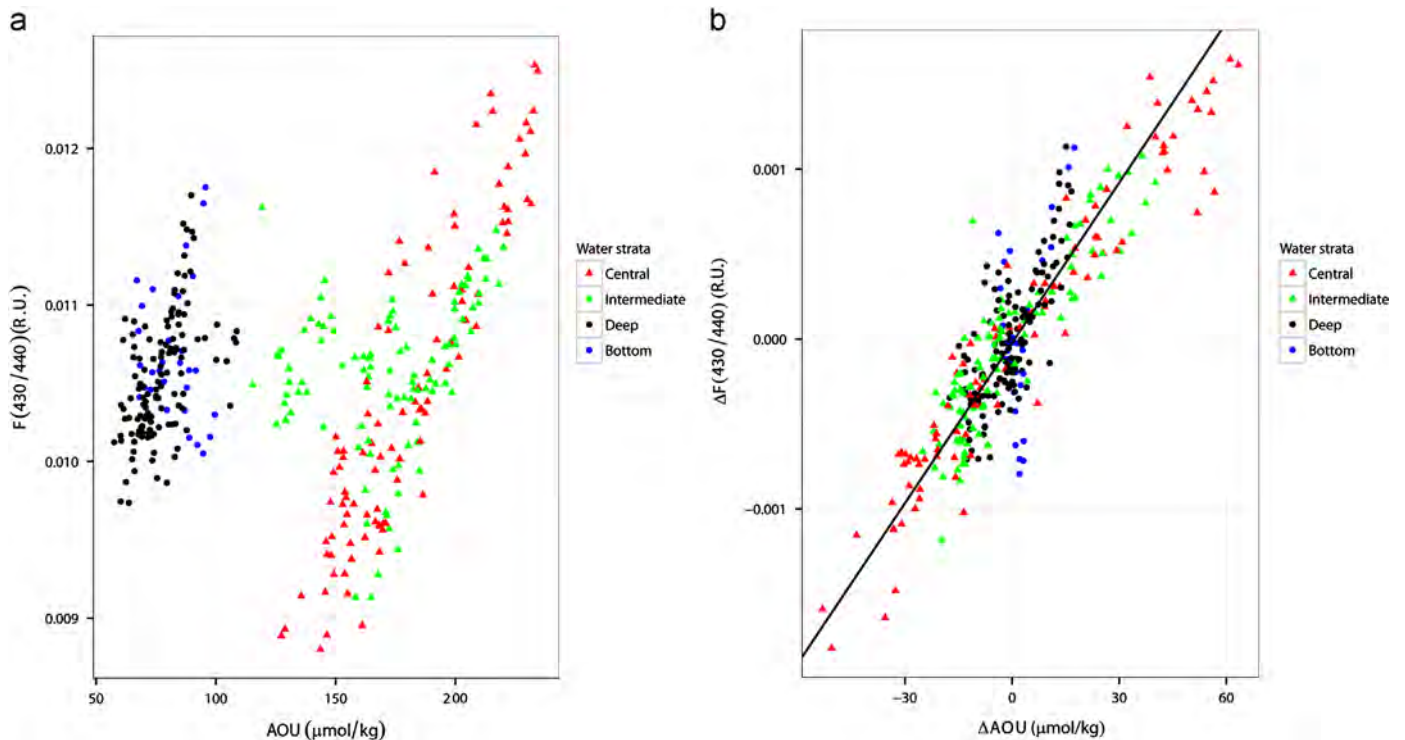


Fig. 8. Property-property plots for the ocean interior (waters deeper than 200 m) for (a) $F(340/440)$ (R.U.) versus AOU ($\mu\text{mol kg}^{-1}$) and (b) $\Delta F(340/440)$ (R.U.) versus ΔAOU ($\mu\text{mol kg}^{-1}$). The regression equation is $\Delta F(340/440) = 3.14 (\pm 0.08) \times 10^{-5} \Delta\text{AOU}$ with $R^2 = 0.79$, $p < 0.001$. Water strata are distinguished by neutral density surfaces. Central waters (SACW, NACW, $26.65 < \gamma^n < 27.3$) represented by red triangles, intermediate waters (AAIW, $27.3 < \gamma^n < 27.8$) represented by green triangles, deep waters (NADW, $27.8 < \gamma^n < 28.12$) represented by black dots, and bottom waters (AABW, $\gamma^n > 28.12$) represented by blue dots. (For interpretation of the references to color in this figure legend, the reader is referred to the web version of this article.)

upper part of the intermediate waters range ($27.3 < \gamma^n < \sim 27.5$, approximately a depth range of 500–900 m), the linear relation between $F(340/440)$ and AOU is high (slope = $(3.70 \pm 0.16) \times 10^{-5}$ R.U., $R^2 = 0.88$, $n = 66$, p -value < 0.001). These results are in agreement with Yamashita and Tanoue (2008), which reported that the mesopelagic layer was the main site for production of FDOM by microbial respiration in the ocean interior.

3.2.2.2. Abyssal layer (1000 m–Sea bottom); deep and bottom waters. For deep waters ($27.8 < \gamma^n < 28.12$), a weak but positive

linear relationship is found between $F(340/440)$ and AOU (slope = $(3.60 \pm 0.31) \times 10^{-5}$ R.U., $R^2 = 0.27$, $n = 126$, p -value < 0.001 , Table 1); bottom waters ($\gamma^n > 28.12$) do not present any significant linear relationship ($R^2 < 0.01$, $n = 30$, p -value = 0.81, Table 1). Both deep and bottom waters show relatively high values of $F(340/440)$ associated with AOU values, lower than expected if humic-like FDOM came only from in situ production (Fig. 8a). The high-latitude North Atlantic region, where NADW is formed each winter, is a region of high spring primary production (Ducklow and Harris, 1993) which also receives large amounts of terrestrial organic matter from the Arctic rivers (Álvarez-Salgado

et al., 2013; Jørgensen et al., 2011; Dittmar and Kattner, 2003). All over, these water masses introduce high levels of O_2 and humic-like FDOM into the deep equatorial Atlantic Ocean. Respect to the AABW, a plausible explanation for the relative high FDOM/AOU ratio is linked to the conditions in those formation regions located near the Antarctic continental margin. A large fraction of recalcitrant DOM moves up to the surface, mainly in the Southern Ocean via the upwelling of NADW (Chen, 2011). This, together with low light incidence and the high depth of the surface mixed layer in this region (Siegel et al., 2002), results in CDOM-rich (and therefore FDOM-rich) surface waters.

3.3. FDOM and AOU residuals ($\Delta F(340/440)$, ΔAOU)

3.3.1. Non-linear models

A significant relationship between deep humic-like FDOM (Coble's M-peak) and AOU has been reported by Yamashita and Tanoue (2008) for the Pacific Ocean basin. They found positive and strong linear FDOM–AOU correlations for all water masses within the mesopelagic layer but with substantial differences in slope and intercept. Such differences were associated to the mixing of source waters with different initial levels of FDOM. In order to evaluate the in situ production rate of FDOM from the respiration rate, Yamashita and Tanoue (2008) considered only the FDOM–AOU linear relationship in the abyssal layer (> 1000 m) where one single dominant water mass is found (slope = 0.0047 N.FI.U., $R^2 = 0.85$, $n = 210$, p -value < 0.001). Yamashita et al. (2010), using Fluorescence Excitation Emission Matrix (EEM) spectroscopy and multivariate data analysis Parallel Factor (PARAFAC), found a humic-like component similar to that traditionally assigned to terrestrial humic-like fluorophore (C-peak). They showed that C-peak and AOU were linearly correlated in both the mesopelagic (200–1000 m) and bathypelagic (1000–4000 m) layers. Taking into account the mixing of waters with different source in the mesopelagic layer of the Pacific Ocean, the authors only discussed the FDOM–AOU relationship in the bathypelagic layer (slope = 0.0029 Q.S.U., $R^2 = 0.89$, $n = 16$, p -value < 0.001). Jørgensen et al. (2011) found a significant relationship between component 1 (the humic-like FDOM component associated to C-peak) and AOU for the dark global ocean excluding waters from the North Atlantic (O_2 and humic-FDOM rich in origin) (slope = 3.493×10^{-5} R.U., $R^2 = 0.72$, $p < 0.05$). However, as in previous studies (Yamashita and Tanoue, 2008; Yamashita et al., 2010), the variability related to the different concentrations at origin was not considered. Álvarez-Salgado et al. (2013) found a strong relationship between marine humic-like FDOM (Coble's M-peak) and AOU (slope = 0.009 ± 0.002 Q.S.U., $R^2 = 0.83$, $n = 9$, $p < 0.001$) in the deep northern North Atlantic, but the Denmark Strait overflow water (DSOW), initially rich in O_2 and remarkably high in humic-FDOM content, was also omitted because it deviated from the general trend.

Our results (Section 3.2) show a significant but weak relationship between $F(340/440)$ and AOU (slope = $(1.20 \pm 0.01) \times 10^{-5}$ R.U., $R^2 = 0.05$, $n = 360$, p -value < 0.001 , Table 1) for the dark equatorial Atlantic (> 200 m). The presence of deep and bottom waters, rich in humic-like FDOM and low in AOU at origin, would explain the weak $F(340/440)$ –AOU relationship for the ocean interior. This is consistent with reports for the Atlantic Ocean (Jørgensen et al., 2011; Álvarez-Salgado et al., 2013; Nelson and Siegel, 2013) which point at a dependence of both $F(340/440)$ and AOU values on the conditions where the different water masses were formed.

In order to remove the variability associated to the distinct $F(340/440)$ and AOU “initial” conditions of each water mass, a multiple non-linear regression has been carried out between either $F(340/440)$ or AOU with salinity and temperature

(Eqs. (1) and (2)); the underlying premise is that a water mass is identified by a point, or region, in the temperature–salinity space. The results show that only a small portion of the $F(340/440)$ variability is explained by temperature and salinity ($R^2 = 0.20$, p -value < 0.001 ; Eq. (1)); instead, the AOU distribution is highly dependent on temperature and salinity, with an $R^2 = 0.89$ and p -value < 0.001 (Eq. (2))

$$F(340/440) = -14.1 + 0.8S - 1.2 \times 10^{-2}S^2 - 5.4 \times 10^{-2}\theta - 4.0 \times 10^{-5}\theta^2 + 1.6 \times 10^{-3}S\theta + \Delta F(340/440),$$

$$R^2 = 0.20, n = 369, p < 0.001. \quad (1)$$

$$AOU = -5.8 \times 10^5 + 3.4 \times 10^4S - 502S^2 - 2438\theta - 2.0\theta^2 + 71.0S\theta + \Delta AOU,$$

$$R^2 = 0.89, n = 399, p < 0.001. \quad (2)$$

The residuals ($\Delta F(340/440)$ and ΔAOU), as deduced after subtracting the values estimated through the optimal model (Eqs. (1) and (2)) from the observed values, represent the variability of $F(340/440)$ and AOU that is not explained by temperature and salinity. The significant relationship between AOU with salinity and temperature (Eq. (2)) indeed leads to an important reduction in the ΔAOU standard deviation ($SD_{\Delta AOU} = 17.8 \mu\text{mol kg}^{-1}$), as compared with the AOU standard deviation ($SD_{AOU} = 52.8 \mu\text{mol kg}^{-1}$). The major reduction is observed for intermediate ($SD_{\Delta AOU} = 26.4 \mu\text{mol kg}^{-1}$ versus $SD_{AOU} = 16.0 \mu\text{mol kg}^{-1}$), deep ($SD_{\Delta AOU} = 10.6 \mu\text{mol kg}^{-1}$ versus $SD_{AOU} = 7.8 \mu\text{mol kg}^{-1}$) and bottom waters ($SD_{\Delta AOU} = 10.3 \mu\text{mol kg}^{-1}$ versus $SD_{AOU} = 4.8 \mu\text{mol kg}^{-1}$) and it is minimal for central waters ($SD_{\Delta AOU} = 27.5 \mu\text{mol kg}^{-1}$ versus $SD_{AOU} = 28.4 \mu\text{mol kg}^{-1}$).

In contrast, the standard deviation of $\Delta F(340/440)$ for the ocean interior ($SD_{\Delta F(340/440)} = 5.7 \times 10^{-4}$ R.U.) only shows a slight reduction when compared with the standard deviation of the $F(340/440)$ data ($SD_{F(340/440)} = 6.4 \times 10^{-4}$ R.U.). Such a result confirms the relatively low dependence of $F(340/440)$ on salinity and temperature for all water strata (Eq. (1)). As the FDOM residuals represent the major source of the $F(340/440)$ variability, we can conclude that in situ processes have an important role in FDOM production.

A remarkable result is the low FDOM variability explained by temperature and salinity, as compared with AOU. Fig. 5 shows that both AOU and $F(340/440)$ have a noteworthy west-east gradient, not present in the salinity and potential temperature profiles (Fig. 3). In contrast, AOU presents much more depth variability than $F(340/440)$, which correlates well with the salinity and potential temperature vertical profiles. We have no conclusive explanation for these differences, but they clearly reflect that $F(340/440)$ is much less correlated to the water masses than AOU, the latter being strongly related to the temperature-dependent O_2 content at origin.

3.3.2. A general $\Delta F(340/440)$ – ΔAOU relationship for the ocean interior

The distributions of residuals $\Delta F(340/440)$ and ΔAOU along 75°N do follow similar patterns (Fig. 9). This fact suggests that the variability of $\Delta F(340/440)$ (Fig. 9a) is associated with the variability of ΔAOU (Fig. 9b) and endorses the idea of a clear relationship between $\Delta F(340/440)$ and ΔAOU for the ocean interior.

Our results indeed show a significant, positive and high $\Delta F(340/440)$ – ΔAOU relationship for this particular area when considering the full dataset below 200 m, i.e. when considering all water masses present in the zone of study (Eq. (3), Fig. 8b)

$$\Delta F(340/440) = (3.14 \pm 0.08) \times 10^{-5} \Delta AOU,$$

$$R^2 = 0.79, n = 360, p < 0.001. \quad (3)$$

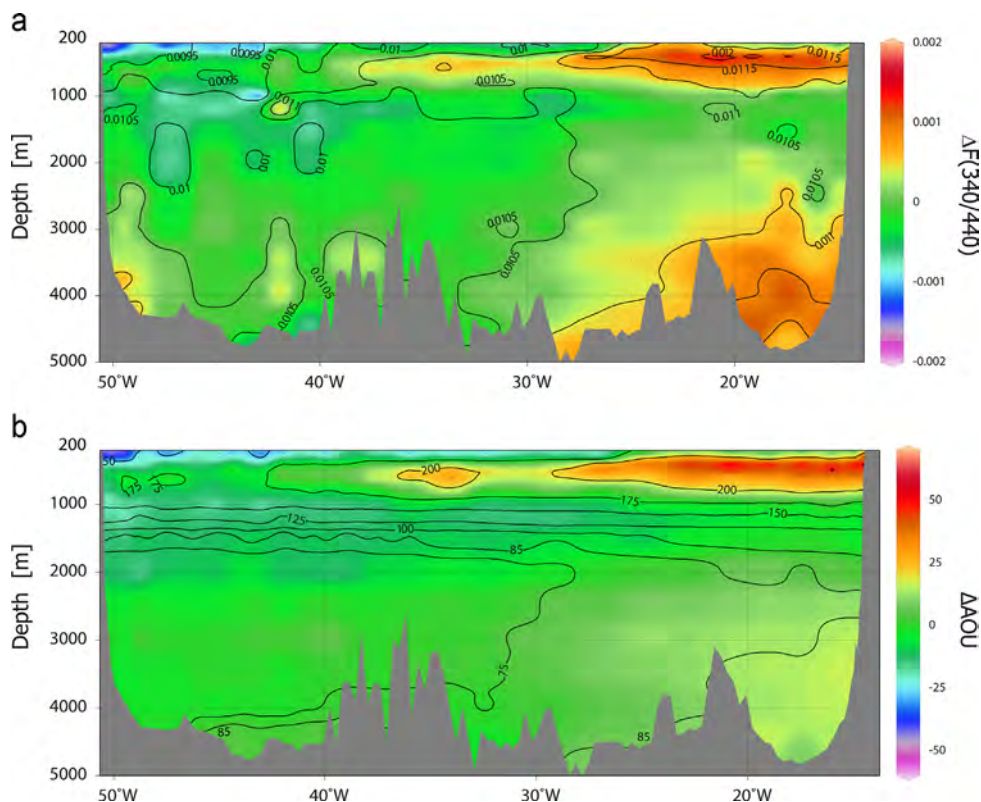


Fig. 9. Contour maps of (a) $F(340/440)$ (black isolines) and $\Delta F(340/440)$ (R.U.) (colour filled contour) and (b) AOU (black isolines) and ΔAOU ($\mu\text{mol kg}^{-1}$) (colour filled contour). (For interpretation of the references to color in this figure legend, the reader is referred to the web version of this article.)

This significant general relationship points a biological oxidation of organic matter by microbial activity as the main source of $F(340/440)$ in the dark ocean.

Despite the existence of this general relationship, the correlation between $\Delta F(340/440)$ – ΔAOU changes among the different water strata. Model II covariance analysis (Table 2) shows a $\Delta F(340/440)$ – ΔAOU linear relationship higher for central ($R^2=0.92$, p -value < 0.001) and intermediate waters ($R^2=0.79$, p -value < 0.001) than for deep ($R^2=0.57$, p -value < 0.001) and bottom waters ($R^2=0.25$, p -value < 0.05) (Table 2). The slopes for the linear relationships change significantly among different water strata ($r_3=89.93$, p -value < 0.001), except between central and intermediate waters (p -value=0.71).

Furthermore, with the exception of the intermediate waters, for each water stratum the slope of the linear relationship differs significantly from the general slope, $(3.14 \pm 0.08) \times 10^{-5}$ R.U. ($r_4=89.93$, p -value < 0.001): p -value < 0.05 for central waters, < 0.001 for deep waters and < 0.001 for bottom waters, while p -value=0.58 for intermediate waters (Table 2). The slope of the deep and bottom waters is indeed substantially larger than for central and intermediate waters, and also larger than the slope of the general trend (Eq. (3)).

Our results agree qualitatively with those obtained by Álvarez-Salgado et al. (2013) for the northern North Atlantic Ocean. These authors justified the different slopes of the humic-like FDOM–AOU relationships in terms of the ventilation of the corresponding water mass realms. According to Álvarez-Salgado et al. (2013), during deep water formation, freshly produced organic matter is injected below the main thermocline acting as a source of DOM for bacteria in the abyssal layer. A similar result was found by Nelson et al. (2007, 2010) for CDOM in the Atlantic Ocean. These authors suggested that rapid formation and advection of NADW masks the existence of a high-correlation between CDOM and

AOU. As $F(340/440)$ is closely related to CDOM, the high rate of NADW and AABW ventilation could also mask the $\Delta F(340/440)$ – ΔAOU relationship found in the present study. For bottom waters, an additional source of $\Delta F(340/440)$ could come from the sediments, caused by the current-induced resuspension (Lappo et al., 2001; Nelson et al., 2007).

Considering the statistical significance of the $\Delta F(340/440)$ – ΔAOU relationship ($R^2=0.79$, p -value < 0.001), a major source of $F(340/440)$ in the equatorial Atlantic dark ocean could be related to in situ biological oxidation of organic matter by microbial activity. This is particularly relevant as there are other FDOM possible sources, as mentioned in previous studies. Jørgensen et al. (2011) speculated that FDOM can be produced abiotically via extracellular precursors released not only by microbial activity but also through viral lysis and grazing activities among others. Recently, Andrew et al. (2013) suggested that chemical or microbial modification of an existing terrestrial source material could be also an importance source of humic-like FDOM. However, it has been shown that C-peak, traditionally assigned with a terrestrial origin, can be also produced by marine bacterial activity (Romera-Castillo et al., 2011b) and that terrestrial material is not necessary to generate FDOM (for example, marine bacteria cultivated in artificial sea water with glucose and inorganic nutrients can produce C-peak FDOM, Kramer and Herndl (2004)).

Finally, when comparing our results with earlier works, an important issue to take into account is the difference in definitions and units for the humic-like fluorescence. Yamashita and Tanoue (2008) and Álvarez-Salgado et al. (2013) studied the fluorescence intensity at Ex/Em at 320 nm/420 nm, i.e. what Coble (1996) defined as the peak M characteristic of marine humic-like substances. Jørgensen et al. (2011) and Yamashita et al. (2010) obtained Ex/Em matrices instead of Ex/Em pairs and used PAR-AFAC modelling to define fluorescent components.

4. Conclusions

The observed distributions of $F(340/440)$ and AOU along the 7.5°N section complement early results for this region (Determann et al., 1996; Karstensen et al., 2008; Jørgensen et al., 2011) and in other ocean basins (Yamashita and Tanoue, 2008; Yamashita et al., 2010). For the ocean interior (> 200 m), the $F(340/440)$ and AOU distributions share some similarities, but also substantial differences, particularly within the deep and bottom waters which are O_2 and humic-FDOM rich at origin. As a result we find a significant but very weak relationship between $F(340/440)$ and AOU.

A multiple non-linear regression analysis for the ocean interior shows that more than 80% of the AOU variability along the 7.5°N Atlantic cross section may be explained by the hydrographic characteristics, with temperature and salinity as a proxy of water masses. However, only 20% of the variability of fluorescence intensity is explained by these hydrographic characteristics. We use optimal non-linear models, for both $F(340/440)$ and AOU as a function of temperature and salinity, in order to remove the variability associated to the water masses. Then, a general and significant relationship is found between the residuals $\Delta F(340/440)$ and ΔAOU , with a slope of $(3.14 \pm 0.08) \times 10^{-5}$ R.U. ($R^2=0.79$, p -value < 0.001). This relationship is obtained using the full dataset below 200 m, i.e. considering all water masses present in the zone of study regardless of the mixture of waters with different levels of preformed FDOM and AOU. This is a remarkable result because, until now, a strong and significant FDOM–AOU association has been found for the Atlantic Ocean only when omitting those waters that are O_2 and humic-FDOM rich at origin (Álvarez-Salgado et al., 2013; Jørgensen et al., 2011; Nelson and Siegel, 2013).

Despite the existence of such a significant general relationship, we still find significant differences among individual water stratum. In particular, within the deep and bottom waters the production of $F(340/440)$ associated to oxidation or organic matter appears to be higher than for central and intermediate waters. This seems to be mainly related with the ventilation of water masses but may also reflect the existence of different processes and transformations in each individual stratum.

The strong and significant general relationship between $\Delta F(340/440)$ and ΔAOU reveals that 79% of the $\Delta F(340/440)$ variability is associated to ΔAOU for the interior equatorial Atlantic Ocean. This result endorses the idea that, after removing the potential differences at origin, the major source of $F(340/440)$ in the dark ocean is the in situ biological oxidation of organic matter by microbial activity.

Acknowledgments

The MOC2-Equatorial cruise was carried out with the R/V *Hespérides*, we are happy to acknowledge support by the crew and on board technicians. Funding comes from the Spanish government through the MOC2 (CTM2008-06438-CO2), TIC-MOC (CTM2011-28867), and DOREMI (CTM2012-34294) projects of the R+D Spanish research program, and from the ECLIPSE project financed by Total Foundation. P. De La Fuente would like to thank the Agència de Gestió d'Ajuts Universitaris i de Recerca de la Generalitat de Catalunya (AGAUR) for their financial support through a FI-AGAUR fellowship. A. Canepa was funded by CONICYT (PFCHA/Doctorado al Extranjero 4a Convocatoria, 72120016). C. Romera-Castillo was funded by a Beatriu de Pinós post-doctoral fellowship from the AGAUR of the Generalitat de Catalunya. Images 2, 4, 6 and 9 have been created using Ocean Data View (Schlitzer, 2011, <http://odv.awi.de>).

References

- Álvarez-Salgado, X.A., Nieto-Cid, M., Álvarez, M., Pérez, F.F., Morin, P., Mercier, H., 2013. New insights on the mineralization of dissolved organic matter in central, intermediate, and deep-water masses of the northeast North Atlantic. *Limnol. Oceanogr.* 58 (2), 681–696, <http://dx.doi.org/10.4319/lo.2013.58.2.0000>.
- Andrew, A.A., Del Vecchio, R., Subramaniam, A., Blough, N. V., 2013. Chromophoric dissolved organic matter (CDOM) in the Equatorial Atlantic Ocean: optical properties and their relation to CDOM structure and source. *Mar. Chem.* 148 (33–43), <http://dx.doi.org/10.1016/j.marchem.2012.11.001>.
- Arhan, M., Mercier, H., Bourlès, B., Gouriou, Y., 1998. Hydrographic sections across the Atlantic at 7°30N and 4°30S. *Deep Sea Res. Part I* 45, 829–872.
- Benson, B.B., Krause Jr., D., 1984. The concentration and isotopic fractionation of oxygen dissolved in freshwater and seawater in equilibrium with the atmosphere. *Limnol. Oceanogr.* 29 (3), 620–632.
- Carlson, C.A., et al., 2010. Dissolved organic carbon export and subsequent remineralization in the mesopelagic and bathypelagic realms of the North Atlantic basin. *Deep Sea Res. Part II* 57, 1433–1445, <http://dx.doi.org/10.1016/j.dsr.2.2010.02.013>.
- Castro, C.G., Nieto-Cid, M., Álvarez-Salgado, X.A., Pérez, F.F., 2006. Local remineralization patterns in the mesopelagic zone of the eastern North Atlantic, off the NW Iberian Peninsula. *Deep Sea Res. Part I* 53, 1925–1940.
- Chen, C.T.A., 2011. Microbial carbon pump: additional considerations. *Nat. Rev. Microbiol.* , <http://dx.doi.org/10.1038/nrmicro2386-c4>.
- Chen, R.F., Bada, J.L., 1992. The fluorescence of dissolved organic matter in seawater. *Mar. Chem.* 37, 191–221.
- Coble, P.G., Green, S.A., Blough, N.V., Gagosian, R.B., 1990. Characterization of dissolved organic matter in the Black Sea by fluorescence spectroscopy. *Nature* 348, 432–435.
- Coble, P.G., 1996. Characterization of marine and terrestrial DOM in seawater using excitation-emission matrix spectroscopy. *Mar. Chem.* 51, 325–346.
- Coble, P.G., 2007. Marine optical biogeochemistry: the chemistry of ocean color. *Chem. Rev.* 107, 402–418.
- Del Castillo, C.E., Coble, P.G., Morell, J.M., López, J.M., Corredor, J.E., 1999. Analysis of the optical properties of the Orinoco River plume by absorption and fluorescence spectroscopy. *Mar. Chem.* 66, 35–51.
- Determann, S., Reuter, R., Willkomm, R., 1996. Fluorescence matter in the eastern Atlantic Ocean: Part 2. Vertical profiles and relation to water masses. *Deep Sea Res.* 43, 345–360.
- Dittmar, T., Kattner, G., 2003. The biogeochemistry of the river and shelf ecosystem of the Arctic Ocean: a review. *Mar. Chem.* 83, 103–120.
- Ducklow, H., Harris, R., 1993. Introduction to the JGOFS North Atlantic bloom experiment. *Deep Sea Res.* 40, 1–8.
- Flugister, F.L., 1960. Atlantic Ocean Atlas of Temperature and Salinity Profiles and Data from the International Geophysical Year of 1957–1958. Atlas Series, Woods Hole Oceanographic Institution 1
- Hansell, D.A., Carlson, C.A., Repeta, D.J., Reiner, S., 2009. Dissolved organic matter in the ocean: new insights stimulated by a controversy. *Oceanography* 22, 52–61, <http://dx.doi.org/10.5670/oceanog.2009.109>.
- Hansell, D.A., 2013. Recalcitrant dissolved organic carbon fractions. *Annu. Rev. Mar. Sci.* 5, 3.1–3.25.
- Hayase, K., Tsubota, H., Sunada, I., 1989. Relationships of fluorescence and AOU in three north Pacific water samples. *Sci. Total Environ.* 81/82, 315–318.
- Hayase, K., Shinozuka, N., 1995. Vertical distribution of fluorescent organic matter along with AOU and nutrients in the equatorial Central Pacific. *Mar. Chem.* 48, 283–290.
- Ito, T., Follows, M.J., Boyle, E.A., 2004. Is AOU a good measure of respiration in the oceans? *Geophys. Res. Lett.* 31 (17305–17305).
- Jackett, T.R., McDougall, T.J., 1997. A neutral density variable for the world's ocean. *J. Phys. Oceanogr.* 27, 237–263.
- Jiao, N., Herndl, G.J., Hansell, D.A., Benner, R., Kattner, G., Wilhelm, S.W., Kirchman, D.L., Weinbauer, M.G., Luo, T., Chen, F., 2010. Microbial production of recalcitrant dissolved organic matter: long-term carbon storage in the global ocean. *Nat. Rev. Microbiol.* 8, 593–599.
- Jørgensen, L., Stedmon, C.A., Kragh, T., Markager, S., Middelboe, M., Søndergaard, M., 2011. Global trends in the fluorescence characteristics and distribution of marine dissolved organic matter. *Mar. Chem.* 126, 139–148.
- Karstensen, J., Stramma, L., Visbeck, M., 2008. Oxygen minimum zones in the eastern tropical Atlantic and Pacific oceans. *Prog. Oceanogr.* 77, 331–350.
- Kramer, G.D., Herndl, G.J., 2004. Photo- and bioreactivity of chromophoric dissolved organic matter produced by marine bacterioplankton. *Aquat. Microb. Ecol.* 36, 239–246.
- Lappo, S.S., Lozovatsky, I.D., Morozov, E.G., Sokov, A.V., Shapovalov, S.M., 2001. Variability of water structure in the equatorial Atlantic. *Dokl. Earth Sci. Sect* 379, 739–743.
- Lawaetz, A.J., Stedmon, C.A., 2009. Fluorescence intensity calibration using the Raman scatter peak of water. *Appl. Spectrosc.* 63 (8), 936–940.
- Legendre, P., Legendre, L., 1998. Numerical Ecology. Number 20 in Developments in Environmental Modellingsecond ed. Elsevier, Amsterdam.
- Logan, M., 2010. Biostatistical design and analysis using R, A Practical Guide. Wiley-Blackwell, Oxford, UK, ISBN: 978-1-4443-3524-8 p. 546.
- Machín, F., Pelegrí, J.L., 2009. Northward penetration of Antarctic Intermediate Water off northwest Africa. *J. Phys. Oceanogr.* 39, 512–535.
- Mamayev, O.I., 1975. Temperature–Salinity Analysis of World Ocean Waters, Amsterdam-Oxford-New York. Elsevier Scientific p. 374.

- McDougall, T.J., Barker, P.M., 2011. Getting Started with TEOS-10 and the Gibbs Seawater (GSW) Oceanographic Toolbox, 28 pp., SCOR/IAPSO WG127, 978-0-646-55621-5.
- Mopper, K., Zhou, X., Kieber, R.J., Kieber, D.J., Sikorski, R.J., Jones, R.D., 1991. Photochemical degradation of dissolved organic carbon and its impact in oceanic carbon cycle. *Nature* 353, 60–62.
- Nelson, N.B., Siegel, D.A., Carlson, C.A., Swan, C., Smethie, W.M., Khaliwala, S., 2007. Hydrography of chromophoric dissolved organic matter in the North Atlantic. *Deep Sea Res. Part I* 54, 710–731.
- Nelson, N.B., Siegel, D.A., Carlson, C.A., Swan, C.M., 2010. Tracing global biogeochemical cycles and meridional overturning circulation using chromophoric dissolved organic matter. *Geophys. Res. Lett.* 37, L03610.
- Nelson, N.B., Siegel, D.A., 2013. Global distribution and dynamics of chromophoric dissolved organic matter. *Annu. Rev. Mar. Sci.* 5, 447–476.
- Nieto-Cid, M., Álvarez-Salgado, Gago, J., X.A., Pérez, F.F., 2005. DOM fluorescence a tracer for biogeochemical processes in a coastal upwelling system (NW Iberian Peninsula). *Mar. Ecol. Prog. Ser.* 297, 33–50.
- Nieto-Cid, M., Álvarez-Salgado, X.A., Pérez, F.F., 2006. Microbial and photochemical reactivity of fluorescent dissolved organic matter in a coastal upwelling system. *Limnol. Oceanogr.* 51, 1391–1400.
- Oudot, C., 1993. Carbon data obtained during the R/V L'Atalante cruise in the Atlantic Ocean (WOCE Section A07, 13 February–19 March 1993). Carbon Dioxide Information Analysis Center, Oak Ridge National Laboratory, US Department of Energy, A07. Oak Ridge, Tennessee p. 1993b, [http://dx.doi.org/10.3334/CDIAC/otg.WOCE\(http://cdiac.ornl.gov/ftp/oceans/a07/woce/\)](http://dx.doi.org/10.3334/CDIAC/otg.WOCE(http://cdiac.ornl.gov/ftp/oceans/a07/woce/)).
- Orsi, A.H., Johnson, G.C., Bullister, J.L., 1999. Circulation, mixing, and production of Antarctic Bottom Water. *Prog. Oceanogr.* 43, 55–109.
- Romera-Castillo, C., Sarmento, H., Álvarez-Salgado, X.A., Gasol, J.M., Marrasé, C., 2010. Production of chromophoric dissolved organic matter by marine phytoplankton. *Limnol. Oceanogr.* 55 (1), 446–454.
- Romera-Castillo, C., Nieto-Cid, M., Castro, C.G., Marrasé, C., Largier, J., Barton, E.D., Álvarez-Salgado, X.A., 2011a. Fluorescence: absorption coefficient ratio—tracing photochemical and microbial degradation processes affecting coloured dissolved organic matter in a coastal system. *Mar. Chem.* 125, 26–38.
- Romera-Castillo, C., Sarmento, H., Álvarez-Salgado, X.A., Gasol, J.M., Marrasé, C., 2011b. Net production/consumption of fluorescent coloured dissolved organic matter by natural bacterial assemblages growing on marine phytoplankton exudates. *Appl. Environ. Microbiol.* 77, 7490–7498.
- Core Team, R., 2012. R: A Language and Environment for Statistical Computing. R Foundation for Statistical Computing, Vienna, Austria, ISBN: 3-900051-07-0 (URL).
- Salisbury, J., Vandermark, D., Campbell, J., Hunt, C., Wisser, D., Reul, N., Chapron, B., 2011. Spatial and temporal coherence between Amazon River discharge, salinity, and light absorption by colored organic carbon in western tropical Atlantic surface waters. *J. Geophys. Res.* 116, <http://dx.doi.org/10.1029/2011JC006989>.
- San Antolín, M.A., Pelegrí, J.L., Machín, F.J., Benítez, V., 2012. Inter decadal changes in stratification and double diffusion in a transatlantic section along 7.5°N. *Sci. Mar.* 76S1, 189–207 (ISSN:0214–8358).
- Sarafanov, A., Sokov, A., Demidov, A., 2007. Water mass characteristics in the equatorial North Atlantic: a section nominally along 6.5°N, July 2000. *J. Geophys. Res.* 112, C12023, <http://dx.doi.org/10.1029/2007JC004222>.
- Siedler, G., Zangenberg, N., Onken, R., Morlière, A., 1992. Seasonal changes in the tropical Atlantic circulation: observation and simulation of the Guinea Dome. *J. Geophys. Res.* 97, 703–7150.
- Siegel, D., Maritorena, S., Nelson, N., Hansell, D., Lorenzi-Kayser, M., 2002. Global distribution and dynamics of colored dissolved and detrital organic materials. *J. Geophys. Res.* 107, 3228.
- Stedmon, C.A., Markager, S., 2005. Resolving the variability in dissolved organic matter fluorescence in temperate estuary and its catchment using PARAFAC analysis. *Limnol. Oceanogr.* 50, 686–697.
- Schlitzer, R., Ocean Data View, (<http://odv.awi.de>), 2011.
- Stramma, L., Schott, F., 1999. The mean flow field of the tropical Atlantic Ocean. *Deep Sea Res. Part II* 46, 279–303.
- Stramma, L., 2008. Expanding oxygen—minimum zones in the tropical oceans. *Science* 320, 655.
- Talley, L.D., Pickard, G.L., Emery, W.J., Swift, J.H., 2011. *Descriptive Physical Oceanography: An Introduction* sixth ed. Elsevier, Boston p. 560.
- Yamashita, Y., Tsukasaki, A., Nishida, T., Tanoue, E., 2007. Vertical and horizontal distribution of fluorescence dissolved organic matter in the Southern Ocean. *Mar. Chem.* 106, 498–509.
- Yamashita, Y., Tanoue, E., 2008. Production of bio-refractory fluorescent dissolved organic matter in the ocean interior. *Nature* 1, 579–582.
- Yamashita, Y., Cory, R.M., Nishioka, J., Kuma, K., Tanoue, E., Jaffé, R., 2010. Fluorescence characteristics of dissolved organic matter in the deep waters of the Okhotsk Sea and the northwestern North Pacific Ocean. *Deep Sea Res. Part II* 57, 1478–1485, <http://dx.doi.org/10.1016/j.dsr2.2010.02.016>.
- Warton, D.I., Duursma, R.A., Falster, D.S., Taskinen, S., 2012. *Smatr 3—an R package for estimation and inference about allometric lines*. *Methods Ecol. Evol.* 3, 257–259.
- Weiss, R.F., 1970. The solubility of nitrogen, oxygen and argon in water and seawater. *Deep Sea Res.* 17, 721–735.
- WOCE, 1994. *WOCE Operations Manual: Vol. 3, Sect. 3.1, Part 3.1.3: WHP Operations and Methods Oxygen Determination*. Woods Hole, MA, USA p. 12 (Rev. 1, Nov. 1994).
- Zuur, A.F., Ieno, E.N., Walker, N.J., Saveliev, A.A., Smith, G.M., 2009. *Mixed Effects Models and Extensions in Ecology with R*. Springer, New York p. 574.

TWO-BOX OCEAN MODEL TO UNDERSTAND THE ROLE OF THE RDOC, VIA THE MICROBIAL CARBON PUMP, IN THE GLACIAL-INTERGLACIAL TRANSITIONS



Global constraints on net primary production and inorganic carbon supply during glacial and interglacial cycles

Pelegrí, J.L., De La Fuente, P., Olivella, R. and García-Olivares, A., (2013), Global constraints on net primary production and inorganic carbon supply during glacial and interglacial cycles. *Paleoceanography*. 28, 713 - 725. <https://doi.org/10.1002/2012PA002419> Wiley. Used with permission.

Global constraints on net primary production and inorganic carbon supply during glacial and interglacial cycles

Josep L. Pelegrí,^{1,2} Patricia De La Fuente,¹ Roger Olivella,¹ and Antonio García-Olivares¹

Received 26 October 2012; revised 1 August 2013; accepted 12 November 2013; published 16 December 2013.

[1] Relaxation-type models have good skill at reproducing glacial-interglacial transitions in climatic variables. Here we propose a simple two-box and two-state relaxation-type model for the upper ocean (surface and permanent thermocline layers) where dissolved inorganic carbon/nutrients are supplied by the deep ocean and through remineralization within the upper ocean. The model is tuned using genetic algorithms to simulate the atmospheric CO₂ time series for the last four glacial-interglacial cycles. The fit to the data is very good, with correlations above 0.8, as the upper ocean responds to shifts in (1) the intensity of the meridional overturning circulation, from off to on during the glacial-interglacial transition, and (2) the size and sign of net primary production, with respiration greatly exceeding primary production during interglacial periods and production larger than respiration during the glacial phase. The glacial-interglacial transitions are interpreted as shifts between two distinct metabolic states of the Earth system, with high/low supply of dissolved inorganic carbon and nutrients to the productive upper ocean during interglacial/glacial periods.

Citation: Pelegrí, J. L., P. De La Fuente, R. Olivella, and A. García-Olivares (2013), Global constraints on net primary production and inorganic carbon supply during glacial and interglacial cycles, *Paleoceanography*, 28, 713–725, doi:10.1002/2012PA002419.

1. Introduction

[2] The Earth system has presented an alternation between glacial and interglacial states during the last circa 3 Myr [e.g., *Imbrie et al.*, 1993; *Sigman and Boyle*, 2000; *Paillard*, 2001; *Raymo and Nisancioglu*, 2003; *Sigman et al.*, 2010]. These two states display substantial changes in diverse global variables, such as high/low atmospheric CO₂ values during interglacial/glacial periods [e.g., *Petit et al.*, 1999; *Siegenthaler et al.*, 2005; *Lüthi et al.*, 2008]. Considering that the amount of dissolved inorganic carbon (DIC) available in the ocean is much larger than that contained within the atmosphere and biosphere, and given the rates of exchange between these different compartments, it turns out that the oceans are the principal responsible for glacial-interglacial changes in atmospheric CO₂ [e.g., *Sundquist and Visser*, 2003]. Therefore, the main processes that have been invoked to explain these atmospheric variations are thought to operate on the intensity of the physical, biological, and chemical ocean pumps.

[3] The physical pump is traditionally related to seasonal and latitudinal changes in sea surface temperature, as the

partial pressure of CO₂ within the ocean surface depends largely on temperature [e.g., *Siegenthaler and Sarmiento*, 1993]. The concept, however, is easily extended to consider actual changes in the content of total DIC within the surface ocean, related to the presence of waters of different origin [*Sarmiento and Toggweiler*, 1984; *Siegenthaler and Wenk*, 1984; *Toggweiler*, 1999]. The biological pump depends directly on variations in net primary production, as it transforms DIC into organic carbon [*Broecker*, 1982a, 1982b; *Sarmiento and Toggweiler*, 1984; *Knox and McElroy*, 1984; *Martin*, 1990]. Finally, the chemical pump relies on changes in calcium carbonate (CaCO₃), either due to external fluxes or through the dissolution of carbonate organisms: An increase in carbonate raises the ocean's alkalinity which affects the partition of DIC and leads to the sequester of atmospheric CO₂ [*Broecker*, 1982a; *Broecker and Peng*, 1987]. All three pumps rely, to a large degree, on the rate at which bottom waters (relatively cold, nutrient rich and DIC rich) are brought in contact with the atmosphere, i.e., they rely on the intensity of the meridional overturning circulation (MOC) [*Stommel*, 1961; *Broecker*, 1991].

[4] A number of box-type models, focused on reproducing the interglacial and glacial maximum conditions, have investigated the relative importance of these pumps [e.g., *Sarmiento and Toggweiler*, 1984; *Siegenthaler and Wenk*, 1984; *Paillard et al.*, 1993; *Toggweiler*, 1999; *Peacock et al.*, 2006; *Skinner*, 2009]. Estimates on the drawdown of CO₂ change substantially depending on the diffusive and advective circulation patterns, the assumptions on the conservation and distribution of properties, and whether external factors (such as sediment and dust sources) are allowed. The complexity of a model, and likely its realism, increases with the number of boxes,

Additional supporting information may be found in the online version of this article.

¹Departament d'Oceanografia Física i Tecnològica, Institut de Ciències del Mar, CSIC, Barcelona, Spain.

²LINCGlobal, Institut de Ciències del Mar, CSIC, Barcelona, Spain.

Corresponding author: J. L. Pelegrí, Departament d'Oceanografia Física i Tecnològica Institut de Ciències del Mar, CSIC, Passeig Marítim de la Barceloneta, 37-49, E-08003 Barcelona, Spain. (pelegrí@icm.csic.es)

©2013. American Geophysical Union. All Rights Reserved.
0883-8305/13/10.1002/2012PA002419

but the large scatter among all results tells us that the relative importance of the mechanisms operating during glacial and interglacial periods remains to be elucidated.

[5] Given the evident difficulty for determining the different contributions during steady state conditions, it is no surprise that time-dependent box models are not used to simulate glacial-interglacial transients. The alternatives are idealized two-state relaxation-type heuristic models for one or more coupled variables [e.g., *Calder, 1974; Imbrie and Imbrie, 1980; Watson and Maddock, 1993; Paillard, 1998; Paillard and Parrenin, 2004; Hogg, 2008; García-Olivares and Herrero, 2012, 2013*]. These models assume the existence of two different ocean states (glacial and interglacial) and allow DIC, and other oceanic variables, to relax toward different reference values; for example, the control equation for ice volume, I , has the form $dI/dt = (I_r - I)/\tau_{ice}$, where I_r is a reference ice volume and τ_{ice} is a relaxation time.

[6] The behavior of relaxation models depends on three types of parameters: the timing for the system to switch state, the reference concentrations during each state, and the length of time required for the system to relax toward the reference value. A proper formulation for these parameters requires good knowledge of those mechanisms forcing the behavior of the physical, biological, and chemical pumps, particularly of those processes setting the MOC intensity and the concentration of the transported properties. The parameters may not be constant; for example, the relaxation time typically changes depending on the state and variable under consideration. Many mechanisms have been proposed, such as atmospheric (wind and thermal) forcing, deep ocean stratification, sea ice coverage in the southern ocean, and oscillations in the burial of carbonates [*Paillard et al., 1993; Paillard, 1998; Toggweiler, 1999; Stephens and Keeling, 2000; Paillard and Parrenin, 2004; Hogg, 2008; Toggweiler et al., 2006; Skinner, 2009; García-Olivares and Herrero, 2013*]. However, no deterministic formulation is yet available so these parameters are usually specified through (properly tuned) heuristic dependences on external and internal forcing.

[7] The *Paillard and Parrenin [2004]* relaxation-type model illustrates the good skill of heuristic models at reproducing the time series of diverse climatological proxies; *García-Olivares and Herrero [2013]* have recently optimized the model's formulation to obtain correlations with data as high as 0.90 for ice volume and 0.79 for atmospheric CO_2 . This model has three time-dependent variables (ice volume, Antarctic ice extent, and atmospheric carbon dioxide), with the reference value for each variable expressed as a linear function that may involve insolation and all three variables. A step-like change of state is specified through an additional dependent variable, efficiency in bottom water formation, which is directly related to ice volume and inversely linked to the amount of insolation over Antarctica and the extent of the Antarctic ice sheet. The argument is that high efficiency implies the formation of salty, well-stratified and high- CO_2 , bottom waters; when this variable falls below certain threshold, the formation of stratified bottom waters is substantially reduced, and there is a discontinuous increase in the CO_2 reference concentration. The *Paillard and Parrenin [2004]* model has the virtue of identifying the existence of multiple processes and, therefore, represents an important step forward in our understanding of climate transitions. Nevertheless, as in all heuristic arguments, it is unquestionable that there is no

unique interpretation for the forcing mechanisms and, furthermore, different versions for the formulations are possible with equally good results [*García-Olivares and Herrero, 2012, 2013*]. For example, a high rate of deep water formation, no matter how salty and stratified these waters are, implies a fast recirculation of DIC-rich deep waters to the surface. Actually, even a very slow rate of deep water formation would imply relatively short time scales for the MOC, e.g., only one Sverdrup ($1 \text{ Sv} = 10^6 \text{ m}^3 \text{ s}^{-1}$) would fill the world's oceans in a time scale of the order of 10 kyr. Therefore, the relevant argument should not focus on the formation of bottom waters but rather on how isolated these waters are, in terms of both negligible diapycnal mixing (because of high vertical stratification) and a small sea-surface print (possibly helped by sea surface ice capping). This brief discussion illustrates that heuristic relaxation-type models are capable of grasping some of the relations between variables and the dependences to external forcing but, as they are not based on fundamental principles, other unknown interactions are certainly possible.

[8] In this study we propose a very simple time-dependent DIC model for an upper ocean that changes at glacial-interglacial time scales. This upper ocean is understood as that part of the ocean holding an active wind- and/or buoyancy-driven thermocline circulation and having relatively short (order 10 years) characteristic time scales, connected to a nutrient-rich deep ocean through the MOC. The model, inspired on the way local and remote energy supply allows a living being to sustain transitions between basal and enhanced metabolic states [*Pelegri, 2008*], is capable of reproducing the glacial-interglacial transitions with the sole action of a peculiar version of the physical-biological pump. The net autotrophic community production in the upper ocean sets the metabolic rate of the ocean system, sustained through remineralization within the upper ocean (local or proximal reserves) and deep-ocean supply through a changing MOC (remote sources). The results lead us to interpret interglacial periods as times of enhanced metabolic rate, sustained by high heterotrophic respiration (greater than net autotrophic community production) and intense MOC supply, and glacial periods as times when community production exceeds total respiration. An innovative character of the model is the role assigned to the pool of dissolved organic carbon (DOC) in the upper ocean, building up during glacial periods and being consumed during interglacial times, analogous to proximal (and fast) energy reserves in living beings.

[9] The DIC equation arises from conservation arguments in a very simple two-box ocean; therefore, no heuristic interpretations are necessary, its structure being that of a relaxation-type model. The model is tuned with genetic algorithms to hindcast the atmospheric CO_2 during the last four interglacial-glacial cycles. It can neither predict the timing when the system switches state nor the reference concentrations during both states, which are set from the data through simple criteria, but finds the size and temporal dependence of the MOC (the inverse of relaxation time) and sets constraints on the amount of primary production and remineralization in the upper ocean.

2. A Simple Transient Model for the Upper Ocean

2.1. Transient Box Model for the Upper Ocean

[10] *Pelegri [2008]* has proposed the Earth to be an optimized pulsating system, analogous to many other living

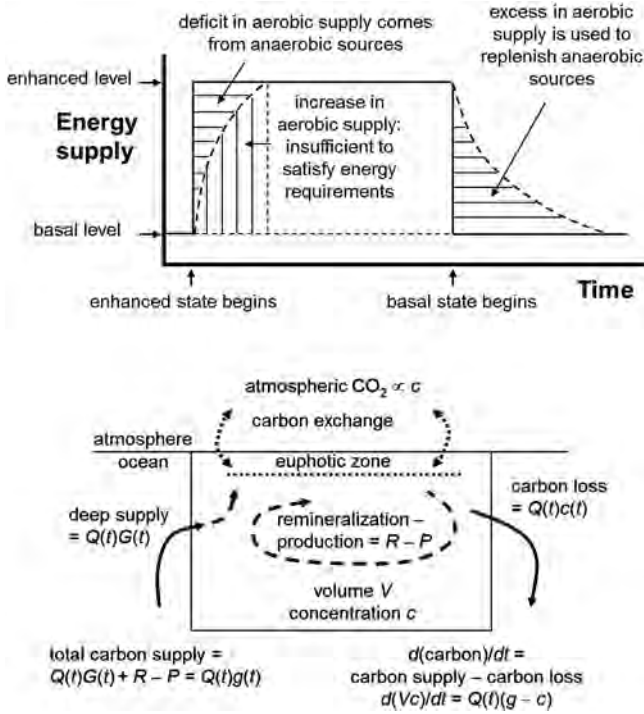


Figure 1. (top) Schematics of the change in energy supply to mammals, as an example of complex system, as it switches from one metabolic state to another. In this plot, the supply discretely changes between two different, low and high, energy supply levels. (bottom) Main elements of the two-box model for DIC concentration in the upper ocean. The closed rectangle represents the upper ocean. The net advective DIC supply is given by $Q(G - c)$ and the aerobic processes $R - P$ account for the deficit or excess supply. Adapted from Pelegrí [2008].

beings, and has endorsed the idea that it may be studied using global, physiological-like, variables. In particular, he argued that the glacial and interglacial periods correspond to times of rest and exercise for an autotrophic planet, in terms of its skill to convert solar energy through photosynthesis (see also Appendix A in the supporting information). The efficiency of this conversion is set by the availability of DIC and inorganic nutrients, supplied both through remineralization of DOC in the upper ocean (local and fast sources) and by the MOC advection of nutrient- and carbon-rich deep waters (Figure 1 (top)). In this paper we will further explore these ideas using, as our reference variable, the concentration of DIC in the upper ocean simply because it may be calibrated against the paleorecord of atmospheric CO_2 . We must keep in mind, however, that DIC is always in excess at the sea surface so that inorganic nutrients, with substantial differences in concentration between the upper and deep ocean, are the truly limiting factors for primary production; hence, hereafter we shall think of carbon as accompanying the nutrient supply in proportions close to the stoichiometric Redfield ratios [e.g., Anderson and Sarmiento, 1994] so that we will indistinctly talk about (inorganic) nutrients or carbon supply.

[11] A complementary view is obtained by considering a simple ocean composed of a time-changing upper box and a deep immutable chamber, as shown in Figure 1 (bottom) [Pelegrí, 2008]. The upper box contains surface and thermocline waters, in direct or indirect contact with the atmosphere,

the latter via Ekman or buoyancy pumping [Stommel, 1979; Luyten and Stommel, 1986]. The rate of water recirculation within the upper box is much greater than the rate of water exchange between both compartments; hence, at glacial-interglacial time scales, we consider the upper ocean recirculation to solely be responsible for homogenizing the carbon and nutrient concentrations in the upper box. The upper and deep compartments are connected through the MOC: Water from the upper box sinks into the deep chamber at high latitudes, indistinctly in the Northern and Southern Hemispheres, and eventually recirculates back to the upper ocean. The rate of exchange between the two compartments may change in time through variations in the MOC, shifting between two stable (although not necessarily steady) states [Stommel, 1961].

[12] Temperature, salinity, and alkalinity play no role in our highly idealized two-box model. The arrival of deep waters to the upper compartment only affects its inorganic carbon (and nutrients) content and will bring no other property anomalies. Therefore, we focus on the biological pump related to the transformation of new and remineralized carbon (nutrients), ignoring any changes in air-sea CO_2 exchange associated to possible thermodynamic and chemical upper ocean variations. This approach allows us to examine the evolution of DIC in the upper ocean, during the last four glacial-interglacial cycles, solely through the Vostok record of atmospheric CO_2 . This is because (for constant temperature, salinity, and alkalinity) the relation between DIC in the upper ocean (carbon dioxide, bicarbonate, and carbonate) and atmospheric CO_2 is approximately linear in the 180 to 280 ppm $p\text{CO}_2$ range (see also Appendix D in the supporting information).

[13] Obviously, we do not attempt to produce a fully diagnostic model; rather, we propose a conceptual approach that focuses on understanding what the CO_2 time series tells us about global constraints on primary production and inorganic carbon supply during glacial and interglacial cycles. Some of the underlying approximations are indeed reasonable; for example, alkalinity does not change through the introduction of CO_2 into the water, and it is neither much affected as a result of the synthesis or remineralization of organic matter [Paillard et al., 1993; Brewer and Peltzer, 2009]. However, we disregard any (potentially important) effects on atmospheric CO_2 related to the introduction of cold waters to the surface ocean or to relative changes in the concentration of calcium carbonate during enhanced primary production; in section 5, we will come back to some of these issues.

[14] After arrival of deep water to the upper ocean, some of its inorganic carbon and nutrients are photosynthesized and converted into organic matter while some are left unused and returned back to the deep ocean during winter deep water formation (Figure 1). The equations for DIC, c , and DOC, c_r , in the upper ocean are

$$\frac{d(cV)}{dt} = R - P + Q(G - c) \xrightarrow{s.s.} P_s - R_s = Q_s(G_s - c_s), \quad (1)$$

$$\frac{d(c_r V)}{dt} = P - R - Qc_r \xrightarrow{s.s.} P - R_s = Q_s c_{r,s}, \quad (2)$$

where $Q(t)$ is the volume transport (or overturning rate), V is the upper ocean volume, $G(t)$ is the DIC concentration reaching the upper ocean through the returning MOC, and

$R(t)$ and $P(t)$ are the remineralization and primary production of the upper ocean, respectively; the s subindex denotes steady state (s.s.) conditions. In these expressions, the respiration comes from both the autotrophic R_{aut} and heterotrophic R_{het} communities, i.e., $R = R_{aut} + R_{het}$ (see Appendix A in the supporting information). A similar formulation was proposed by Pelegrí [2008] and Pelegrí *et al.* [2011] but with the important difference that the deep ocean input was taken as $Q c_d$ instead of $Q G$, with c_d being the high-DIC concentration of the deep ocean; the deep ocean concentration was assumed constant and always larger than c therefore conditioning the size and sign of $R - P$.

[15] Equations (1) and (2) are conservative for the upper ocean. Equation (2) shows that DOC is transferred from the upper to the deep ocean, where these materials will have plenty of time to remineralize. The model is largely idealized as it ignores any thermal and chemical ocean change, such as the deep-ocean carbonate system, and does not consider the high-nutrient and low-chlorophyll Southern Ocean. Further, it assumes the system is closed, i.e., it does not address processes such as iron fertilization, export of particulate organic matter, and changes in coastal erosion between glacial and interglacial cycles. Finally, it is not clear whether the concentrations of inorganic carbon and nutrients have significantly changed within the deep ocean in the past [Ganeshram *et al.*, 1995; Sigman and Haug, 2003; Sigman *et al.*, 2010], so the simplest hypothesis is to choose them constant. The model, therefore, focuses on the transformation between inorganic and organic matter within the upper ocean and on the exchange of dissolved carbon between the upper and deep ocean compartments through the MOC.

[16] The steady state form of equation (1) is identical to equation (A1) in the supporting information. This is a relevant result, as it suggests that the two-box ocean model may be understood as ruling the metabolic requirements for the upper ocean but with a changing pool of DIC: Equation (1) sets the fraction of solar energy used for photosynthetic transformation of DIC into DOC. For this to occur, the supply of DIC to the upper ocean has to switch between two different metabolic states, indistinctly supported by remote and local sources, with an exponential-like relaxation toward one single reference DIC value for each state.

2.2. Nondimensional Formulation

[17] As explained in section 1, one possible approach to reproduce two-state DIC transitions would be through a nondimensional relaxation-type equation, such as $d(cV)/dt = Q(g - c)$, where each state has its own g value for the reference DIC. In this equation, Q is inversely proportional to the relaxation time, i.e., a rapid transition corresponds to a large overturning rate and vice versa, and a constant g sets the concentration level to be attained by the upper ocean if it remains sufficiently long within one single state. Equation (1) is turned into such an expression by simply letting $R - P = Q(g - G)$, i.e.,

$$\frac{dc}{dt} = Q(g - G) + Q(G - c) = Q(g - c). \quad (3)$$

[18] In equation (3), the total DIC supply $Q(g - c)$ has been decomposed into an advective source from the deep ocean

$Q(G - c)$ and a term arising from biological processes within the upper ocean $Q(g - G)$.

[19] Equation (3) is turned into nondimensional through the following scaling: $t = \tau_0 t'$, $c = c_d c'$, $G = c_d G' \equiv c_d \Gamma$, $g = c_d g' \equiv c_d \gamma$, $Q = Q_0 Q' \equiv Q_0 \varepsilon$, and $R - P = Q_0 c_d (R' - P')$, where τ_0 is a glacial (or basal) time scale, c_d is the DIC concentration of the deep ocean, and $Q_0 = V/\tau_0$ is the basal recirculation rate, expressed in terms of the volume of the upper ocean V . Assuming an upper ocean of constant volume, the corresponding nondimensional equation becomes (dropping primes)

$$\frac{dc}{dt} = \varepsilon(\gamma - \Gamma) + \varepsilon(\Gamma - c) = \varepsilon(\gamma - c). \quad (4)$$

[20] The main advantage of this last equation is its simplicity, as the solution depends solely on two variables: the recirculation rate or inverse recirculation time $\varepsilon(t)$ and the concentration level $\gamma(t)$.

3. Modeling the Antarctic Time Series

3.1. State Changes: Timing and Reference Concentrations

[21] Rather than modeling the absolute value of DIC concentration in the upper ocean, we may look at its anomalies referred to some background state. Formally, this means we restrict our calculations to a relatively small DIC range where an approximate linear relation with atmospheric CO_2 is expected; in practice, this allows us to use atmospheric CO_2 anomalies as a proxy for changes in the upper ocean DIC. Specifically, we define $c = c_0 + \hat{c}$, $g = c_0 + \hat{g}$, and $G = c_0 + \hat{G}$, where c_0 is a constant value, and substitute back into equation (3), so that this equation (after dropping hats) becomes an anomaly equation, and equation (4) is the corresponding nondimensional anomaly relation. In the remaining of this paper, we will use these normalized anomalies and will refer to them simply as the nondimensional variables. Note that in order to recover dimensional values (see section 5), we need to dimensionalize the equations through an appropriate anomaly scale (Δc_d rather than c_d). Table 1 summarizes all dimensional parameters and variables, together with their nondimensional counterparts, appearing in the paper.

[22] In order to tune our DIC anomaly model, we use a nondimensional atmospheric CO_2 signal anomaly, derived from the Vostok time series for the last four interglacial-glacial cycles, i.e., between years 432,375 and 20,750 before present. To produce this normalized anomaly time series, we employ the Lüthi *et al.* [2008] CO_2 time series and follow three steps: (a) select the smallest and largest values of the original time series, (b) calculate the anomalies with respect to the smallest value, and (c) normalize these anomalies by the difference between the largest and smallest values. This normalized time series is shown in Figure 2 (top); it comprises four interglacial-glacial cycles chronologically named cycles 1 to 4, with cycle 4 the most recent one.

[23] To set the DIC supply, we use the two-state approximation: As the high state begins, the DIC requirements increase rapidly while as it ends, these requirements also decrease abruptly, so $\gamma(t)$ must resemble a step function. Specifically, the concentration level γ temporarily rises from a basal-glacial

Table 1. Summary of Parameters and Variables

| Parameters, Variables | Description | Dimensional | Scale | Nondimensional |
|---|--|---------------------------------------|-------------------------------------|--|
| Parameters from ocean data | Nowadays MOC transport (22 Sv, assumed to be the same for all interglacial maxima) | Q_{\max} | Q_0 | ε_{\max} |
| | Upper ocean volume ($4.7 \times 10^{17} \text{ m}^3$) | V | | |
| Parameters from CO ₂ time series | Beginning times for interglacial and glacial periods, respectively | t_1, t_2 | | |
| | Time length of glacial and interglacial periods, respectively | $T_g, T_i = t_2 - t_1$ | | |
| | Time when the smoothed CO ₂ time series reaches maximum values | t_{peak} | | |
| | Reference DIC concentration for deep ocean waters reaching back the upper ocean through the MOC | g | c_d (Δc_d for anomalies) | γ |
| Parameters as estimated through GA | Time when the MOC transport is maximum (eventually set to t_2) | t_{\max} | | |
| | Time when the MOC transport returns back to zero (eventually set to time step after t_2) | t_3 | | |
| | Glacial or basal time scale (inversely proportional to the basal transport Q_0) | $\tau_0 = V/Q_0$ | | |
| Other parameters | Non-dimensional deep ocean DIC reaching the upper ocean at the beginning of the interglacial | $\Gamma_g = \Gamma(t = t_1)$ | | |
| | Fraction of glacial-stored DOC available for remineralization during the subsequent interglacial | α | | |
| Variables | Time | t | τ_0 | t |
| | DOC concentration in the upper ocean | c_r | - | - |
| | DIC concentration in the upper ocean | c | c_d (Δc_d for anomalies) | c |
| | DIC concentration in deep ocean waters reaching back to the upper ocean through the MOC | G | c_d (Δc_d for anomalies) | Γ |
| | MOC water transport | Q | Q_0 | ε |
| | Exchange of DIC between the deep and upper oceans or net DIC advective supply | $Q(G - c)$ | $Q_0 c_d$ | $\varepsilon(\Gamma - c)$ |
| | Upper ocean's primary production | P | $Q_0 c_d$ | P |
| | Upper ocean's autotrophic respiration | R_{aut} | $Q_0 c_d$ | R_{aut} |
| | Upper ocean's heterotrophic respiration | R_{het} | $Q_0 c_d$ | R_{het} |
| | Net autotrophic community production, equals the upper ocean's metabolic rate | $M = P - R_{\text{aut}}$ | $Q_0 c_d$ | $M = P - R_{\text{aut}}$ |
| | Upper ocean's total respiration | $R = R_{\text{aut}} + R_{\text{het}}$ | $Q_0 c_d$ | $R = R_{\text{aut}} + R_{\text{het}}$ |
| | Net community respiration, or negative net community production | $R - P = Q(g - G)$ | $Q_0 c_d$ | $R - P = \varepsilon(\gamma - \Gamma)$ |

γ_g (low DIC requirements) to an enhanced-interglacial level γ_i (high DIC state):

$$\gamma = \begin{cases} \gamma_g, & t < t_1 \\ \gamma_i, & t_1 \leq t < t_2 \\ \gamma_g, & t_2 \leq t \end{cases} \quad (5)$$

where γ_g and γ_i , respectively, set the glacial (rest) and interglacial (exercise) levels. We choose $\gamma_g = 0$ and let γ_i constant during each interglacial period but changing from one cycle to another (Figure 2 (top)). A constant γ reflects the stability of the system, i.e., during one specific glacial or interglacial period, the system tends toward a reference point.

[24] The times for changing state, t_1 and t_2 , and the reference levels during each interglacial period, γ_i , are specified by applying simple criteria to the smoothed CO₂ time series. This smoothed series is obtained by low pass filtering the original time series: After several tests, we selected a 2 kyr filter for the interglacial period and a 7 kyr filter for the glacial period. The interglacial start time t_1 corresponds to the last time when the derivative of the smoothed series becomes zero before the original time series overcomes some threshold, taken as 75% of the interglacial maximum value. An exception occurs if the last two minima are separated by less than 10 kyr; in this case t_1 is taken to be the average between these last two minima. Similarly, the end time t_2 is taken as

the last time when the derivative of the smoothed series becomes zero before the original series decreases toward glacial values, again set as less than 75% of the interglacial maximum value. Figure 2 (bottom) shows a detailed view of cycle 4, with the CO₂ original and smoothed series, indicating those times when the system changes from glacial to interglacial, t_1 , and back to glacial, t_2 . The interglacial γ_i level is taken as the mean value of the CO₂ smoothed time series between t_{peak} and t_2 , with t_{peak} corresponding to the time when the smoothed series is maximum.

3.2. Recirculation Rate

[25] In a previous study [Pelegri *et al.*, 2011], the recirculation rate was nondimensionalized as $Q = Q_0 Q' = Q_0(1 + \varepsilon)$, and different $\varepsilon(t)$ functions, always linearly increasing or decreasing in time, were tested. It was found that the best data fit corresponded to $\varepsilon(t) = 0$ during the glacial period and $\varepsilon(t)$ increasing through the interglacial. This relation pertained to a nondimensional basal glacial recirculation rate, $Q' = 1$, which was greatly enhanced during the interglacial, $Q' = 1 + \varepsilon(t)$, with the maximum $\varepsilon(t)$ much greater than 1. The interpretation was that the glacial state corresponds to a situation with a very slow MOC, bringing highly diluted deep ocean DIC to the upper ocean, while the interglacial state corresponds to an active MOC, capable of bringing relatively undiluted bottom waters to the upper ocean. However, as

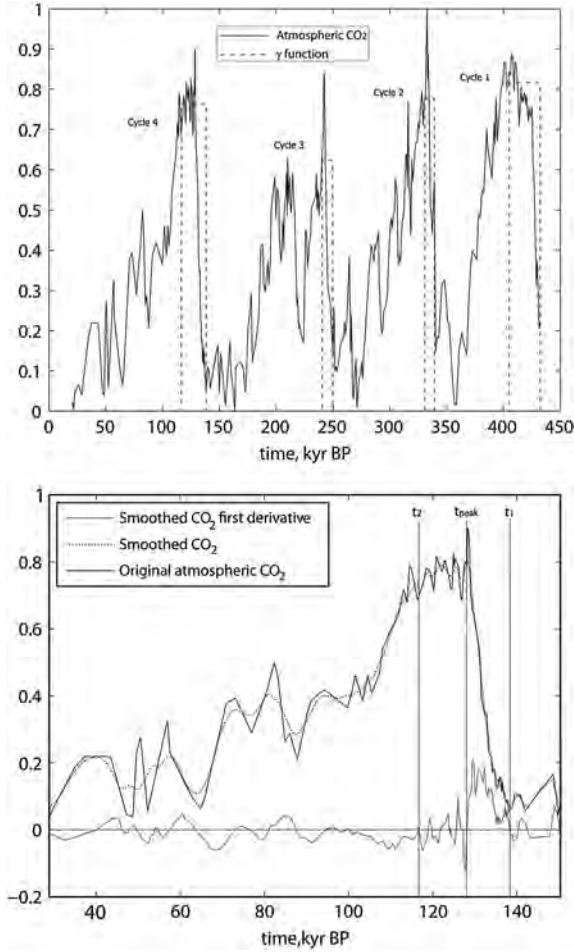


Figure 2. (top) Nondimensional normalized atmospheric CO₂ anomaly as deduced from the Vostok's time series; the rectangles indicate the length and intensity of those periods with enhanced DIC supply. (bottom) Original and smoothed CO₂ time series for cycle 4, together with the time derivative of the smoothed time series, illustrating the timings for the enhanced-supply period. Adapted from *Pelegri et al.* [2011].

argued in section 1, the dilution argument is counterintuitive as even a weak production of deep waters, if maintained during a long enough period, should eventually bring a high concentration level.

[26] Here we pursue an alternative and, we trust, more coherent interpretation: We propose the deep ocean becomes effectively blocked during glacial periods so that, in practice, no high DIC bottom waters reach the upper ocean. In this way, the change of DIC concentration within the upper ocean will only depend on the value of $P - R$. For this purpose, we nondimensionalize the recirculation rate as $Q = Q_0 Q' \equiv Q_0 \varepsilon(t)$ and let $\varepsilon(t)$ change linearly with time between the glacial and interglacial periods. The numerical fit turns out to be very similar to that obtained by *Pelegri et al.* [2011] as all the difference in the current formulation lies on the interglacial recirculation rate being $\varepsilon(t)$ instead of $1 + \varepsilon(t)$. The interpretation for the glacial period, however, is quite different: Rather than a weak recirculation rate ($Q' = 1$), we think of the deep ocean as effectively blocked ($Q' = 0$) so that no deep DIC sources are available. The decaying upper ocean DIC concentration is,

therefore, not the result of diluted deep waters reaching the upper ocean but rather of DIC slowly being transformed into DOC ($P - R > 0$) within an isolated upper ocean.

[27] We examine the sensitivity of the model to simple expressions for the recirculation rate; specifically, we let $\varepsilon(t)$ increase linearly from $\varepsilon(t=t_1)=0$ to a maximum $\varepsilon(t=t_{max})=\varepsilon_{max}$ and then back to $\varepsilon(t=t_3)=0$ (Figure 3). The time t_1 coincides with the beginning of the interglacial, the maximum recirculation takes place some time later, $t_{max} > t_1$, and the recirculation is blocked again at some posterior time within the interglacial or the next glacial period, i.e., $t_3 \geq t_{max}$ can be smaller, equal, or larger than t_2 . Notice t_{max} does not have to equal t_{peak} ; the latter refers to the actual CO₂ measurements and is obtained from the maximum interglacial value in the smoothed time series while the former concerns to the recirculation rate and is determined from the model.

3.3. Best and Mean Value Predictions

[28] The model is calibrated in two steps as described in Appendix B in the supporting information. In the first step, we discretely change parameters until we find a group of values that give an approximate fit to the data (Figure 4 (top)). In the second step, we apply a genetic algorithm (GA) to each interglacial-glacial cycle, initialized with the previously calculated values, to search for the set of parameters that provide the best fit to the data (Figure 4 (middle) and Table 2). Since these parameters change little from one cycle to another, we may calculate the mean parameters for the whole time series: $\bar{\gamma}_i = 0.786$ and $\bar{\tau}_0 = 42.0$ kyr (or, alternatively, $\bar{\varepsilon}_{max} = 60.0$). With these values, and setting $t_{max} = t_2$ and t_3 as the time step immediately after t_{max} , the model output still keeps a quite high correlation ($R^2 = 0.78$) to the data (Figure 4 (bottom)).

[29] This simple model, with only two parameters ($\bar{\gamma}_i$ and $\bar{\tau}_0$) and the knowledge of the transition times (t_1, t_2) for each cycle, is capable of reproducing the overall features of the last four interglacial-glacial cycles (Figure 4). In particular, it matches correctly the asymmetry between the rapid

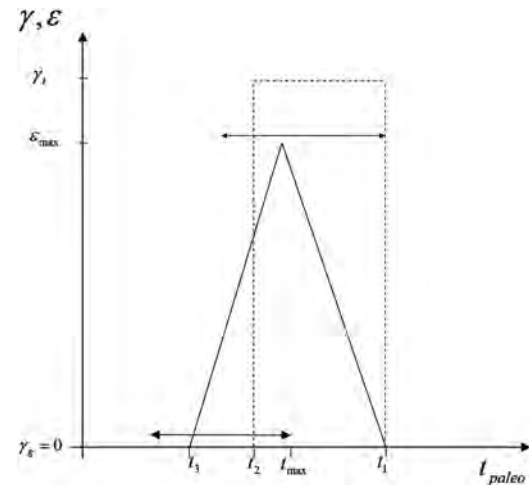


Figure 3. Schematics illustrating the search parameters used in the GA executions; the solid and dashed lines, respectively, correspond to the recirculation rate ε and normalized energy function γ .

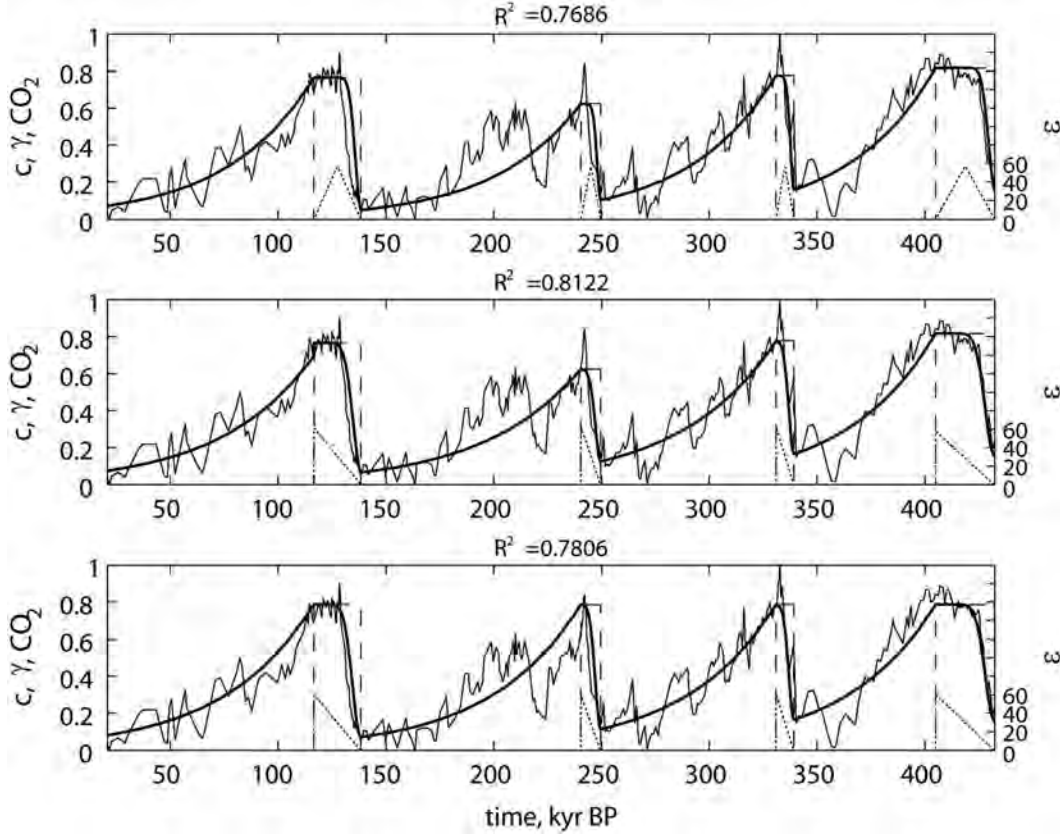


Figure 4. Normalized atmospheric CO₂ anomaly (gray line) and model results of the nondimensional DIC in the upper ocean (black line) for three different cases; the panels also show the normalized energy function γ , which sets the changes in state, and the nondimensional recirculation rate ε which increases rapidly during the interglacial period. (top) Model results for constant $\tau_0 = 40$ kyr, $t_{\max} = (t_1 + t_2)/2$, and $t_3 = t_2$. (middle) Model results for τ_0 and t_{\max} , so that $\varepsilon_{\max} \equiv \varepsilon(t = t_{\max})$, as obtained from the best GA execution, see Table 2. (bottom) Model results with the mean values for cycles 1, 2, and 4 ($\bar{\gamma}_i = 0.786$, $\bar{\tau}_0 = 42.0$ kyr) and $t_3 = t_{\max} = t_2$.

glacial-interglacial transition and the much slower interglacial-glacial decay. This is because the circulation rate $\varepsilon(t)$ rises linearly in time during the interglacial period, $\varepsilon(t) = \varepsilon_{\max} (t - t_1)/(t_2 - t_1)$, which results in an effectively fast circulation rate (short relaxation time), while the transformation of DIC into DOC during the glacial cycles occurs at a very slow rate. The model certainly fails at simulating the abrupt changes, so the ocean-DIC-atmospheric CO₂ correlation cannot become much larger than about 0.8.

[30] The linear $\varepsilon(t)$ increase throughout the interglacial period is in qualitative agreement with evidences of a more

intense MOC during interglacial periods than during glacial periods [Boyle and Keigwin, 1982; Shackleton et al., 1983; Labeyrie et al., 1992]. The interglacial MOC is assumed to have had the same intensity Q_{\max} during all interglacial periods, equal to the current rate of deep water formation (estimated as 22 Sv). The nondimensional MOC peak, ε_{\max} , is expressed as a multiple of a basal rate Q_0 , defined in terms of the glacial relaxation time τ_0 , $\varepsilon_{\max} = Q_{\max}/Q_0 = (Q_{\max}\tau_0)/V$. Its actual value depends on the volume of the upper ocean and the current rate of deep water formation, so its error bars are probably as large as a factor of three. For example, if

Table 2. The Top Three Rows Show the Parameters (t_1 , t_2 , and γ_i) Obtained From the Analysis of the CO₂ Time Series^a

| | Par\Cycle | 1 (Oldest) | 2 | 3 | 4 (Youngest) |
|---|---|---------------------------------|---------------------------------|---------------------------------|---------------------------------|
| | t_1 (yrs BP) | 432,375 | 339,275 | 249,675 | 138,375 |
| | t_2 (yrs BP) | 405,075 | 330,975 | 240,375 | 116,675 |
| | γ_i | 0.816 | 0.776 | 0.624 | 0.765 |
| Best execution | τ_0 (kyr) (ε_{\max}) | 41.0 (58.6) | 44.5 (63.6) | 45.0 (64.3) | 42.8 (61.1) |
| | $(t_{\max} - t_1)/(t_2 - t_1)$ | 0.957 | 0.925 | 0.987 | 1.003 |
| Mean \pm SD for 38 best executions (correlation above 0.81) | τ_0 (kyr) (ε_{\max}) | 40.4 \pm 0.9 (57.7 \pm 1.3) | 43.7 \pm 0.6 (62.4 \pm 0.9) | 44.8 \pm 0.2 (64.0 \pm 0.3) | 42.0 \pm 1.2 (60.0 \pm 1.7) |
| | $(t_{\max} - t_1)/(t_2 - t_1)$ | 0.977 \pm 0.028 | 0.923 \pm 0.021 | 0.993 \pm 0.012 | 1.004 \pm 0.002 |

^aThe remaining rows show the two model parameters (ε_{\max} or τ_0 and $(t_{\max} - t_1)/(t_2 - t_1)$) for the best data fit as obtained after 400 GA executions for each interglacial-glacial cycle (rows 4 and 5, correlation 0.813), and for the mean \pm SD values of those executions (38) whose correlation with the observations is above 0.81 (rows 6 and 7).

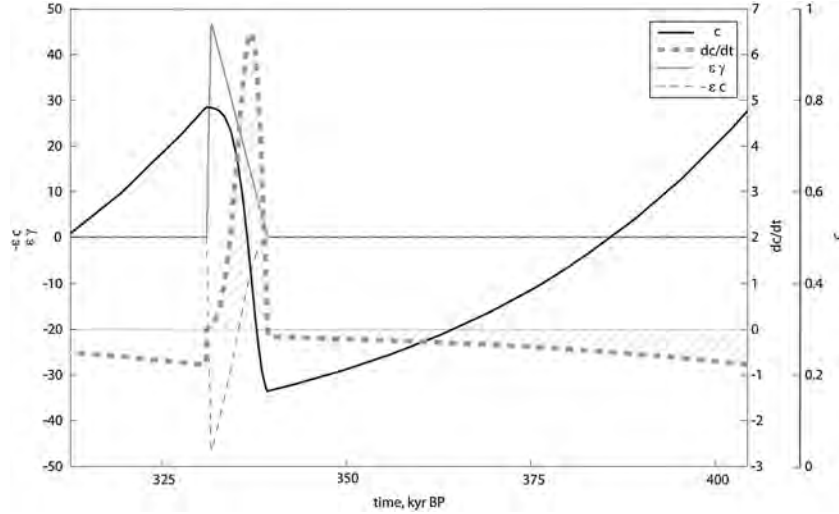


Figure 5. Model results for glacial cycle 1, interglacial cycle 2, and the start of glacial cycle 2 as obtained with the best GA execution (Table 2). The variables plotted are the DIC concentration in the upper ocean c (black solid line), the total input rate $\varepsilon \gamma$ (gray solid line), and the output rate from the upper to the deep ocean $-\varepsilon c$ (dashed gray line); the thick dashed gray line corresponds to the time derivative of the DIC concentration dc/dt and the shaded areas illustrate that condition (6) is approximately satisfied.

today's rate of deep water formation was 50 Sv (instead of 22 Sv) and the upper ocean had a mean depth of 2000 m (instead of 1400 m), ε_{\max} would be about 20. A high ε_{\max} value, either 20 or 180, simply reflects the different processes operating over the DIC budget: an intense MOC and net conversion of DOC into DIC during interglacial periods and net conversion of DIC into DOC during glacial periods.

4. Balancing the Upper Ocean DOC Budget

[31] The nondimensional concentration of DIC reaching the upper ocean through the MOC is set by $\Gamma(t)$. This variable is key to understanding how the DIC input splits between deep-ocean supply and remineralization of DOC within the upper ocean. We may use simple $\Gamma(t)$ dependences, together with DIC conservation arguments, in order to explore this partition. In this section, we will use a linear $\Gamma(t)$ dependence (Appendix C in the supporting information); further, in order to simplify the mathematics, we consider one full glacial-interglacial cycle with time zero set at the start of the glacial period.

[32] The essential argument is that, after one full glacial-interglacial cycle, the DIC in the upper ocean always approximately returns to its initial value. This means that the carbon budget is well balanced, i.e., $\int_0^{T_g+T_i} (dc/dt) dt$ is approximately zero because the area below dc/dt during the glacial approximately equals the area above dc/dt during the posterior interglacial period (Figure 5):

$$-\int_0^{T_g} (dc/dt) dt = \int_{T_g}^{T_g+T_i} (dc/dt) dt, \quad (6)$$

where T_g and T_i , respectively, are the extent of the glacial and interglacial periods (setting $t=0$ at the start of the glacial

gives $T_g=t_1$ and $T_i=t_2-t_1$). In our simple model, the observed oscillations are entirely justified in terms of pure net production during a glacial period and an equally large DIC supply (indistinctly coming from the deep ocean and/or upper ocean DOC remineralization) during the adjacent interglacial period. Equation (6) becomes

$$\int_0^{T_g} (P-R) dt = \int_{T_g}^{T_g+T_i} (R-P) dt + \int_{T_g}^{T_g+T_i} \varepsilon(\Gamma-c) dt. \quad (7)$$

where $\Gamma(t) = \Gamma_g + (\gamma_i - \Gamma_g)(t - t_1)/T_i$ and the value at the start of the interglacial period, Γ_g , is given by equation (C5) (Appendix C in the supporting information).

[33] The DIC reaching the upper ocean at the start of the interglacial depends on the amount of DOC available for remineralization, specifically on the fraction α of DOC accumulated during the glacial period that is to be used during the subsequent interglacial. The sources and sinks of DIC within the upper ocean may be assessed for different values of α , e.g., the smaller the α , the larger will be the MOC contribution. Figure 6 zooms at the model solution at times before, during, and after an interglacial period for $\alpha = 1.0$ and 0.5 (top and bottom panels, respectively). The rate of change of DIC, dc/dt , and the deep ocean net input, $\varepsilon(\Gamma - c)$, are computed from the model exact solutions (Appendix C in the supporting information). The net interglacial respiration is calculated as $R - P = \varepsilon(\gamma_i - \Gamma)$, and the net community primary production during the glacial stage is given by $R - P = -c$. At the start of the interglacial period, the deep ocean input may dominate the DIC budget, but later in the interglacial, because of high remineralization, the DIC concentration within the upper ocean temporarily exceeds those values arriving from the deep ocean, leading to a net loss of DIC through the MOC. We may see that as α decreases, the initial input of DIC from the deep ocean is more relevant, and the contribution from remineralization becomes less important.

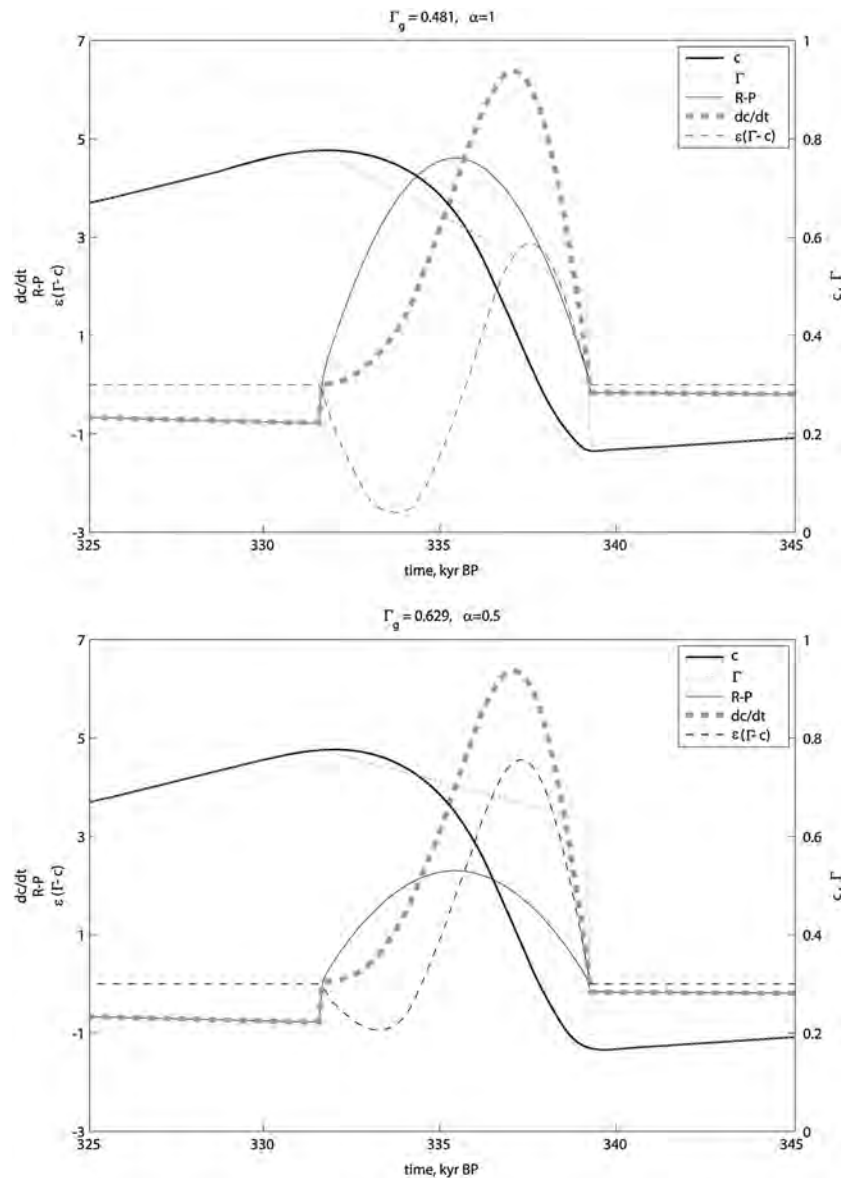


Figure 6. Model results zooming at interglacial cycle 2, as obtained with the best GA execution (Table 2), for (top) $\alpha = 1$ and (bottom) $\alpha = 0.5$. The variables plotted are the DIC concentration in the upper ocean c (solid black line), the net input rate through the MOC $\varepsilon(\Gamma - c)$ (dashed gray line), the net rate of remineralization $R - P$ (solid gray line), and the time derivative of the DIC concentration dc/dt (thick dashed gray line); the function $\Gamma(t)$ is plotted as a dotted line.

[34] The results, in particular the fractioning between deep ocean DIC supply and upper ocean remineralization during the interglacial period, depend on the expressions used for $\Gamma(t)$ and $\varepsilon(t)$ and on the portion $1 - \alpha$ of DOC lost through the MOC. This is simply because we are solving one single equation with two unknowns. Further progress in this direction would require the joint solution of the DIC and DOC equations, subject to proper initial conditions.

5. Discussion

[35] There are evidences which suggest that two important properties of the upper ocean have been substantially different in glacial and interglacial periods: The MOC connection between the deep and upper oceans is enhanced during the

interglacial period [Boyle and Keigwin, 1982; Shackleton *et al.*, 1983; Labeyrie *et al.*, 1992; Sigman and Boyle, 2000; Sigman *et al.*, 2010], and during the glacial stage, in subantarctic waters, primary production exceeds respiration [Mortlock *et al.*, 1991; Kumar *et al.*, 1995; Harris *et al.*, 1996; François *et al.*, 1997; Robinson *et al.*, 2005; Robinson and Sigman, 2008; Martínez-García *et al.*, 2009]. Our simple model has shown that these evidences are consistent with a highly idealized scenario for glacial-interglacial changes in the supply of DIC to the upper ocean.

[36] At the beginning of the interglacial periods, there are two sources of net DIC supply to the upper ocean: The MOC brings deep ocean waters which have an excess DIC concentration, and the upper ocean DOC reservoir becomes progressively depleted as DOC is transformed into DIC

Table 3. Values as Inferred From the Mean of the Best Executions in Table 2^a

| Cycles Glacial-Interglacial | 1–2 | 2–3 | 3–4 |
|--------------------------------------|-------------|-------------|-------------|
| T_g (kyr) | 65.8 | 81.3 | 102.0 |
| T_i (kyr) | 8.3 | 9.3 | 21.7 |
| γ_i | 0.776 | 0.624 | 0.765 |
| τ_0 (kyr) (ϵ_{\max}) | 40.4 (62.4) | 43.7 (64.0) | 44.8 (60.0) |
| Γ_g ($\alpha=1$) | 0.481 | 0.389 | 0.623 |
| Γ_g ($\alpha=0.9$) | 0.511 | 0.412 | 0.637 |
| Γ_g ($\alpha=0.5$) | 0.629 | 0.506 | 0.694 |

^aCycles 1–2, 2–3, and 3–4 correspond to composites done using a glacial-interglacial full cycle (τ_0 belongs to the glacial decay, and ϵ_{\max} corresponds to the interglacial period). All quantities except times are nondimensional.

through enhanced remineralization ($R > P$). Both DIC sources reach maxima some time during the interglacial period, leading to the highest rate of DIC (and inorganic nutrients) increase but go back to zero by the end of the interglacial period as the system approaches a steady state. The MOC source goes to zero simply because the DIC in the upper ocean approaches the concentration of the deep ocean waters that reach back to the surface. The eventual decrease in the net DOC to DIC transformation within the upper ocean is related to the behavior of the metabolic rate, defined as the net autotrophic community production, $M \equiv P - R_{\text{aut}}$. During the (enhanced) interglacial period, the metabolic rate reaches toward a maximum value which equals the heterotrophic remineralization, i.e., $P - R$ tends to zero simply because both $P - R_{\text{aut}}$ and R_{het} are equal and maxima.

[37] During the glacial periods, the upper and deep oceans are virtually disconnected, so very small amounts of DIC and inorganic nutrients are supplied from the deep ocean, and primary production relies on the interglacial upper ocean pool of DIC. During these periods, the upper ocean reached beyond some 2000 m, dominated by the presence of the glacial North Atlantic intermediate waters (GNAIW) [Curry and Oppo, 2005; Lynch-Stieglitz et al., 2007]. It seems likely that the glacial upper ocean maintained a relatively rapid recirculation [Oppo and Lehman, 1993], alike that of the modern ocean, characterized by subduction of surface waters, DOC remineralization during their subsurface trip, and their return to the surface layers at high latitudes [Kawase and Sarmiento, 1985; Pelegri and Csanady, 1991; Pelegri et al., 2006]. Such a swift and long glacial recirculation would lead to an increase in the flux of regenerated inorganic nutrients reaching the euphotic layer and to a proportionally enhanced primary production. The machinery simply becomes more efficient, the only condition being that the thermocline recirculation takes longer than the time scale for remineralization. By the end of the glacial period, the amount of stored DOC would reach a maximum.

[38] Our simple model satisfies the condition that the DIC returns periodically to the initial condition, implying a tight relation between consecutive glacial and interglacial periods: A relatively long glacial period is followed by a proportionally intense interglacial (Figure 2 (top) and Table 3). If the upper ocean was locked, this would imply that the interglacial remineralization could balance the glacial net primary production. However, the interglacial upper ocean does drain both organic carbon and DIC to the deep ocean, meaning that both net (integrated over a glacial-interglacial cycle) primary production and DIC supply from the deep to the upper ocean are positive.

[39] The idea of long-term organic carbon storage in the oceans has recently become the focus of substantial interest (see reviews by Hansell et al. [2009] and Jiao et al. [2010]). Hansell et al. [2009] argue that the deep ocean observations of refractory DOC are consistent with lifetimes of about 15 kyr, the same order as the relevant time scale during interglacial periods. This fits the idea that the large upper ocean pool of DOC, accumulated by the end of the glacial period, becomes a source of DIC and inorganic nutrients during the interglacial stage. A simple calculation may be carried out to assess potential DOC glacial-interglacial changes within the upper ocean reservoir. Nowadays, the DOC reservoir has been estimated to be about 700 Pg, with mean concentrations in the upper ocean of about 45 mmol C m⁻³, while the DIC reservoir is some 55 times larger [Sundquist and Visser, 2003; Hansell et al., 2009]. Assuming that we are close to the end of the (anthropogenic unperturbed) interglacial, the above DOC balance implies that during the glacial maximum, the DOC reservoir could have been of the order of 2000 Pg C, with upper ocean concentrations of about 132 mmol C m⁻³ (Appendix D in the supporting information). This threefold DOC glacial increase would have taken place at the expense of the DIC reservoir, it decreasing by only about 1%.

[40] It is important to emphasize that these figures should be only considered as gross indicators of potential glacial-interglacial changes in DOC stored within the upper ocean, as determined from the best fit of our idealized model to the observed atmospheric CO₂ patterns. Our model has indeed ignored processes which could have a large impact on the DOC budget of the upper ocean. One such process is DOC return to the upper ocean through the MOC. Today's DOC concentrations in the deep ocean are about 35 mmol C m⁻³ [Hansell et al., 2009] so that today's DOC returned to the upper ocean (estimated as the product of the DOC concentration in the deep ocean times the transport of the MOC) amounts to about 0.3 Pg C yr⁻¹. The action of this process during the interglacial period could be expressed as effectively increasing the α parameter. Another neglected process is export of particulate organic carbon (POC) into the deep ocean, nowadays estimated at about 0.4 Pg C yr⁻¹ [Honjo et al., 2008]. During an interglacial period, this effect tends to compensate the previous one, effectively reducing the α parameter. Its role during the glacial period is much more difficult to appraise, it could either imply net primary production larger than here estimated or even the existence of a MOC-driven compensating deep ocean DIC supply. These two combined processes give an interglacial rate of about 0.1 Pg C yr⁻¹ export to the deep ocean, similar to our estimate for the DOC to DIC interglacial rate of transformation in the upper ocean, about 1300 Pg C in some 10,000 years.

[41] The solution of our model depends critically on the temporal changes of a highly idealized MOC, one that does not differentiate between northern and southern limbs and between advective and diffusive return paths. We have reduced the complexity of the actual MOC, either the present or past one, to one main mode of operation with regards to carbon air-sea exchange. Today's MOC, for example, is characterized by sinking of carbon-rich waters in subpolar regions and the return of DIC-rich waters, and CO₂ outgassing, both in the equatorial Atlantic and in the Southern Ocean (the latter without considering anthropogenic effects [Gruber

et al., 2012]). Our model suggests that during glacial periods, there was no such an analogous return path. The largest areas of the globe were dominated by the GNAIW and the formation of very dense bottom waters was localized at high latitudes in the Southern Ocean, taking place in relatively small surface areas but stretching worldwide under the GNAIW [Curry and Oppo, 2005; Lynch-Stieglitz *et al.*, 2007]. The density difference between these water masses was very high, so negligible mixing took place between them [Watson and Naveira-Garabato, 2006; Skinner, 2009], and the Antarctic waters returned to the sea surface near its high-latitude formation areas, probably in regions with substantial sea ice capping; observed latitudinal differences in primary production may actually reflect the presence of these different water masses [Mortlock *et al.*, 1991]. The atmospheric CO₂ was therefore controlled by the transformations of carbon within the GNAIW, with DIC slowly turning into DOC because of positive net community production.

[42] The upper ocean has been defined as waters driven by wind or buoyancy pumping with relatively short recirculation times (order 10 years), for the glacial period corresponding to the quite thick GNAIW. The above considerations are not in conflict with our idealization of an upper ocean of constant volume, as our nondimensional results depend only on the size of the interglacial volume (section 2.1). It is true, however, that this variability has to be taken into account when estimating the glacial maximum DOC concentrations: A doubling of the glacial size would mean halving the glacial increase in DOC, i.e., the upper ocean DOC concentrations at the end of the glacial period would have been about 89 rather than 132 mmol C m⁻³. Clearly, in order to obtain more accurate results, our model would require both including a third box to represent the Southern Ocean, as early done by Sarmiento and Toggweiler [1984] and Siegenthaler and Wenk [1984], and allowing a variable-size upper ocean.

[43] We wish to emphasize that by no means has our approach intended to be a comprehensive approximation to the Earth system. The two-box model, with the upper ocean in equilibrium with the atmosphere, has definitely been inspired on the way energy is distributed and transformed in living beings as they change their metabolic state [Pelegri, 2008]. The approach has focused on a few global variables, therefore ignoring any spatial variability, in a similar way as the health of a living being is quickly assessed through a handful of physiological variables. In particular, we have explored the potential relevance of both a changing MOC and a varying pool of dissolved organic matter in the upper ocean. We believe this perception, yet far from complete, may eventually lead to fundamentally new perspectives in our understanding of the Earth system.

[44] Many other processes may have certainly played a very significant role in controlling the glacial-interglacial variations (see reviews by Sigman and Boyle [2000], Paillard [2001], Kohfeld *et al.* [2005], Sarmiento and Gruber [2006], and Sigman *et al.* [2010]). For example, Kohfeld *et al.* [2005] pointed that increased glacial export production could account for about half the observed CO₂ changes, and Toggweiler [1999] justified the full range in terms of MOC variations combined with the calcium carbonate compensation mechanism. Their description goes well beyond our objectives, but it is worth to end this section with a brief mention of the most promising candidates.

[45] Our model's biological pump has been most rudimentary, disregarding particulate matter and making no distinction between plankton species, and the carbonate pump has been totally neglected. Shifts in the dominant plankton types may have had important consequences on the ocean's DIC. For example, our proposition of increased glacial net production is consistent with a glacial increase in biological rain; if such an increase was accompanied by a reduced calcium-carbonate to organic-carbon ratio, it would have driven an important decrease in atmospheric CO₂ [Sigman and Boyle, 2000]. The physical pump has neither considered any feedback mechanisms, such as how changes in surface temperature (brought about by the MOC) may affect the incorporation of heat to the upper ocean. Other mechanisms playing a potential role in the air-sea CO₂ equilibrium have also been completely ignored: wind-driven upwelling in the Southern Ocean related to the meridional shift in the westerlies, changes in ice coverage and iron fertilization at high latitudes, and dust fluxes to the subtropical gyres. Finally, in our model, the upper ocean DIC concentration is controlled by one single glacial (DIC to DOC transformation) and two interglacial (DOC respiration and deep-ocean supply) processes. In particular, the two interglacial processes are assumed to begin at the same time; however, it is possible that these interglacial mechanisms had not operated simultaneously but sequentially. Similarly, during the glacial period, the DIC to DOC transformation may have been complemented with other processes, for example, the initial MOC interruption could have been followed by iron fertilization of the Southern Ocean [Sigman *et al.*, 2010].

6. Concluding Remarks

[46] We have proposed a two-box ocean model for DIC in the upper ocean, with simple parameterizations for the intensity of the MOC and the net community production during glacial and interglacial periods, whose solution displays exponential decays toward reference DIC values. The model is tuned with a GA in order to obtain the basal (or glacial) time scale τ_0 and the time dependence of the interglacial recirculation rate anomaly $\varepsilon(t)$ that provide the best model fit to the data. The model, despite its simplicity, does well at reproducing the atmospheric CO₂ glacial-interglacial pattern, with data correlations close to 0.8 when only two parameters (basal time scale and interglacial DIC level) and the state-switching times are specified. The model predicts a relatively long (basal) glacial relaxation period, 42 kyr, which is related to the decay time for the conversion of DIC into DOC, surprisingly similar to the period of the Earth's obliquity cycle. It also predicts interglacial relaxation periods 1 to 2 orders of magnitude shorter, associated to high heterotrophic respiration and a swift MOC.

[47] The metabolic rate of the ocean system has been identified with the net primary production of the autotrophic community. This concept has allowed us to explore the idea that the ocean (and probably the Earth) system switches between two different metabolic states, characterized by quite different rates of inorganic carbon and nutrient supply to the upper ocean and, therefore, photosynthetic solar energy transformation. As the system shifts to an enhanced (interglacial) state, the DIC and inorganic nutrients are supplied by the deep ocean through a progressive increase in the MOC. This match is not attained instantly, so the system must resource to inorganic

nutrients and carbon resulting from oxidation of organic matter. The metabolic rate experiences a large increase, but the heterotrophic respiration is so large that total respiration exceeds primary production. When the system returns to the basal (glacial) state, it slowly recovers its reserves of organic matter. During this period, the metabolic rate, despite being small, exceeds the heterotrophic respiration.

[48] We have not proposed what may be the mechanisms that lead to such substantial changes in ocean state. Whatever the triggering mechanisms, for a review, see Paillard and Parrenin [2004], they must have intense positive feedback within the Earth system. Instead, our simple model has focused on assessing what the atmospheric CO₂ glacial-interglacial patterns may be telling us about the carbon transformations taking place within the upper ocean. Our results suggest that upper ocean DIC supply during an interglacial period, both from the deep ocean and through DOC remineralization, equals the DIC employed through net primary production during the adjacent glacial period. A novel element is the role played by dissolved organic matter in the upper ocean as a proximal and relatively fast source of inorganic carbon and nutrients, building up during glacial periods and becoming available through enhanced heterotrophic respiration during the interglacial times. This mode of operation is indicative of the existence of a pulsating homeostatic organization, e.g., the longer and deeper a glacial period, the more intense will be the next interglacial.

[49] Analogous temporal patterns have been observed in other complex systems, as they change between two distinct metabolic states [Scheffer et al., 2001, 2009; Dakos et al., 2008]. For example, as mammals begin exercise, they experience changes in the rate of oxygen and nutrient supply to the different organs, coming from both nearby (reserves within cells) and remote (brought by the circulatory system) sources [Pelegri, 2008]. The corollary of this study may possibly be that future work on the climate of the Earth system shall benefit from observations of the organization and response of other complex systems, such as living beings, hence using physiology as a source of inspiration.

[50] **Acknowledgments.** We sincerely thank our colleagues for many useful comments, particularly Xosé Álvarez-Salgado, Eva Calvo, Marta Estrada, Carmen Herrero, Denny Kirwan, Celia Marrasé, Carles Pelejero, and Fiz Pérez. We would also like to extend our gratitude to our reviewers for numerous constructive suggestions, including Christopher Charles, the journal's chief editor. This work has been funded through projects MOC2 (CTM2008-06438-C02) and TIC-MOC (CTM2011-28867) of the R+D Spanish research program and through project Fisiocan (PIF08-006-1) of CSIC's frontier program. PDLF has been partly supported through a FI-AGAUR fellowship from the Catalan government.

References

Anderson, L. A., and J. L. Sarmiento (1994), Redfield ratios of remineralization determined by nutrient data analysis, *Global Biogeochem. Cycles*, *8*, 65–80.

Boyle, E. A., and L. D. Keigwin (1982), Deep circulation of the North Atlantic over the last 200,000 years: Geochemical evidence, *Science*, *218*, 784–787.

Brewer, P. G., and E. T. Peltzer (2009), Limits to marine life, *Science*, *324*, 347–348.

Broecker, W. S. (1982a), Glacial to interglacial changes in ocean chemistry, *Progr. Oceanogr.*, *11*, 151–197.

Broecker, W. S. (1982b), Ocean chemistry during glacial time, *Geochim. Cosmochim. Acta*, *46*, 1689–1706.

Broecker, W. S. (1991), The great ocean conveyor, *Oceanography*, *4*, 78–89.

Broecker, W. S., and T.-H. Peng (1987), The role of CaCO₃ compensation in the glacial to interglacial atmospheric CO₂ change, *Global Biogeochem. Cycles*, *1*, 15–29.

Calder, N. (1974), Arithmetic of ice ages, *Nature*, *252*, 216–218.

Curry, W. B., and D. W. Oppo (2005), Glacial water mass geometry and the distribution of δ¹³C of ΣCO₂ in the western Atlantic Ocean, *Paleoceanography*, *20*, PA1017, doi:10.1029/2004PA001021.

Dakos, V., M. Scheffer, E. H. van Nes, V. Brovkin, V. Petoukhov, and H. Held (2008), Slowing down as an early warning signal for abrupt climate change, *Proc. Natl. Acad. Sci. U. S. A.*, *105*, 14,308–14,312.

François, R., M. A. Altabet, E.-F. Yu, D. M. Sigman, M. P. Bacon, M. Frank, G. Bohman, G. Boreille, and L. Labeyrie (1997), Contribution of Southern Ocean surface-water stratification to low atmospheric CO₂ concentrations during the last glacial period, *Nature*, *389*, 929–935.

Ganeshram, R. X., T. F. Pedersen, S. E. Calvert, and J. W. Murray (1995), Large changes in oceanic nutrient inventories from glacial to interglacial periods, *Nature*, *376*, 755–758.

García-Olivares, A., and C. Herrero (2012), Fitting the last Pleistocene delta O-18 and CO₂ time-series with simple box models, *Sci. Mar.*, *76SI*, 209–218.

García-Olivares, A., and C. Herrero (2013), Simulation of glacial-interglacial cycles by simple relaxation models: Consistency with observational results, *Clim. Dyn.*, *41*, 1307–1331.

Gruber, N., et al. (2012), Oceanic sources, sinks, and transport of atmospheric CO₂, *Global Biogeochem. Cycles*, *23*, GB1005, doi:10.1029/2008GB003349.

Hansell, D. A., C. A. Carlson, D. J. Repeta, and R. Schlitzer (2009), Dissolved organic matter in the ocean: A controversy stimulates new insights, *Oceanography*, *22*, 202–211.

Harris, P. G., M. Zhao, A. Rosell-Melé, R. Tiedemann, M. Sarnthein, and J. R. Maxwell (1996), Chlorin accumulation as a proxy for Quaternary marine primary productivity, *Nature*, *383*, 63–65.

Hogg, A. M. (2008), Glacial cycles and carbon dioxide: A conceptual model, *Geophys. Res. Lett.*, *35*, L01701, doi:10.1029/2007GL032071.

Honjo, S., S. J. Manganini, R. A. Krishfield, and R. Francois (2008), Particulate organic carbon fluxes to the ocean interior and factors controlling the biological pump: A synthesis of global sediment trap programs since 1983, *Progr. Oceanogr.*, *76*, 217–285.

Imbrie, J., and J. Z. Imbrie (1980), Modelling the climatic response to orbital variations, *Science*, *207*, 943–953.

Imbrie, J., et al. (1993), On the structure and origin of major glaciation cycles 2. The 100,000-year cycle, *Paleoceanography*, *8*, 699–735.

Jiao, N., G. J. Herndl, D. A. Hansell, R. Benner, G. Kattner, S. W. Wilhelm, D. L. Kirchman, M. G. Weinbauer, T. Luo, and F. Chen (2010), Microbial production of recalcitrant dissolved organic matter: Long-term carbon storage in the global ocean, *Nat. Rev. Microbiol.*, *8*, 593–599.

Kawase, M., and J. L. Sarmiento (1985), Nutrients in the Atlantic thermocline, *J. Geophys. Res.*, *90*, 8961–8979.

Knox, F., and M. McElroy (1984), Changes in atmospheric CO₂ influence of the marine biota at high latitude, *J. Geophys. Res.*, *89*, 4629–4637.

Kohfeld, K. E., C. Le Quéré, S. P. Harrison, and R. F. Anderson (2005), Role of marine biology in glacial-interglacial CO₂ cycles, *Science*, *308*, 74–78.

Kumar, N., R. F. Anderson, R. A. Mortlock, P. N. Froelich, P. Kubik, B. Ditttrichhann, and M. Suter (1995), Increased biological productivity and export production in the glacial Southern Ocean, *Nature*, *378*, 675–680.

Labeyrie, L. D., J. C. Duplessy, J. Duprat, A. Juillet-Leclerc, J. Moyes, E. Michel, N. Kallel, and N. J. Shackleton (1992), Changes in the vertical structure of the North Atlantic Ocean between glacial and modern times, *Quaternary Sci. Rev.*, *11*, 401–413.

Lüthi, D., et al. (2008), High-resolution carbon dioxide concentration record 650,000–800,000 years before present, *Nature*, *378*, 379–382.

Luyten, J. R., and H. Stommel (1986), Gyres driven by combined wind and buoyancy flux, *J. Phys. Oceanogr.*, *16*, 1551–1560.

Lynch-Stieglitz, J., et al. (2007), Atlantic meridional overturning circulation during the Last Glacial Maximum, *Science*, *316*, 66–69.

Martin, J. (1990), Glacial-Interglacial CO₂ change: The iron hypothesis, *Paleoceanography*, *5*, 1–13.

Martínez-García, A., A. Rosell-Melé, W. Geibert, R. Gersonde, P. Masqué, V. Gaspari, and C. Barbante (2009), Links between iron supply, marine productivity, sea surface temperature, and CO₂ over the last 1.1 Ma, *Paleoceanography*, *24*, PA1207, doi:10.1029/2008PA001657.

Mortlock, R. A., C. D. Charles, P. N. Froelich, M. A. Zibello, J. Saltzman, J. D. Hays, and L. H. Burckle (1991), Evidence for lower productivity in the Antarctic Ocean during the last glaciation, *Nature*, *351*, 220–223.

Oppo, D. W., and S. J. Lehman (1993), Mid-depth circulation of the subpolar North Atlantic during the Last Glacial Maximum, *Science*, *259*, 1148–1152.

Paillard, D. (1998), The timing of Pleistocene glaciations from a simple multiple-state climate model, *Nature*, *391*, 378–381.

- Paillard, D. (2001), Glacial cycles: Toward a new paradigm, *Rev. Geophys.*, *39*, 325–346.
- Paillard, D., and F. Parrenin (2004), The Antarctic ice sheet and the triggering of deglaciations, *Earth Planet. Sci. Lett.*, *227*, 263–271.
- Paillard, D., M. Ghil, and H. Le Treut (1993), Dissolved organic matter and the glacial-interglacial pCO₂ problem, *Global Biogeochem. Cycles*, *7*, 901–914.
- Peacock, S., E. Lane, and J. M. Restrepo (2006), A possible sequence of events for the generalized glacial-interglacial cycle, *Global Biogeochem. Cycles*, *20*, GB2010, doi:10.1029/2005GB002448.
- Pelegri, J. L. (2008), A physiological approach to oceanic processes and glacial-interglacial changes in atmospheric CO₂, *Sci. Mar.*, *72*, 125–202.
- Pelegri, J. L., and G. T. Csanady (1991), Nutrient transport and mixing in the Gulf Stream, *J. Geophys. Res.*, *96*, 2577–2583.
- Pelegri, J. L., A. Marrero-Díaz, and A. W. Ratsimandresy (2006), Nutrient irrigation of the North Atlantic, *Progr. Oceanogr.*, *70*, 366–406.
- Pelegri, J. L., R. Olivella, and A. García-Olivares (2011), A simple metabolic model of glacial-interglacial energy supply to the upper ocean, *Earth Syst. Dyn. Disc.*, *2*, 271–313.
- Petit, J. R., et al. (1999), Climate and atmospheric history of the past 420,000 years from the Vostok ice core, Antarctica, *Nature*, *399*, 429–436.
- Raymo, M. E., and K. Nisancioglu (2003), The 41 kyr world: Milankovitch's other unsolved mystery, *Paleoceanography*, *18*, 1011, doi:10.1029/2002PA000791.
- Robinson, R. S., and D. M. Sigman (2008), Nitrogen isotopic evidence for a poleward decrease in surface nitrate within the ice age Antarctic, *Quat. Sci. Rev.*, *27*, 1076–1090.
- Robinson, R., D. Sigman, P. DiFiore, M. Rohde, T. Mashiotta, and D. Lea (2005), Diatom-bound ¹⁵N/¹⁴N: New support for enhanced nutrient consumption in the ice age subantarctic, *Paleoceanography*, *20*, PA3003, doi:10.1029/2004PA001114.
- Sarmiento, J. L., and N. Gruber (2006), *Ocean Biogeochemical Dynamics*, Princeton University Press, Princeton.
- Sarmiento, J. L., and J. R. Toggweiler (1984), A new model for the role of the oceans in determining atmospheric PCO₂, *Nature*, *308*, 621–624.
- Scheffer, M., S. Carpenter, J. A. Foley, C. Folke, and B. Walker (2001), Catastrophic shifts in ecosystems, *Nature*, *413*, 591–596.
- Scheffer, M., J. Bascompte, W. A. Brock, V. Brovkin, S. R. Carpenter, V. Dakos, H. Held, E. H. van Nes, M. Rietkerk, and G. Sighara (2009), Early-warning signals for critical transitions, *Nature*, *461*, 53–59.
- Shackleton, N. J., J. Imbrie, and M. A. Hall (1983), Oxygen and carbon isotope record of East Pacific core V19–30: Implications for the formation of deep-water in the late Pleistocene North-Atlantic, *Earth Planet. Sci. Lett.*, *65*, 233–244.
- Siegenthaler, U., and J. L. Sarmiento (1993), Atmospheric carbon dioxide and the ocean, *Nature*, *365*, 119–125.
- Siegenthaler, U., and T. Wenk (1984), Rapid atmospheric CO₂ variations and ocean circulation, *Nature*, *308*, 624–626.
- Siegenthaler, U., et al. (2005), Stable carbon cycle-climate relationship during the Late Pleistocene, *Science*, *310*, 1313–1317.
- Sigman, D. M., and E. A. Boyle (2000), Glacial/interglacial variations in atmospheric carbon dioxide, *Nature*, *407*, 859–869.
- Sigman, D. M., and G. H. Haug (2003), The biological pump in the past, in *Treatise on Geochemistry*, vol. 6, edited by D. Holland and K. K. Turekian, pp. 491–528, Elsevier, London.
- Sigman, D. M., M. P. Hain, and G. H. Haug (2010), The polar ocean and glacial cycles in atmospheric CO₂ concentration, *Nature*, *466*, 47–55.
- Skinner, L. C. (2009), Glacial-interglacial atmospheric CO₂ change: A possible “standing volume” effect on deep-ocean carbon sequestration, *Clim. Past*, *5*, 537–550.
- Stephens, B. B., and R. F. Keeling (2000), The influence of Antarctic sea ice on glacial-interglacial CO₂ variations, *Nature*, *404*, 171–174.
- Stommel, H. (1961), Thermohaline convection with two stable regimes of flow, *Tellus*, *13*, 224–230.
- Stommel, H. (1979), Determination of water mass properties of water pumped down from the Ekman layer to the geostrophic flow below, *Proc. Natl. Acad. Sci. U. S. A.*, *76*, 3051–3055.
- Sundquist, E. T., and K. Visser (2003), The geological history of the carbon cycle, in *Treatise on Geochemistry*, vol. 6, edited by D. Holland and K. K. Turekian, pp. 425–472, Elsevier, London.
- Toggweiler, J. R. (1999), Variation of atmospheric CO₂ by ventilation of the ocean's deepest water, *Paleoceanography*, *14*, 571–588.
- Toggweiler, J. R., J. L. Russell, and S. R. Carson (2006), Midlatitude westerlies, atmospheric CO₂, and climate change during ice ages, *Paleoceanography*, *21*, PA2005, doi:10.1029/2005PA001154.
- Watson, A. J., and L. Maddock (1993), A geophysiological model for glacial-interglacial oscillations in the carbon and phosphorus cycles, in *Scientists on Gaia: Proceedings of the AGU Chapman Conference on the Gaia Hypothesis*, edited by S. H. Schneider and P. J. Boston, pp. 240–246, MIT press, Cambridge.
- Watson, A. J., and A. C. Naveira-Garabato (2006), The role of Southern Ocean mixing and upwelling in glacial-interglacial atmospheric CO₂ change, *Tellus*, *58B*, 73–87.

Appendix A: Stable states in complex systems

The existence of different functional states is not exclusive for the Earth system, living beings and ecosystems also display two or more possible metabolic states where energy is supplied and utilized at very different rates. The transitions between different states in the Earth system share a number of statistical properties with other complex systems, including living beings [Scheffer *et al.*, 2001, 2009; Dakos *et al.*, 2008]. Further, there is a suggestive resemblance between the temporal patterns of several physiological variables in mammals during rest-exercise-rest transitions, like heart-beat and artery-venous oxygen difference, and those of climatological proxies during glacial-interglacial-glacial transitions. It has been proposed that these similarities may occur because of analogous changes in the patterns of nutrient supply, allowing the system to meet sudden shifts in energetic requirements [Pelegri, 2008]. The top panel of Figure 1 illustrates such shifts of energy supply in mammals [e.g., Guyton and Hall, 2005; Randall *et al.*, 2002]. The metabolic rate MR is the energy per unit time used to sustain all body functions. As exercise begins there is a time delay for aerobic energy production in mammals (biomass oxidised through oxygen brought by the circulatory system) to meet the new MR, this oxygen deficit requiring utilization of anaerobic energy (reserve molecules in cells), but eventually the MR is fully sustained aerobically; as exercise ends the MR drops before the aerobic rate of supply does and there is an oxygen debt that is used to rebuild the energy reserves.

We may imagine a similar (physiological) approach for the upper ocean, with two different stable states that depend on the amount of solar energy transformed through photosynthesis. The efficiency in the conversion of solar energy is set by the DIC and inorganic nutrients available in the upper ocean, supplied both from local-fast sources

and through slow deep-water advection and diffusion (therefore, DIC and inorganic nutrients in the ocean would play a role analogous to oxygen and organic nutrients in a heterotrophic living being). A fast source of DIC and dissolved inorganic nutrients is respiration by the heterotrophic community: semi-labile or ancient dissolved organic nutrients and carbon within the upper ocean are swiftly available, although its rate of transformation slows down from labile to recalcitrant forms [see reviews by *Hansell et al.*, 2009; *Jiao et al.*, 2010]. On the other hand, the rate at which deep DIC and dissolved inorganic nutrients reach the upper ocean depends on the intensity of the MOC [*Sarmiento and Toggweiler*, 1984; *Siegenthaler and Wenk*, 1984; *Watson and Naveira-Garabato*, 2006]. Hereafter we shall think of carbon as always accompanying nutrient supply so we will indistinctly refer to (inorganic) nutrients or carbon supply.

Let us consider what would be a sustainable or stable state for the upper ocean. Let c be the DIC concentration within the upper ocean and let G be the DIC concentration of the deep-ocean waters as they reach back to the upper-ocean. The continuity of the MOC implies that the same amount of water that escapes to the deep ocean during deep-water formation has to reach back to the upper ocean; hence, the exchange of DIC between the deep and upper oceans, or net DIC advective supply, is $(G - c)Q$, where Q is the water transported by the MOC. We also allow for the two-way transformation between organic and inorganic carbon through respiration and primary production. The autotrophic upper-ocean photosynthesizes this DIC supply into organic matter at a rate P , although in the process it also uses some organic matter through autotrophic respiration, R_{aut} ; additionally, the system transforms organic into inorganic matter through heterotrophic respiration, R_{het} . Therefore, a stable state is expressed as

$$M \equiv P - R_{aut} = (G - c)Q + R_{het} , \quad (A1)$$

The difference between primary production and autotrophic respiration is the net autotrophic community production, given by $M \equiv P - R_{aut}$. This may also be understood as (solar) energy effectively transformed per unit time through photosynthesis by the autotrophic community; throughout this paper, in analogy with the energy that becomes available to mammals per unit time through the oxidation of organic matter, we will identify this variable with the upper-ocean's MR. (The equivalence is not complete as, while converting energy, the autotrophic community transforms inorganic into organic matter but, in the process, also respire organic matter; in contrast, an heterotroph will transform organic into inorganic matter but will not respire inorganic matter).

Equation (A1) may also be written as $P = (G - c)Q + R$, where total community respiration is defined as $R \equiv R_{aut} + R_{het}$, which may be interpreted as setting the DIC supply necessary to meet the system's total primary production. When the system changes into a state that requires more supply it happens that the net DIC advective supply, $(G - c)Q$, is temporarily insufficient and the system has to resource to reserves in the form of net remineralization of DOC, $R > P$; during the opposite change the net advective supply is in excess, which is used to recover the DIC reserves, $P > R$. These physiological-like arguments are incomplete as they ignore changing DOC and DIC pools within the upper ocean, in the same way as they ignore any nutrient and oxygen reserves within the exercising muscles of a mammal; the case for varying DOC and DIC pools is examined in Section 2.1.

It is worth adding that a stable state does not have to be steady, as the state variables may continuously revolve within certain domain or attractor [Stommel, 1961;

Lorenz, 1963]. The good performance of relaxation-type models indeed suggests that glacial-interglacial oscillations may be understood as a relaxation oscillator response, where the system relaxes towards quasi-equilibrium solutions before being ejected away into a different attractor [*Crucifix*, 2012]. In the model to be developed next we ignore any source of high frequency variability and search for solutions that relax in time towards a steady state.

Appendix B: Model tuning

Our tuning strategy is to explore the model's sensitivity to different values of the controlling parameters in order to get the initial conditions for a more refined search method. The first step is to examine the response to different glacial (or basal) time scales $\tau_0 = V/Q_0$ and combinations of t_{\max} and t_3 . The maximum non-dimensional circulation rate, ε_{\max} , is taken as set by the intensity of today's MOC, Q_{\max} , non-dimensionalized in terms of the basal rate $Q_0 = V/\tau_0$, i.e., $\varepsilon_{\max} = Q_{\max}/Q_0$. We estimate the upper-ocean area to be $3.3 \times 10^{14} \text{ m}^2$, or about 65% of the Earth's surface (71% of water coverage less some 6% for the continental shelves), and take a mean depth of 1400 m to get $V = 4.7 \times 10^{17} \text{ m}^3$. For today's rate of deep water formation we set $Q_{\max} = 22 \text{ Sv}$ ($1 \text{ Sv} \equiv 10^6 \text{ m}^3 \text{ s}^{-1}$), as a rough average estimate from several authors (for brief reviews see *Pelegri* [2008] and *Marchal and Curry* [2008]); this rate sets a limit to the maximum rate of deep water formation and provides an estimate for the minimum recirculation time, $\tau_{\min} = V/Q_{\max} = 700 \text{ yrs}$.

We compute the solution of the model allowing τ_0 to vary between 10 and 100 kyr in intervals of 10 kyr. The correlation coefficient between the CO_2 original time series and the DIC modelled values serves as a useful indicator for the goodness of the

solution. The most satisfactory results correspond to $\tau_0 = 40$ kyr, with t_{\max} somewhere between $(t_1 + t_2)/2$ and t_2 , and t_3 quite close to t_2 . For example, for $\tau_0 = 40$ kyr and $t_3 = t_2$ the correlations for $t_{\max} = (t_1 + t_2)/2$ and $t_{\max} = t_2$ respectively are 0.769 and 0.794. The top panel of Figure 4 illustrates the results when $t_{\max} = (t_1 + t_2)/2$ and $t_3 = t_2$ for $\tau_0 = 40$ kyr; hereafter, in all figures we use the normalized non-dimensional concentrations but, for the sake of clarity, we recover the dimensional time scale. The model cannot reproduce the abrupt changes, as they take place at time scales between several hundred and a few thousand years, but reproduce quite well the long-scale (10 to 100 kyr) oscillations.

The second step is to use a genetic algorithm (GA) [e.g., *Bäck*, 1996] in order to obtain the set of parameters that provides, for each interglacial-glacial cycle, the best model fit to the data. In our model we have one single differential equation whose output is controlled by several parameters. We may therefore define a fitness function that compares the model output with the experimental time-series. The GA looks for the combination of parameters (associated to an individual) which maximizes such a fitness function, i.e., minimizes the residual. The name itself (GA) and the nomenclature commonly used reflect a process of natural selection. The procedure starts with a population of randomly generated individuals, with the parameters specified within certain limits prescribed from our preliminary analysis. The fitness of every individual is assessed and only those that show the best fit are used to recombine parameters and produce the new generation of individuals. The process continues until a certain level of fitness is attained, or a maximum number of iterations is exceeded.

For our application we ask the GA to search for (a) a value of τ_0 during each interglacial-glacial cycle (the starting value is set to 40 kyr), and (b) for the pair (t_{\max}, t_3) , under the condition that $t_3 \geq t_{\max} > t_1$, that set $\varepsilon(t)$ (linearly increasing between t_1 and t_{\max} and decreasing between t_{\max} and t_3). Note τ_0 is allowed to change between different cycles but we assume Q_{\max} has been the same for all interglacial periods, so that the non-dimensional recirculation rate for each interglacial-glacial cycle becomes a function of the glacial time scale, $\varepsilon_{\max} = Q_{\max}/Q_0 = (Q_{\max} \tau_0)/V$. Setting Q_{\max} constant for all four interglacial-glacial cycles is an additional approximation which presumes that the maximum deep-water formation rate has been constrained within some narrow range at each time in the history of the Earth.

The GA is executed for 1600 combinations of the controlling parameters (400 times for each glacial-interglacial cycle) and the correlation between the model output and the normalized CO₂ anomaly time-series is computed. The combination of parameters that provides the highest correlation with the data (0.813) is computed and the corresponding numerical solution is shown in the middle panel of Figure 4. These parameters are t_{\max} and τ_0 , one set for each interglacial-glacial cycle (Table 2, rows 4-5); t_3 is not shown as it always turns out to be equal to t_2 . Those realizations with correlation above 0.81 are chosen to get the mean values and standard deviations of the controlling parameters (Table 2, rows 6-7). The solution using the mean values in Table 2 is hardly distinguishable from the best fit and is not shown.

The four cycles have relatively similar γ_i , τ_0 and $(t_{\max} - t_1)/(t_2 - t_1)$ values, except for cycle 3 which has the smallest γ_i and the largest τ_0 value among all cycles; it appears as if during cycle 3 the interglacial period did not have time enough to reach a

steady state. Therefore, we may calculate mean values for these three parameters using the values from cycles 1, 2 and 4 (Table 2): $\bar{\gamma}_i = 0.786$ and $\bar{\tau}_0 = 42.0$ kyr (or, alternatively, $\bar{\varepsilon}_{\max} = 60.0$). Further, we may reasonably choose $t_{\max} = t_2$ as $(t_{\max} - t_1)/(t_2 - t_1)$ differs from 1.0 by less than 8%. We can use these mean numbers, together with t_1 and t_2 that set the start of the transitions, to predict the full time series for all four interglacial-glacial cycles. The result is shown in the bottom panel of Figure 4, the data-prediction correlation is 0.782, remaining rather high.

Appendix C: Glacial and interglacial DIC solutions and $\Gamma(t)$ approximation

Here we first provide the glacial and interglacial DIC solutions and then use a simple conservation argument in order to obtain a simple expression for $\Gamma(t)$. In order to have simple mathematical expressions, we consider one single glacial-interglacial cycle, with the glacial period starting at time zero and followed by the interglacial period starting at $t = t_1$ and ending at $t = t_2$.

A low-DIC glacial period, with no MOC supply to the upper ocean, is obtained by setting $\gamma = \gamma_g = 0$ and $\Gamma = c$. In this case the DIC in the upper ocean changes solely because production exceeds respiration by an amount εc , the controlling equation being $dc/dt = -\varepsilon c$. By setting $\varepsilon = 1$ this equation becomes $dc/dt = -c$ which tells us the DIC concentration decays with the time scale τ_0 because of excess production over remineralization, i.e., the non-dimensional solution (but, as for the plots, retaining the dimensional time) is

$$c = \gamma_i \exp\left(-\frac{t}{\tau_0}\right). \quad (\text{C1})$$

The integral of the excess in primary production over respiration during the glacial period becomes

$$\int_0^{t_1} (P - R) dt = \int_0^{t_1} c dt = \gamma_i \tau_0 \left[1 - \exp\left(-\frac{T_g}{\tau_0}\right) \right], \quad (\text{C2})$$

where $T_g = t_1$ is the length of the glacial period.

A high-DIC interglacial period with both MOC supply and remineralization of DOC within the upper ocean is obtained by setting $\gamma = \gamma_i$ and $0 < \Gamma \leq \gamma_i$. In this case the partition between deep-water DIC supply, $\varepsilon(\Gamma - c)$, and input through regeneration of DIC within the upper ocean, $\varepsilon(\gamma_i - \Gamma)$, changes with time depending on $\Gamma(t)$. However, the solution for $c(t)$ during the interglacial is independent of this partition, the non-dimensional solution being (again retaining the dimensional time)

$$c(t) = c_1 + (\gamma_i - c_1) \left[1 - \exp\left(-\frac{E_1}{\tau_0}\right) \right], \quad (\text{C3})$$

where $c_1 \equiv c(t_1)$ is the concentration of DIC at the start of the interglacial; using $\varepsilon(t) = \varepsilon_{\max} (t - t_1) / T_i$ leads to the time-integrated non-dimensional circulation rate, $E_1 = \int_{t_1}^t \varepsilon(t) dt = \varepsilon_{\max} (t - t_1)^2 / 2T_i$, where t_1 and t_2 respectively correspond to the start and end of the interglacial period so that its duration is given by $T_i = t_2 - t_1$.

During the interglacial period we let $\Gamma(t)$ increase from some initial value $c \leq \Gamma_g \leq \gamma_i$ at the end of the glacial period (at time t_1) to the γ_i interglacial reference value at the end of the interglacial period (at time $t_{\max} \cong t_2$). At the beginning of the interglacial period both $\varepsilon(\Gamma - c)$ and $\varepsilon(\gamma_i - \Gamma)$ are null because $\varepsilon(t) = 0$, i.e., the MOC is initially blocked. At the end of the interglacial period they both again become zero

because c reaches γ_i (the DIC effectively reaches its steady state value and the deep-ocean supply becomes null) and Γ is set as γ_i (to ensure that there cannot be indefinite remineralization within an upper ocean of finite size).

Consider a simple case where the function $\Gamma(t)$ is left to increase linearly in time during the interglacial period, from the initial value Γ_g to the γ_i value, i.e., $\Gamma(t) = \Gamma_g + (\gamma_i - \Gamma_g)(t - t_1)/T_i$. In this case the integral for the excess in respiration over primary production during the interglacial period is

$$\int_{t_1}^{t_2} (R - P) dt = \int_{t_1}^{t_2} \varepsilon (\gamma_i - \Gamma) dt = \frac{\varepsilon_{\max} T_i (\gamma_i - \Gamma_g)}{6} \quad (\text{C4})$$

In order to determine Γ_g we require that net production over the glacial period equals the excess respiration during the interglacial period less the loss of organic matter from the upper to the deep ocean associated to the MOC. Notice this is an additional constraint which arises from conservation of DOC in the upper ocean (equation 2). A limitation is that we have no simple ways to estimate the loss term $-Qc_r$, as it would require solving equation (2) for c_r subject to some (unknown) initial condition. Alternatively, we may specify what fraction α of the DOC stored in the upper ocean during the glacial period is available for remineralization during the subsequent interglacial period; this is equivalently to setting the fraction $1 - \alpha$ of organic carbon produced during a glacial period that is lost through recirculation out of the upper ocean during the following interglacial period. With these considerations relations (C2) and (C4) lead to

$$\Gamma_g = \left\{ 1 - \left(\frac{6\alpha\tau_0}{\varepsilon_{\max} T_i} \right) \left[1 - \exp\left(-\frac{T_g}{\tau_0} \right) \right] \right\} \gamma_i. \quad (\text{C5})$$

This last relation shows that the smaller α the greater Γ_g will be. This is because the DIC of the deep-waters arriving to the upper ocean has to increase in order to account for the DIC lost during the interglacial period through conversion into DOC and sinking with the MOC. Following this procedure we obtain Γ_g for several values of α (1.0, 0.9 and 0.5) for the different glacial-interglacial cycles; Γ_g is, as expected, always larger than the DIC in the upper ocean at the start of the interglacial period and this difference increases as α is reduced (Table 3).

So far we have explored a linear expression for $\Gamma(t)$, believed to be indicative of the sort of fractioning that occurs. Another possibility of interest is obtained by setting $\Gamma(t) = c(t) + \delta(t)$, where $\delta(t)$ is a positive function that decreases as time approaches the interglacial maximum; this function guarantees the MOC supply to be always positive, i.e., $\varepsilon(\Gamma - c) \geq 0$. The results again depend on the fraction α of glacial DOC used for remineralization during the interglacial. If this fraction is close to one then it turns out that almost no deep-ocean input is necessary, i.e., δ remains close to zero, meaning that the DOC stored in the upper ocean during the glacial period is sufficient to sustain, through remineralization, the interglacial DIC requirements. On the contrary, the smaller α (large amounts of DOC are lost through the MOC during the interglacial period) the larger the DIC supply from the deep ocean.

Appendix D: Estimating dimensional DIC and DOC changes in the upper ocean

Equations (C2) and (C4) are non-dimensional relations for the amount of DIC converted to DOC during one full glacial cycle. However, in these equations γ_i was obtained from the anomaly non-dimensional CO_2 time series. Therefore, if we wish to calculate the corresponding dimensional quantity we should not use the deep-water

DIC, c_d , but rather the change in DIC related to the glacial-interglacial CO₂ variations, Δc_d . Given the atmospheric CO₂ concentrations, we would require knowing the temperature, salinity and alkalinity of the surface waters in order to obtain the corresponding equilibrium DIC values [Broecker, 1974; Skirrow, 1975]. In coherence with the assumptions behind our simple two-box model, for our purposes it is sufficient to estimate (with constant temperature, salinity and alkalinity) the range of DIC concentrations that corresponds to the observed range of atmospheric CO₂ concentrations.

Carrying out this exercise for waters with temperature of 15°C, salinity 35 and alkalinity 2350 mmol m⁻³, we find that a good approximation in the pCO₂ range from 180 to 280 ppmv (deviations always less than 0.5%) is given by the following linear relation:

$$\text{DIC} = 1955 + 0.96 (\text{pCO}_2 - 180) \quad (\text{D1})$$

where DIC is expressed in mmol C m⁻³ and the concentration of CO₂ is given in ppmv. This relation tells us that the change in DIC between maximum glacial and interglacial periods will approximately be $\Delta c_d = 100 \text{ mmol C m}^{-3}$.

Therefore, the actual amount of DIC (in mmol of carbon) converted into DOC during one glacial period is obtained from equation (C2) as

$$\int_0^{T_g} (P - R) dt = \tau_0 \left[1 - \exp\left(-\frac{T_g}{\tau_0}\right) \right] \frac{V \Delta c_d}{\tau_0} \quad (\text{D2})$$

Using, for example, the values for the 2-3 glacial-interglacial cycle ($T_g = 81.9 \text{ kyr}$, $\tau_0 = 43.7 \text{ kyr}$; Table 3) gives that $40.0 \times 10^{12} \text{ kmol C}$ were converted from inorganic to organic. Dividing by the volume of the upper ocean ($4.7 \times 10^{17} \text{ m}^3$), leads to a carbon transformation of about 85 mmol C m^{-3} . Repeating the calculations for the other two

cycles in Table 2, the mean transformation is $87 \pm 9 \text{ mmol C m}^{-3}$. According to *Hansell et al.* [2009], the DOC concentration in today's upper ocean is about 45 mmol C m^{-3} . Assuming that this value is characteristic for the end of an interglacial period, our estimate for the amount of carbon transformed tells us that by the end of the glacial period the DOC concentration would have had approximately been $132 \text{ mmol C m}^{-3}$, representing an increase by a factor of almost 3 with respect to the modern ocean.

In order for the upper-ocean to be balanced, the same amount of DOC stored during a glacial period would need to become available as DIC during the subsequent interglacial period. If there is no carbon leakage through the MOC ($\alpha = 1$) then all inorganic carbon would be available from the DOC stored in the upper-ocean through remineralization. However, if there is a fraction of DOC lost to the deep ocean through the MOC then it will have to be supplied by deep-ocean sources; for example, if $\alpha = 0.5$ then half of the interglacial DIC supply will come from the remineralization of DOC within the upper ocean and the other half will be new carbon arriving from the deep ocean.

References

- Bäck, T. (1996), *Evolutionary Algorithms in Theory and Practice*, Oxford University Press, Oxford.
- Broecker, W. S. (1974), *Chemical Oceanography*, Harcourt Brace Jovanovich, New York.
- Crucifix, M. (2012), Oscillators and relaxation phenomena in Pleistocene climate theory, *Phil. Trans. R. Soc. A*, 370, 1140-1165.

- Dakos, V., M. Scheffer, E. H. van Nes, V. Brovkin, V. Petoukhov, and H. Held (2008), Slowing down as an early warning signal for abrupt climate change, *Proc. Natl. Acad. Sci. USA*, *105*, 14308-14312.
- Guyton, A. C., and J. E. Hall (2005), *Textbook of medical physiology*, 10th edition, Philadelphia, W. B. Saunders Company.
- Hansell, D. A., C. A. Carlson, D. J. Repeta, and R. Schlitzer (2009), Dissolved Organic Matter in the Ocean: A Controversy Stimulates New Insights, *Oceanogr.*, *22*, 202-211.
- Jiao, N., G. J. Herndl, D. A. Hansell, R. Benner, G. Kattner, S. W. Wilhelm, D. L. Kirchman, M. G. Weinbauer, T. Luo, and F. Chen (2010), Microbial production of recalcitrant dissolved organic matter: long-term carbon storage in the global ocean, *Nat. Rev. Microbiol.*, *8*, 593-599.
- Lorenz, E. N. (1963), Deterministic nonperiodic flow, *J. Atmos. Sci.*, *20*, 130-141.
- Marchal, O., and W. G. Curry (2008), On the abyssal circulation in the Glacial Atlantic, *J. Phys. Oceanogr.*, *38*, 2014-2037.
- Pelegrí, J. L. (2008), A physiological approach to oceanic processes and glacial-interglacial changes in atmospheric CO₂, *Sci. Mar.*, *72*, 125-202.
- Randall, D., W. Burggren, and K. French (2002), *Eckert animal physiology: mechanisms and adaptations*, 5th edition, New York, W. H. Freeman and Company.
- Sarmiento, J. L., and J. R. Toggweiler (1984), A new model for the role of the oceans in determining atmospheric PCO₂, *Nature*, *308*, 621-624.
- Scheffer, M., S. Carpenter, J. A. Foley, C. Folke, and B. Walker (2001), Catastrophic shifts in ecosystems, *Nature*, *413*, 591-596.

Scheffer, M., J. Bascompte, W. A. Brock, V. Brovkin, S. R. Carpenter, V. Dakos, H. Held, E. H. van Nes, M. Rietkerk, and G. Sigihara (2009), Early-warning signals for critical transitions, *Nature*, *461*, 53-59.

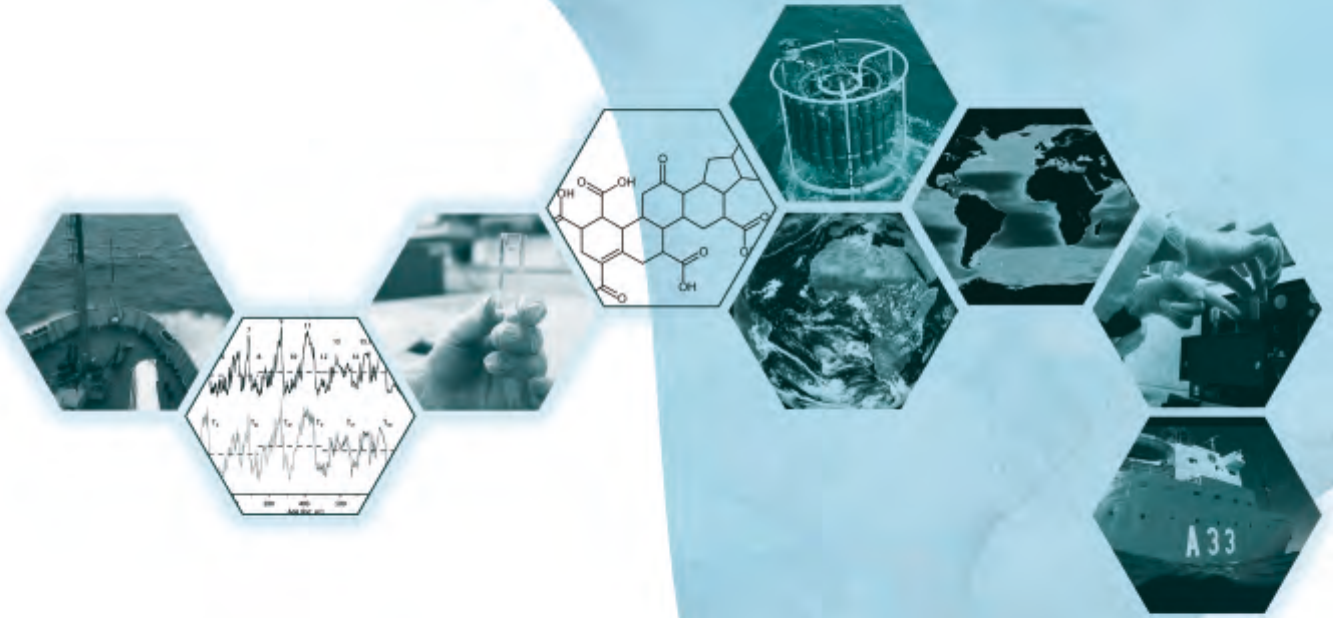
Siegenthaler, U., and T. Wenk (1984), Rapid atmospheric CO₂ variations and ocean circulation, *Nature*, *308*, 624-626.

Skirrow, G. (1975), The dissolved gases - Carbon dioxide, in *Chemical Oceanography*, edited by J. P. Riley and G. Skirrow, pp. 1-192, Academic Press, London.

Stommel, H. (1961), Thermohaline convection with two stable regimes of flow, *Tellus*, *13*, 224-230.

Watson A. J., and A. C. Naveira-Garabato (2006), The role of southern ocean mixing and upwelling in glacial-interglacial atmospheric CO₂ change, *Tellus*, *58B*, 73-87.

GENERAL DISCUSSION AND CONCLUSIONS



In order to fully understand the MCP, its role on past climate and its sensitivity to global change, it is necessary not only to study the different signatures in the paleo-oceanographic record but also to gain knowledge about RDOC sources and the mechanisms and constraints of its decomposition in the modern ocean. Advances in this direction will provide more accurate model-based projections for future climate scenarios (*Dittmar, 2015; Jiao et al., 2014; Ridgwell & Arndt, 2015*). To reach this purpose, a coordinated multidisciplinary research effort is required, combining different research approaches with wide-minded perspectives and covering the full spatio-temporal range of all relevant processes (*Pelegri et al., 2001; Kohfeld and Ridgwell, 2009; Jiao et al., 2010; Jiao et al., 2014; Worden et al., 2015; Jiao et al., 2018; Chen et al., 2018; Robinson et al., 2018; Zhang et al., 2018*).

The main objective of this thesis work has been to address the above challenge through *in situ* measurements and the use of statistical and model approaches at different spatio-temporal scales. For this objective, the approach has incorporated the analysis of concepts of paleoclimate, paleoceanography, biogeochemistry, and physical and biological oceanography, incorporated to the study of the behaviour of complex systems. A clear example is the novel perspective of Ocean Physiology, which uses physiological analogies to understand the potential constraints in the oceanic cycling of carbon during the last four glacial-interglacial cycles.

The several specific topics of this thesis have been discussed at depth in the previous chapters. Here, more than a proper discussion, we reflect about the links between RDOC production and ocean metabolism, at present and during geological times, and its potential relationship with the current climate crisis.

The present: understanding the connections between RDOC production and the metabolism of the ocean

The Anthropocene (*Crutzen, 2002*) represents the beginning of a very rapid trajectory of the Earth system away from the glacial-interglacial limit cycle (of ca. 100,000 years periodicity), as a result of human impacts on the essential planetary processes (*Falkowsky et al., 2000; Steffen et al., 2018*). Nowadays, the Earth system has definitively left the CO_2 domain characteristic for the last 800 kyr, reaching an atmospheric CO_2 level of about 400 ppm, more than 100 ppm higher than the preindustrial values (about 280 ppm) and rising at a rate faster than ever during the Quaternary glacial-interglacial cycles (*Falkowsky et al., 2000; Lüthi et al., 2008; Ciais et al., 2013; Foster et al., 2017*). Although a complete solution to the question of glacial-interglacial variability in atmospheric CO_2 has yet to be found, it is known that a transition

pathway to a new state is difficult to reverse when the transgression of some tipping elements occurs, such as reaching certain critical levels of warming/cooling (Scheffer *et al.*, 2001; Lenton *et al.*, 2008; Lenton, 2011; Lenton *et al.*, 2012).

Steffen and collaborators (2018) suggest that, due global warming caused by human emissions of greenhouse gases and biosphere degradation, the Earth system is currently on a Hothouse Earth pathway (with conditions resembling the mid-Miocene). This might occur when the average Earth's surface temperature exceeds about 2°C above the pre-industrial baseline (Schellnuber *et al.*, 2016); exceeding this planetary threshold is thought to lead the Earth system towards an essentially irreversible pathway driven by internal dynamics, especially strong nonlinearities in biogeophysical feedback processes, and tipping cascades.

The ocean is the largest sink for the anthropogenic CO_2 emissions with a net up take of roughly 40% since the beginning of the industrial era (De Vries *et al.*, 2014; De Vries *et al.*, 2017; Gruber *et al.*, 2019). Therefore, one of the biogeophysical feedbacks that could accelerate the Hothouse Earth pathway is a weakening in the strength of the marine carbon pumps associated with nowadays global warming (Ciais *et al.*, 2013; Segsneider & Bendtsen, 2013; Steffen *et al.*, 2018; Yamamoto *et al.*, 2018; Jiao *et al.*, 2018a; Jiao *et al.*, 2018b).

Many efforts during the last decade have addressed the consequences of human actions over carbon storage via MCP. This is especially relevant because of the feedbacks loops that could potentially exacerbate climate change rate through variations in the RDOC pool size, as it has been suggested for past epochs (Rothman *et al.*, 2003; Royer, 2006; Peltier *et al.*, 2007; Swanson-Hysell *et al.*, 2010; Sexton *et al.*, 2011; Wang *et al.*, 2014; Ridgwell & Arndt, 2015; Ma *et al.*, 2017).

Recently, important advances in knowledge have been possible thanks to (1) the study of geological records and dynamics of biomarkers and isotopic tracers, (2) the employment of novel chemical and genomic methods, (3) the record of *in situ*, remote sensing and experimental observations, (4) the advances on bioinformatics and (5) the global ocean monitoring and Earth-system modelling efforts (Jiao *et al.*, 2014; Jiao *et al.*, 2018a; Zhang *et al.*, 2018). These advances have identified the main drivers of RDOC production under global warming scenario, such as the projected increase in sea water temperature, the enhancement of bacterial respiration, the increase of ocean acidification, the ocean des-oxygenation and also the predicted changes in ocean circulation and mixing.

The present concern is that the sign and direction of the feedbacks are still highly uncertain (Jiao *et al.*, 2014; Ridgwell & Arndt, 2015; Legendre *et al.*, 2015; Jiao *et al.*, 2018a; Polimene *et al.*, 2018; Steffen *et al.*, 2018; Robinson *et al.*, 2018). This means that, despite the progress made over the past decade related to microbial carbon pump framework (*for a review see*

Zhang et al., 2018), there are still large unknowns about the mechanisms and processes of RDOC production, which prevent from predicting how the RDOC reservoir will respond to climate change (*Jiao et al., 2014; Jiao et al., 2018a*).

This thesis clarifies some of these issues and provides new insights on the *in situ* production of RDOC via MCP in water masses with high terrestrial humic-like FDOM concentrations at origin (i.e, the Equatorial Atlantic Ocean). Thanks to the employment of a polynomial mixing model, we have identified the magnitude of the FDOM and AOU variability associated with biogeochemical and physical forcing. This finding allows, for the first time, formulating a general relationship between humic-like FDOM (C-peak) and AOU in the dark equatorial Atlantic Ocean, including the mesopelagic layer and the abyssal layer regardless of the mixture of waters with different preformed levels.

One principal conclusion is that RDOC concentration depends on the characteristics of the water mass at origin but the production rates do not. This piece of work not only provides valuable results for modelling purposes but also gives practical statistical tools to quantify the relative importance of these different drivers on RDOC dynamics. Our results advocate for testing the power of this methodology in other areas with different thermohaline and biogeochemical distributions, with the eventual purpose of assessing global RDOC production rates.

The past: contribution of the MCP to the glacial-interglacial abrupt climatic transitions of the Earth system

The study of the geological records has shed light to the natural changes in the climate and global biogeochemical cycles on planet Earth, which have occurred over periods ranging between decades and millions of years (*Kohfeld & Ridgwell, 2009; Ridgwell & Arndt, 2015*). The sedimentary records provide information on the range of natural variability within the Earth system, hence improving our knowledge of the global biogeochemical processes and their relationship with climate and providing a rigorous test for hindcast and forecast models, from the simplest to the most complex. In this way, through the numerous hypothesis proposed to understand the polar-ice records of glacial-interglacial changes in atmospheric carbon dioxide (*Sigman & Boyle, 2000; Kohfeld and Ridgwell, 2009; Ciais et al., 2013*), the knowledge of the global carbon cycle, the cycle of nutrients and their relationship with Earth's climate has been further improved.

In recent years many studies have focused on the carbon dynamics and the global carbon cycle perturbations, with special attention to the dissolved organic fraction (DOC and RDOC)

(Rothman *et al.*, 2003; Royer, 2006; Peltier *et al.*, 2007; Swanson-Hysell *et al.*, 2010; Sexton *et al.*, 2011; Wang *et al.*, 2014; Ridgwell & Arndt, 2015; Ma *et al.*, 2017). Nevertheless, the processes in the ancient global ocean that may have influenced carbon flux through RDOC are still largely hypothetical and hence far from being conclusive (Ridgwell & Arndt, 2015).

In this thesis, the global constraints on carbon transformations in the upper ocean for the last 420 kyr have been assessed. This has been done with the help of an idealized two-box ocean model, tuned to fit the glacial-interglacial atmospheric CO_2 variations as obtained from the Vostok ice record (Lüthi *et al.*, 2008). The model, inspired on physiological temporal rhythms in living beings (Pelegrí, 2008), associates the glacial/interglacial transitions with shifts between two distinct ocean metabolic states, each one with different rates of dissolved inorganic carbon and nutrients supply to the upper ocean. The results lead us to interpret that the interglacial phases were periods of enhanced metabolic rate, with enhanced DIC/nutrient supply to the upper ocean arising from both relatively high heterotrophic respiration and swift MOC rates. At the beginning of the interglacial state, while the progressive increase of the MOC was taking place, the ocean system resources primarily to inorganic nutrients and carbon arising from the oxidation of the long-lived organic carbon accumulated during the basal (glacial) metabolic state.

From the model's results two key questions appear. First, what are the mechanisms through which the refractory DOC pool formed during the glacial stage becomes available to the heterotrophic community respiration at the beginning of the interglacial period? And, second, what are the processes that allow the formation and accumulation of the RDOC pool during the glacial period?

Using the knowledge about current RDOC dynamics, one plausible explanation for the first question relies on the photo-oxidation of RDOC by sunlight, as the main removal processes for refractory DOC (Carlson & Hansell, 2015). Photochemical reactions not only produce CO_2 but also release labile nitrogen and phosphorous compounds and transform RDOC to DOC forms that are more biologically available to for the heterotrophic microbes (Mopper *et al.*, 1991; Moran and Zepp, 1997; Benner and Biddanda, 1998; Moran and Zepp, 2000; Beaupre and Druffel, 2012; Carlson & Hansell, 2015). Thus, the enhanced solar radiation at the beginning of the interglacial period could have propitiated the photochemical oxidation of long-lived DOC formed during the glacial period, favouring the subsequent uptake by heterotrophic bacteria. The photolytic conversion from RDOC to labile DOC may have been contributed also to an increased remineralization of RDOC through the microbial priming effect (Bianchi, 2011; Guenet *et al.*, 2010; Carlson & Hansell, 2015).

During the glacial period, the model results suggest that the upper ocean metabolic rate (understood as the net autotrophic community production in the upper ocean) exceeds the total respiration. Cooling of the water column reduces the rate of bacterial metabolism (Matsumoto *et al.*, 2007; Matsumoto, 2007), which produce a deepening of the average depth at which organic matter is remineralized (Kohfeld & Ridgwell, 2009; Legendré *et al.*, 2015). This process, together with a more stratified glacial deep ocean (Sigman & Boyle, 2000; Sigman *et al.*, 2010; Skinner *et al.*, 2017), may have played a key role in the accumulation of long-lived carbon during the glacial states for the last 420 kyr (Shen *et al.*, 2018).

Finally, the conclusion that RDOC accumulated during the glacial period plays a key role in the intensity of the subsequent interglacial points at the existence of a pulsating homeostatic organization that is characteristic of the complex adaptive systems, such as planet Earth and human beings (Donner *et al.*, 2009; Dyke & Weaver, 2013). In the last decades, a holistic approach for the study of the complex system Earth has contributed to evidence that the local perturbation of the environment by humans has influenced the global scale processes of planet Earth, at such a level that a different planetary-scale self-organization can emerge. This line of thinking has also contributed to see the planet closer to us than we had ever thought, recognizing humanity as one among many components that set the complexity of the final system. Finally, this work corroborates that humans should improve their relationship with the rest of the Earth's system in order to allow for a dignified survival of all living beings (Schellnuber, 1999; Schellnuber *et al.*, 2004; Steffen *et al.*, 2018).

References

- Beaupré, S., Druffel, R.M., (2012). Photochemical reactivity of ancient marine dissolved organic carbon. *Geophys. Res. Lett.* 39, 0–5.
- Benner, R., Biddanda, B., (1998). Photochemical transformations of surface and deep marine dissolved organic matter : Effects on bacterial growth. *Limnol. Oceanogr.* 1373–1378.
- Bianchi, T.S., (2011). The role of terrestrially derived organic carbon in the coastal ocean: A changing paradigm and the priming effect. *Proc. Natl. Acad. Sci.* 108, 19473 -19481.
- Carlson, T., Hansell, D. A., (2015). DOM Sources, Sinks, Reactivity, and Budgets. In *Biogeochemistry of Marine Dissolved Organic Matter* (Eds Hansell, D. A. & Carlson, C. A.) 369–388 (Academic Press, 2015).
- Chen, J.M., Legendre, L., Benner, R., (2018). A recent project shows that the microbial carbon pump is a primary mechanism driving ocean carbon uptake. *Nat. Sci. Rev.* 5(4), 458.
- Ciais, P., Sabine, C., Bala, G., Bopp, L., Brovkin, V., al., E., & House, J. I. (2014). Carbon and Other Biogeochemical Cycles. In O. Edenhofer, R. Pichs-Madruga, Y. Sokona, E. Farahani, S. Kadner, K. Seyboth, A. Adler, I. Baum, S. Brunner, P. Eickemeier, B. Kriemann, J. Savolainen, S. Schlömer, C. von Stechow, Z. T., ... M. J.C. (Eds.), *Climate Change 2013: The Physical Science Basis. Contribution of Working Group I to the Fifth Assessment Report of the Intergovernmental Panel on Climate Change* (pp. 465-570). Cambridge University Press.

- Crutzen, P.J., (2002). Geology of mankind—The Anthropocene. *Nature*. 415(6867),23.
- Dyke, J. G., & Weaver, I. S., (2013). The Emergence of Environmental Homeostasis in Complex Ecosystems. *PLOS Comput. Biol.* 9(5), e1003050.
- DeVries, T., Holzer, M., & Primeau, F., (2017). Recent increase in oceanic carbon uptake driven by weaker upper-ocean overturning. *Nature.*, 542(7640), 215–218.
- DeVries, T., (2014). The oceanic anthropogenic CO₂ sink: Storage, air-sea fluxes, and transports over the industrial era. *Global Biogeochem. Cycles*. 28, 631–647.
- Dittmar, T., (2015). Reasons Behind the Long-Term Stability of Dissolved Organic Matter. In: Hansell DA, Carlson CA (eds). *The biogeochemistry of marine dissolved organic matter, 2nd edition*. Elsevier 369–388.
- Donner, R., Barbosa, S., Kurths, J., Marwan, N., (2009). Understanding the Earth as a Complex System – recent advances in data analysis and modelling in Earth sciences. *Eur. Phys. J. Spec. Top.* 174(1), 1–9.
- Falkowski, P., *et al.*, (2000). The Global Carbon Cycle : A Test of Our Knowledge of Earth as a System. *Science. New Series*. 290 (5490), 291–296.
- Guenet, B., Danger, M., Abbadie, L., Lacroix, G., (2010). Priming effect: bridging the gap between terrestrial and aquatic ecology. *Ecology*. 91(10), 2850–2861.
- Gruber, N., *et al.*, (2019). The oceanic sink for anthropogenic CO₂ from 1994 to 2007. *Science*. 363(6432), 1193–1199.
- Foster, G.L., Royer, D.L., Lunt, D.J., (2017). Future climate forcing potentially without precedent in the last 420 million years. *Nat. Commun.* 8, 1–8.
- Jiao, N., *et al.*, (2010). Microbial production of recalcitrant dissolved organic matter: long-term carbon storage in the global ocean. *Nat. Rev. Microbiol.* 8, 593–599.
- Jiao, N., Robinson, C., Azam, F., Thomas, H., Baltar, F., Dang, H., Johnson, M., (2014). Mechanisms of microbial carbon sequestration in the ocean – future research directions. *Biogeosciences*. 11, 5285–5306.
- Jiao N, *et al.*, (2018a). Unveiling the enigma of refractory carbon in the ocean. *Natl Sci Rev.* 5, 459–63.
- Jiao, N., Wang, H., Xu, G., Aricò, S., (2018b). Blue Carbon on the Rise : Challenges and Opportunities. *Nat. Sci. Rev.* 5(4), 464–468.
- Kohfeld KE, Ridgwell A (2009) Glacial-interglacial variability in atmospheric CO₂. In: Le Quéré C, Saltzman ES (eds) *Surface ocean-lower atmosphere processes, vol 187., Geophysical monograph series AGU, Washington, pp 251–286*
- Lenton, T.M., Held, H., Kriegler, E., Hall, J.W., Lucht, W., Rahmstorf, S., Schellnhuber, H.J., (2008). Tipping elements in the Earth's climate system. *P. Natl. A. Sci.* 105 (6) 1786–1793.
- Lenton, T.M., (2011). Early warning of climate tipping points. *Nat. Publ. Gr.* 1, 201–209.
- Lenton T.M., Livina, V.N., Dakos, V., van Nes, E.H., Scheffer, M. (2012). Early warning of climate tipping points from critical slowing down: comparing methods to improve robustness. *Philos. Trans. A Math. Phys. Eng. Sci.* 370(1962), 1185–1204.
- Legendre, L., Rivkin, R.B., Weinbauer, M.G., Guidi, L., Uitz, J., (2015). The microbial carbon pump concept: Potential biogeochemical significance in the globally changing ocean. *Prog. Oceanogr.* 134, 432–450
- Lüthi, D., *et al.*, (2008). High-resolution carbon dioxide concentration record 650,000–800,000 years before present. *Nature* 453, 379–382
- Ma, W., Wang, P., Tian, J., (2017). Modeling 400–500-kyr Pleistocene carbon isotope cyclicity through variations in the dissolved organic carbon pool. *Global Planet. Change*, 152, 187–198.
- Matsumoto, K., Hashioka, T., Yamanaka, Y., (2007). Effect of temperature-dependent organic carbon decay on atmospheric pCO₂. *J. Geophys. Res.* 112(G2).

- Matsumoto, K., (2007). Biology-mediated temperature control on atmospheric pCO₂ and ocean biogeochemistry. *Geophys. Res. Lett.* 34(20).
- Mopper, K., Zhou, X., Kieber, R. J., Kieber, D. J., Sikorski, R. J., Jones, R. D., (1991). Photochemical degradation of dissolved organic carbon and its impact on the oceanic carbon cycle. *Nature*. 353(6339), 60–62.
- Moran, M. A., Zepp, R. G., (1997). Role of photoreactions in the formation of biologically labile compounds from dissolved organic matter. *Limnol. Oceanogr.* 42(6), 1307–1316.
- Moran, M. A., Sheldon, W. M., Zepp, R. G., (2000). Carbon loss and optical property changes during long-term photochemical and biological degradation of estuarine dissolved organic matter. *Limnol. Oceanogr.* 6.
- Pelegrí, J., Alonso, I., Arístegui, J., (2001). The ocean, our climate and the earth's health. *Sci. Mar.*, 65(S1), 3-6.
- Pelegrí, J.L., (2008). A physiological approach to oceanic processes and glacial-interglacial changes in atmospheric CO₂. *Sci. Mar.* 72(1), 185-202.
- Peltier, W. R., Liu, Y., Crowley, J. W., (2007). Snowball Earth prevention by dissolved organic carbon remineralization. *Nature*, 450(7171), 813–818.
- Polimene, L. et al., (2018), Modelling marine DOC degradation time scales, *Natl. Sci. Rev.* 5 (4), 468–474.
- Ridgwell, A., Arndt, S., (2015). Why Dissolved Organics Matter: DOC in Ancient Oceans and Past Climate Change. in: *Hansell, D.A., Carlson, C.A.B.T.-B. of M.D.O.M. (Second E. (Eds.), . Academic Press, Boston, pp. 1–20.*
- Robinson, C., Wallace, D., Hyun, J., Polimene, L., Benner, R., Zhang, Y., (2018). An implementation strategy to quantify the marine microbial carbon pump and its sensitivity to global change.. *Nat. Sci. Rev.* 5(4), Pages 474–480.
- Rothman, D.H., Hayes, J.M., Summons, R.E., (2003). Dynamics of the Neoproterozoic carbon cycle. *Proc. Natl. Acad. Sci. USA* 100, 8124–29.
- Royer, D.L., (2006). CO₂-forced climate thresholds during the Phanerozoic. *Geochim. Cosmochim. Acta* 70, 5665–5675.
- Segschneider, J., Bendtsen, J., (2013). Temperature-dependent remineralization in a warming ocean increases surface pCO₂ through changes in marine ecosystem composition. *Global Biogeochem. Cycles.* 27, 1214– 1225.
- Schellnhuber, H.J., (1999). ‘Earth system’ analysis and the second Copernican revolution. *Nature* 402, C19.
- Schellnhuber, H.J., (2004). Earth System Analysis for Sustainability. *Cambridge, Mass: MIT Press in cooperation with Dahlem University Press, 2004. Print.*
- Schellnhuber, H.J., Rahmstorf, S., Winkelmann, R., (2016). Why the right climate target was agreed in Paris. *Nat. Publ. Gr.* 6, 649–653.
- Scheffer, M. et al., (2001). Catastrophic shifts in ecosystems. *Nature.* 413, 591.
- Shen, Y., Benner, R., (2018). Mixing it up in the ocean carbon cycle and the removal of refractory dissolved organic carbon. *Sci. Rep.*, 8(1), 2542
- Skinner, L. C., (2009). Glacial-interglacial atmospheric CO₂ change: a possible “standing volume” effect on deep-ocean carbon sequestration. *Clim.Past.* 5(3), 537–550.
- Steffen, W., et al., (2018). Trajectories of the Earth System in the Anthropocene. *PNAS.* 115(33), 8252–8259.
- Sexton, P.F., Norris, R.D., Wilson, P. A, Pälike, H., Westerhold, T., Röhl, U., Bolton, C.T., Gibbs, S., (2011). Eocene global warming events driven by ventilation of oceanic dissolved organic carbon. *Nature* 471, 349–352.

- Sigman, D.M., Boyle, E.A., (2000). Glacial/Interglacial variations in atmospheric CO₂. *Nature*. 407, 859–869
- Sigman, D. M., Hain, M. P., & Haug, G. H., (2010). The polar ocean and glacial cycles in atmospheric CO₂ concentration. *Nature*. 466(7302), 47–55.
- Swanson-Hysell, N. L., Rose, C. V., Calmet, C. C., Halverson, G. P., Hurtgen, M. T., & Maloof, A. C., (2010). Cryogenian Glaciation and the Onset of Carbon-Isotope Decoupling. *Science*. 328(5978), 608–611.
- Wang, P., Li, Q., Tian, J., Jian, Z., Liu, C., Li, L., Ma, W., (2014). Long-term cycles in the carbon reservoir of the Quaternary ocean: a perspective from the South China Sea. *Natl. Sci. Rev.* 1, 119–143.
- Worden, A. Z., Follows, M. J., Giovannoni, S. J., Wilken, S., Zimmerman, A. E., & Keeling, P. J., (2015). Rethinking the marine carbon cycle: Factoring in the multifarious lifestyles of microbes. *Science*. 347(6223), 1257594.
- Yamamoto, A., Abe-Ouchi, A., Yamanaka, Y., (2018). Long-term response of oceanic carbon uptake to global warming via physical and biological pumps. *Biogeosciences* 15, 4163–4180.
- Zhang, C., Dang, H., Azam, F., Benner, R., (2018). Evolving Paradigms in Biological Carbon Cycling in the Ocean. *Natl. Sci. Rev.* 5, 481–499.

Influence of water-mass mixing and microbial activity in the spatial variability of RDOC in the deep ocean

- I. In order to properly assess the effect of biogeochemical processes in the dark ocean onto the non-conservative variables, it is fundamental and necessary to take into consideration the potential differences associated with their different origins.
- II. A novel methodology that overcomes past constraints about mixing of water masses has been presented. This methodology allows determining the distribution of both physical and biogeochemical contributions, lending information not only on the biogeochemical processes and stoichiometric ratios but also on the patterns of connectivity within regions.
- III. A general and significant relationship between humic-like fluorescent DOM (F(340/440)) and AOU (slope $(3.14 \pm 0.08) \times 10^{-5}$ R.U., $R^2=0.79$, p-value < 0.001) is conclusive for the equatorial Atlantic Ocean, considering all water masses present in the zone of study. Such relationship endorses the idea that the major source of F(340/440) in the dark ocean is the *in situ* biological oxidation of organic matter by microbial activity.

Understanding the role of the RDOC, via the microbial carbon pump, in the glacial-interglacial transitions

- IV. The use of physiological-like approach to study the global spatial and temporal organization of the planet Earth, such as other optimized pulsating systems, helps to give a plausible explanation for the glacial and interglacial climate perturbations in the atmospheric CO_2 . In particular, setting the metabolic rate of the ocean system as the net autotrophic community production in the upper ocean, the interglacial-glacial periods have been related to variations in the efficiency to convert solar into chemical energy through photosynthesis, lending the upper ocean to switch between two different metabolic states. This efficiency is modulated by the availability of DIC and nutrients, coming both from the remineralization of organic matter and/or from deep DIC/nutrients supply through the MOC.

- V.** The progressive slow glacial accumulation and relatively swift interglacial utilization of DOC have been reproduced through a very simple two-box and time-dependent model for DIC/nutrients in the upper ocean. The model also allows incorporating the supply of deep DIC/nutrients through a time-varying MOC. The model is capable of reproducing the overall features of the last four atmospheric CO₂ glacial-interglacial transitions. The interglacial periods are interpreted as epochs of enhanced metabolic rate, sustained by high heterotrophic respiration and intense MOC supply of DIC and nutrients. In contrast, the glacial periods are understood as epochs of weak or null MOC, with the upper ocean being effectively blocked from the deep ocean and experiencing a net conversion of DIC into DOC at a relatively slow rate, meaning that community production exceeds total respiration.
- VI.** Our results strongly suggest that dissolved organic matter, which would build up during the glacial periods, could become a very important source of DIC and nutrients for the upper ocean at the beginning of the interglacial periods. This input of nutrients would help sustain an enhanced interglacial metabolic rate. The glacial-interglacial cycle would turn into a principal oscillation that regulates the homeostatic organization of the Earth system.

*Tú que dispones de viento y mar,
haces la calma, la tempestad.
Ten de nosotros Señor, piedad,
piedad, Señor, Señor, piedad.*

Hespérides, buenas noches...

